

NASA Technical Paper 1316

**LOAN COPY: RET**  
**AFWL TECHNICAL**  
**KIRTLAND AFB,**

TECH LIBRARY KAFB, NM  
0134418

# Wind-Tunnel Investigation at Supersonic Speeds of a Canard-Controlled Missile With Fixed and Free-Rolling Tail Fins

A. B. Blair, Jr.

SEPTEMBER 1978







NASA Technical Paper 1316

Wind-Tunnel Investigation  
at Supersonic Speeds of  
a Canard-Controlled Missile With  
Fixed and Free-Rolling Tail Fins

A. B. Blair, Jr.  
*Langley Research Center  
Hampton, Virginia*



National Aeronautics  
and Space Administration

**Scientific and Technical  
Information Office**

1978



The present investigation was conducted to provide some insight into the effectiveness of the free-rolling tail concept for the reduction or elimination of large induced rolling moments that are generally experienced by maneuvering canard-controlled missile configurations at supersonic speeds. In an effort to reduce or eliminate these induced rolling moments, an experimental wind-tunnel investigation has been made to determine the effect of a free-rolling (no fin cant) cruciform tail on the stability and control characteristics of a canard-controlled missile. The results of a similar test conducted by the U.S. Navy with canted free-rolling tail fins can be found in reference 5. The rolling tail concept also offers the potential of enabling the canards to provide some

over the tail fins. The idea of using free-rolling tail fins is not new. From 1950 to 1960, the NASA and its predecessor, NACA, investigated a number of roll-control devices in free flight as part of their aerodynamic control research program for missiles and airplanes. For some of these tests, a free-rolling tail-fin assembly was used on the missile airframes, not only to stabilize the models longitudinally but also to eliminate unwanted, induced rolling moments that were generated by the various roll controls under investigation (e.g., ref. 2). In many cases, the free-rolling tails were on nonmaneuvering missile systems (e.g., boost-glide trajectories at low angles of attack). More recently (1960 to 1973), the U.S. Navy has conducted research on bomb-shaped bodies (free-fall stores) with free-rolling tail fins (refs. 3 and 4) as a means of reducing dispersion and of increasing accuracy by eliminating the effect of flow asymmetries

It is well documented that missile configurations which utilize forward surfaces to provide control experience the problem of induced rolling moments at supersonic Mach numbers. One approach to the solution of this problem, which is described in reference 1, uses a free-rolling tail-fin afterbody on a canard-controlled missile model to reduce induced rolling moments.

## INTRODUCTION

The results indicate that the fixed and free-rolling tail configurations have about the same lift-curve slope and longitudinal stability level at low angles of attack. For the free-rolling tail configuration, the canards provide conventional roll control with no roll-control reversal at low angles of attack. The free-rolling tail configuration reduced induced roll due to model roll angle and canard yaw control.

A wind-tunnel investigation was made at free-stream Mach numbers from 1.70 to 2.86 to determine the effects of fixed and free-rolling tail-fin afterbodies on the static longitudinal and lateral aerodynamic characteristics of a cruciform canard-controlled missile model. The effect of small canard roll- and yaw-control deflections was also investigated.

## SUMMARY

measure of roll control, either increased roll-damping or roll-attitude control at low angles of attack. There is a growing need to give canard-controlled missile configurations more simplicity and modular flexibility. The free-rolling tail concept may satisfy these requirements by allowing a missile configuration to have a single control system utilizing a cruciform canard control system for pitch, yaw, and roll control.

The tests were conducted in the Langley Unitary Plan wind tunnel at Mach numbers from 1.70 to 2.86. The nominal angle-of-attack range was  $-30$  to  $250$  at model (canard) roll angles of  $0^\circ$  to  $45^\circ$  and at a Reynolds number of  $6.6 \times 10^6$  per meter ( $2.0 \times 10^6$  per foot). Results of these tests include the effects of small roll- and yaw-control deflections of the canards on the longitudinal and lateral aerodynamic characteristics of the model with a fixed and free-rolling tail-fin afterbody.

#### SYMBOLS

The aerodynamic coefficient data are referred to the body-axis system except for lift and drag which are referred to the stability-axis system. The moment reference was located aft of the model nose at 49.0 percent of the reference body length.

Measurements and calculations were made in the U.S. Customary Units. Measurements are presented in the International System of Units (SI), with the equivalent values given parenthetically in U.S. Customary Units (ref. 6).

A reference area; maximum cross-sectional area of body,  $0.003425 \text{ m}^2$  ( $0.036870 \text{ ft}^2$ )

$C_A$  axial-force coefficient, Axial force/ $qA$

$C_{A,b}$  base axial-force coefficient, Base axial force/ $qA$

$C_D$  drag coefficient, Drag/ $qA$

$C_{D,b}$  base drag coefficient, Base drag/ $qA$

$C_L$  lift coefficient, Lift/ $qA$

$C_{L\alpha}$  lift-curve slope, per degree

$C_l$  rolling-moment coefficient, Rolling moment/ $qAd$

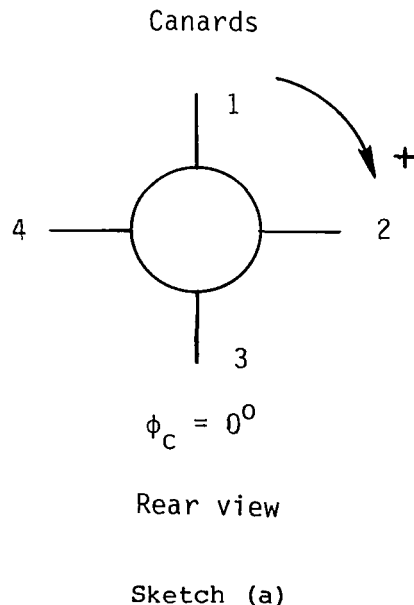
$C_m$  pitching-moment coefficient, Pitching moment/ $qAl$

$C_N$  normal-force coefficient, Normal force/ $qA$

$C_n$  yawing-moment coefficient, Yawing moment/ $qAd$

$C_Y$  side-force coefficient, Side force/ $qA$

$d$	reference diameter, 6.604 cm (2.600 in.)
$l$	reference body length, 99.060 cm (39.000 in.)
$M$	Mach number
$q$	free-stream dynamic pressure, $N/m^2$ (psfa)
$\alpha$	angle of attack, deg
$\delta_{roll}$	differential deflections of two canards (canards 2 and 4, shown in sketch (a)) for roll control; individual canards are deflected indicated amount; negative to provide counterclockwise rotation when viewed from rear, deg
$\delta_{yaw}$	yaw-control deflection of two canards (canards 1 and 3, shown in sketch (a)); positive for leading edge right when viewed from rear, deg
$\phi_C$	model roll angle; positive clockwise when viewed from rear (for $\phi_C = 0^\circ$ , canards are in vertical and horizontal planes), deg
$\dot{\phi}_{tail}$	roll rate of tail-fin afterbody; positive clockwise when viewed from rear, rpm
$\partial C_m / \partial C_L$	static longitudinal stability parameter



## APPARATUS AND TESTS

### Wind Tunnel

The investigation was conducted in the low Mach number test section of the Langley Unitary Plan wind tunnel, which is a variable-pressure, continuous-flow facility. The test section is approximately 2.13 m (7 ft) long and 1.22 m (4 ft) square. The nozzle leading to the test section is of the asymmetric sliding-block type, which permits a continuous variation in Mach number from about 1.5 to 2.9. (See ref. 7.)

### Model

Dimensional details of the model are shown in figure 1(a) and a model photograph is shown in figure 2. The model was a cruciform missile configuration that consisted of a cylindrical body with canards, aft tail fins, and a tangent ogive nose of fineness ratio 3.0. The complete model body had a fineness ratio of 15. The canards and tail fins had slab cross sections with beveled leading and trailing edges. In order for the model to have a free-rolling tail-fin assembly, the tail-fin afterbody was mounted on a set of low-friction ball bearings and was free to rotate through 360° (lock screw out). For the fixed-tail configuration (lock screw in), the tail fins were locked in line with the canards. For both the fixed and free-rolling tail configurations, the canards were deflected to provide roll control and yaw control. The tail fins were not deflected (zero cant angle) and the tail-fin assembly had no braking system.

### Test Conditions

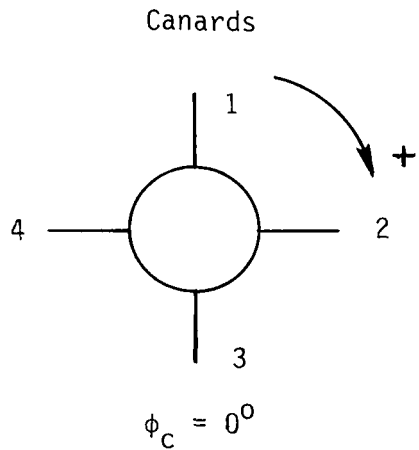
Tests were performed at the following tunnel conditions:

Mach number	Stagnation temperature		Stagnation pressure		Reynolds number	
	K	°F	kPa	psfa	per meter	per foot
1.70	339	150	56.4	1178	$6.6 \times 10^6$	$2.0 \times 10^6$
2.16	339	150	68.5	1430	6.6	2.0
2.36	339	150	75.7	1580	6.6	2.0
2.86	339	150	98.4	2056	6.6	2.0

The dewpoint temperature measured at stagnation pressure was maintained below 239 K (-30° F) to assure negligible condensation effects. All tests were performed with boundary-layer transition strips measured streamwise on both sides of the canards and tail fins and located 3.05 cm (1.20 in.) aft of the body nose and 1.02 cm (0.40 in.) aft of the leading edges. The transition strips were approximately 0.157 cm wide (0.062 in.) and were composed of No. 50 sand grains sprinkled in acrylic plastic. (See ref. 8.)



- d reference diameter, 6.604 cm (2.600 in.)
- l reference body length, 99.060 cm (39.000 in.)
- M Mach number
- q free-stream dynamic pressure,  $N/m^2$  (psfa)
- $\alpha$  angle of attack, deg
- $\delta_{roll}$  differential deflections of two canards (canards 2 and 4, shown in sketch (a)) for roll control; individual canards are deflected indicated amount; negative to provide counterclockwise rotation when viewed from rear, deg
- $\delta_{yaw}$  yaw-control deflection of two canards (canards 1 and 3, shown in sketch (a)); positive for leading edge right when viewed from rear, deg
- $\phi_C$  model roll angle; positive clockwise when viewed from rear (for  $\phi_C = 0^\circ$ , canards are in vertical and horizontal planes), deg
- $\dot{\phi}_{tail}$  roll rate of tail-fin afterbody; positive clockwise when viewed from rear, rpm
- $\partial C_m / \partial C_L$  static longitudinal stability parameter



Rear view

Sketch (a)

## APPARATUS AND TESTS

### Wind Tunnel

The investigation was conducted in the low Mach number test section of the Langley Unitary Plan wind tunnel, which is a variable-pressure, continuous-flow facility. The test section is approximately 2.13 m (7 ft) long and 1.22 m (4 ft) square. The nozzle leading to the test section is of the asymmetric sliding-block type, which permits a continuous variation in Mach number from about 1.5 to 2.9. (See ref. 7.)

### Model

Dimensional details of the model are shown in figure 1(a) and a model photograph is shown in figure 2. The model was a cruciform missile configuration that consisted of a cylindrical body with canards, aft tail fins, and a tangent ogive nose of fineness ratio 3.0. The complete model body had a fineness ratio of 15. The canards and tail fins had slab cross sections with beveled leading and trailing edges. In order for the model to have a free-rolling tail-fin assembly, the tail-fin afterbody was mounted on a set of low-friction ball bearings and was free to rotate through 360° (lock screw out). For the fixed-tail configuration (lock screw in), the tail fins were locked in line with the canards. For both the fixed and free-rolling tail configurations, the canards were deflected to provide roll control and yaw control. The tail fins were not deflected (zero cant angle) and the tail-fin assembly had no braking system.

### Test Conditions

Tests were performed at the following tunnel conditions:

Mach number	Stagnation temperature		Stagnation pressure		Reynolds number	
	K	°F	kPa	psfa	per meter	per foot
1.70	339	150	56.4	1178	$6.6 \times 10^6$	$2.0 \times 10^6$
2.16	339	150	68.5	1430	6.6	2.0
2.36	339	150	75.7	1580	6.6	2.0
2.86	339	150	98.4	2056	6.6	2.0

The dewpoint temperature measured at stagnation pressure was maintained below 239 K (-30° F) to assure negligible condensation effects. All tests were performed with boundary-layer transition strips measured streamwise on both sides of the canards and tail fins and located 3.05 cm (1.20 in.) aft of the body nose and 1.02 cm (0.40 in.) aft of the leading edges. The transition strips were approximately 0.157 cm wide (0.062 in.) and were composed of No. 50 sand grains sprinkled in acrylic plastic. (See ref. 8.)

The primary method for controlling tail-fin rotational speed was by limiting the model angle of attack. In the early stages of this test program, tail-fin rotational speed was nominally limited to 200 rpm as a safety precaution; however, this limit was extended to 500 rpm as more confidence was gained. In order to satisfy these limits, only small canard deflections were made.

### Measurements

Aerodynamic forces and moments on the model were measured by means of a six-component electrical strain-gage balance which was housed within the model. The balance was attached to a sting which was, in turn, rigidly fastened to the model support system. Balance-chamber pressure (base pressure) was measured by means of a single static-pressure orifice located in the vicinity of the balance. One light-emitting diode with a photo-transistor receiver pick-up mounted on the sting was used in conjunction with a color-coded ring at the base of the model to record tail-fin afterbody revolutions. The accuracy of this recording system was  $\pm 20$  rpm. No attempt was made to measure the afterbody torque that was produced by the internal ball-bearing friction, viscous-layer skin friction, or aerodynamic damping.

### Corrections

The angles of attack have been corrected for deflection of the balance and sting due to aerodynamic loads. In addition, angles of attack have been corrected for tunnel-flow misalignment. The drag and axial-force coefficient data have been adjusted to free-stream static pressure acting over the model base. Typical measured values of base axial-force and drag coefficients are presented in figure 3.

## PRESENTATION OF RESULTS

Figure

Effect of free-rolling tail on longitudinal aerodynamic characteristics of model with zero control deflection at -	
$\phi_C = 0^\circ$ . . . . .	4
$\phi_C = 45^\circ$ . . . . .	5
Effect of canards on longitudinal aerodynamic characteristics of model with free-rolling tail at $\phi_C = 0^\circ$ . . . . .	6
Effect of free-rolling tail on lateral aerodynamic characteristics of model with zero control deflection at -	
$\phi_C = 0^\circ$ . . . . .	7
$\phi_C = 26.6^\circ$ . . . . .	8
$\phi_C = 45^\circ$ . . . . .	9

Figure

Effect of canards on lateral aerodynamic characteristics of model with free-rolling tail at  $\phi_C = 0^\circ$  . . . . . 10

Roll-control characteristics of model with fixed and free-rolling tail at -

$\phi_C = 0^\circ$  , . . . . . 11

$\phi_C = 45^\circ$  , . . . . . 12

Yaw-control characteristics of model with fixed and free-rolling tail at  $\phi_C = 0^\circ$  . . . . . 13

Table

Summary of test data from free-rolling tail configuration with -

Zero control deflection , . . . . . I

Canard off . . . . . II

Two canards differentially deflected  $0.5^\circ$  each for negative roll control . . . . . III

Vertical canards deflected  $5^\circ$  for positive yaw control . . . . . IV

DISCUSSION

Longitudinal Aerodynamic Characteristics

The longitudinal aerodynamic characteristics of the model with zero control deflection are presented in figures 4 and 5 for  $\phi_C = 0^\circ$  and  $45^\circ$ , respectively. In general, at low angles of attack ( $\alpha \leq 4^\circ$ ), both the fixed and free-rolling tail configurations have about the same lift-curve slope  $C_{L\alpha}$  and stability

level  $\partial C_m / \partial C_L$ . At the higher angles of attack for  $\phi_C = 0^\circ$ , the free-rolling tail configuration has more nonlinear pitching-moment coefficient characteristics with a slight pitch-up tendency and, in general, less restoring moment than the fixed-tail configuration. These aerodynamic differences between the two configurations for the  $\phi_C = 45^\circ$  case (fig. 5) are less pronounced, with the pitching-moment curves becoming more nearly linear with increases in Mach number for the free-rolling tail configuration. However, the fixed-tail configuration now exhibits the pitch-up tendency that characterized the free-rolling tail configuration at  $\phi_C = 0^\circ$ . This pitch-up trend is typical for a missile with cruciform tail fins in the x-position ( $\phi_C = 45^\circ$ ) at supersonic speeds. Flow-field effects, in conjunction with adverse panel-to-panel interference between the windward and leeward tail-fin surfaces, result in a small overall reduction in tail lift capability. This loss of lift for the fixed-tail configuration ( $\phi_C = 45^\circ$ ) can be seen in the lift-coefficient curves presented in figure 5 and for the free-rolling tail configuration at  $\phi_C = 0^\circ$  in figure 4. Visual observation has shown that for  $\phi_C = 0^\circ$ , the free-rolling tail fins are generally interdigitated to the canards (x-position) when rotation stops and are therefore in a similar flow environment as the fixed-tail case when  $\phi_C = 45^\circ$ . This loss in tail lift would account for the pitch-up tendency.

yaw-control capability than the fixed-tail configuration. Again, the aero lockup is delayed to higher angles of attack. (See table IV.)

#### CONCLUSIONS

A wind-tunnel investigation was made at free-stream Mach numbers from 1.70 to 2.86 to determine the effects of fixed and free-rolling tail-fin afterbodies on the static longitudinal and lateral aerodynamic characteristics of a cruciform canard-controlled missile model. The effect of small canard roll- and yaw-control deflections was also investigated. The results of the investigation are as follows:

1. The fixed and free-tail configurations have about the same lift-curve slope and longitudinal stability level at low angles of attack.
2. For the free-rolling tail configuration, the canards provide conventional roll control with no roll-control reversal at low angles of attack.
3. The free-rolling tail configuration reduced induced roll due to model roll angle and canard yaw control.

Langley Research Center  
National Aeronautics and Space Administration  
Hampton, VA 23665  
August 9, 1978

## REFERENCES

1. Sawyer, Wallace C.; Jackson, Charlie M., Jr.; and Blair, A. B., Jr.: Aerodynamic Technologies for the Next Generation of Missiles. Paper presented at the AIAA/ADPA Tactical Missile Conference (Gaithersburg, Maryland), Apr. 27-28, 1977.
2. Schult, Eugene D.: Free-Flight Measurements of the Rolling Effectiveness and Operating Characteristics of a Bellows-Actuated Split-Flap Aileron on a 60° Delta Wing at Mach Numbers Between 0.8 and 1.8. NACA RM L54H17, 1954.
3. Regan, Frank J.; and Falusi, Mary E.: The Static and Magnus Aerodynamic Characteristics of the M823 Research Store Equipped With Fixed and Freely Spinning Stabilizers. NOLTR 72-291, U.S. Navy, Dec. 1, 1972. (Available from DDC as AD 751 658.)
4. Regan, F. J.; Shannon, J. H. W.; and Tanner, F. J.: The Joint N.O.L./R.A.E./W.R.E. Research Programme on Bomb Dynamics. Part III. A Low-Drag Bomb With Freely Spinning Stabilizers. WRE-Report-904 (WR&D), Australian Def. Sci. Serv., June 1973.
5. Darling, John A.: Elimination of the Induced Roll of a Canard Control Configuration by Use of a Freely Spinning Tail. NOLTR 72-197, U.S. Navy, Aug. 16, 1972.
6. Mechtly, E. A.: The International System of Units - Physical Constants and Conversion Factors (Second Revision). NASA SP-7012, 1973.
7. Schaefer, William T., Jr.: Characteristics of Major Active Wind Tunnels at the Langley Research Center. NASA TM X-1130, 1965.
8. Stallings, Robert L., Jr.; and Lamb, Milton: Effects of Roughness Size on the Position of Boundary-Layer Transition and on the Aerodynamic Characteristics of a 55° Swept Delta Wing at Supersonic Speeds. NASA TP-1027, 1977.
9. Spahr, J. Richard; and Dickey, Robert R.: Wind-Tunnel Investigation of the Vortex Wake and Downwash Field Behind Triangular Wings and Wing-Body Combinations at Supersonic Speeds. NACA RM A53D10, 1953.
10. Dillenius, Marnix F. E.; and Nielsen, Jack N.: Prediction of Aerodynamics of Missiles at High Angles of Attack in Supersonic Flow. NEAR TR 99 (Contract No. N00014-74-C-0050); Nielsen Eng. & Res., Inc., Oct. 1975. (Available from DDC as AD A018 680.)
11. Hardy, Samuel R.: Subsonic Wind Tunnel Tests of a Canard-Control Missile Configuration in Pure Rolling Motion. NSWC/DL TR-3615, U.S. Navy, June 1977. (Available from DDC as AD A044 957.)

TABLE I.- SUMMARY OF TEST DATA FROM FREE-ROLLING TAIL CONFIGURATION  
WITH ZERO CONTROL DEFLECTION

M	$\alpha$ , deg	$\phi_C$ , deg	Tail-fin roll rate, rpm <sup>a</sup>		Remarks
			Counterclockwise		
1.70	-1.9	0	115		
	-.8		122		
	0		115		
	1.2		127		
	2.2		97		
	4.4		88		
	6.6		80		
	8.9		0		Stopped rolling
	11.1		0		Aero lockup
	13.5		0		Very small oscillation angle
	↓				
17.9	0				
1.70	-2.0	26.6	108		
	-.5		133		
	-.1		121		
	1.1		127		
	2.1		116		
	4.5		12		Rotated very slowly
	6.6		116		Roll rate apparently increasing with $\alpha$
1.70	-2.4	45	105		
	-.9		112		
	0		123		
	.9		112		
	2.2		124		
	4.4		0		Stopped rolling
	6.5		0		Very small oscillation angle
	8.8		21		Rotated very slowly
	↓				
	17.8		0		Aero lockup
2.16	-1.2	0	120		
	.1		114		
	1.0		112		
	2.2		110		
	3.3		96		
	5.5		75		
	7.7		0		Stopped rolling; aero lockup
	↓				
	24.7		0		

<sup>a</sup>When viewed from the rear.

TABLE I.- Continued

M	$\alpha$ , deg	$\phi_C$ , deg	Tail-fin roll rate, rpm <sup>a</sup>		Remarks
			Counterclockwise		
2.16	-1.0	26.4	121		Stopped rolling Roll rate apparently increasing with $\alpha$
	-.1		122		
	.9		130		
	2.1		107		
	3.2		96		
	5.4		0		
	7.5		0		
	7.8		199		
2.16	-1.4	45	100		Stopped rolling Started rolling Roll rate increasing with $\alpha$
	-.1		104		
	1.0		99		
	2.1		100		
	3.2		87		
	5.4		0		
	7.5		0		
	9.9		114		
	12.0		128		
	14.1		195		
2.36	-1.5	0	143		Stopped rolling; aero lockup Large oscillation angle
	-.2		129		
	.9		83		
	2.0		78		
	2.9		72		
	5.2		37		
	7.3		27		
	9.6		0		
	↓				
	23.7		0		
2.36	-1.5	26.6	80		Stopped rolling Roll rate apparently increasing with $\alpha$
	0		94		
	.9		98		
	2.0		61		
	3.1		0		
	5.3		0		
	7.4		194		

<sup>a</sup>When viewed from the rear.



TABLE I.- Continued

M	$\alpha$ , deg	$\phi_C$ , deg	Tail-fin roll rate, rpm <sup>a</sup>		Remarks
			Counterclockwise		
2.36	-1.0	45	56		Stopped rolling Started rolling Roll rate increasing with $\alpha$
	.3		70		
	1.3		100		
	2.4		56		
	3.5		54		
	5.6		0		
	7.7		33		
	9.9		118		
	12.0		161		
	14.4		167		
	16.5		122		
	18.7		0		
↓					
23.8	0		Stopped rolling; aero lockup		
2.86	-2.9	0	23		Low roll rates  Stopped rolling; aero lockup
	-1.6		71		
	-.5		64		
	.7		62		
	1.8		36		
	3.8		0		
	↓				
	22.0		0		
2.86	-2.8	26.5	33		Oscillated; 2 or 3 revolutions Started rolling Stopped rolling  Started rolling Stopped rolling Roll rate apparently increasing with $\alpha$
	-1.5		49		
	-.6		51		
	.6		0		
	1.8		50		
	3.7		0		
	5.9		0		
	8.0		131		
	10.0		0		
11.5	230				

<sup>a</sup>When viewed from the rear.

TABLE I.- Concluded

M	$\alpha$ , deg	$\phi_C$ , deg	Tail-fin roll rate, rpm <sup>a</sup>		Remarks
			Counterclockwise		
2.86	-2.5	45		27	Low roll rates
	-1.5		51		
	-.5		93		
	.7		50		
	1.7		0	Stopped rolling	
	3.9		0	Small oscillation angle	
	5.9		0		
	8.1		75	Started rolling	
	10.3		120	Steady rolling	
	12.6		124		
	14.6		0	Stopped rolling	
	17.0		0		
	19.1		0		
	20.2		157	Started rolling	

<sup>a</sup>When viewed from the rear.

TABLE II.- SUMMARY OF TEST DATA FROM FREE-ROLLING TAIL CONFIGURATION  
WITH CANARD OFF

M	$\alpha$ , deg	$\phi_C$ , deg	Tail-fin roll rate, rpm <sup>a</sup>		Remarks
			Clockwise		
1.70	-2.0	0	54	Very low roll rates	
	-.9		37		
	0		39		
	1.0		46		
	2.1		47		
	4.0		31		
	6.0		31		
	8.0		0		Stopped and started to roll
	10.0		0		
	12.1		30		
	14.2		28		Aero lockup
	16.4		26		
	2.16		-1.6		0
-.9		34			
-.1		31			
1.0		47			
2.0		20			
3.0		30			
5.0		23			
7.0		0	Stopped rolling		
9.1		0	Stopped; started for several revolutions at a very slow rate		
11.3		0	Stopped; started; oscillated		
13.4		26	Rolled hesitantly and irregularly		
↓					
23.2		27			

<sup>a</sup>When viewed from the rear.

TABLE II.- Concluded

M	$\alpha$ , deg	$\phi_c$ , deg	Tail-fin roll rate, rpm <sup>a</sup>		Remarks
			Clockwise		
2.36	-1.2	0	74	Low roll rates	
	-.3		47		
	.8		86		
	1.8		52		
	2.8		102		
	4.9		88		
	6.9		45		
	9.0		0		
	↓				
	23.0		42		
2.86	-2.5	0	39	Low roll rates	
	↓				
	5.6		28		
	7.8		0		
	9.8		0		
	↓				
21.6	0				
				Stopped; started; and oscillated Rolled hesitantly and irregularly	
				Stopped rolling Oscillated through small angle	

<sup>a</sup>When viewed from the rear.

TABLE III.- SUMMARY OF TEST DATA FROM FREE-ROLLING TAIL CONFIGURATION  
 WITH TWO CANARDS DIFFERENTIALLY DEFLECTED  $0.5^\circ$   
 EACH FOR NEGATIVE ROLL CONTROL

M	$\alpha$ , deg	$\phi_C$ , deg	Tail-fin roll rate, rpm <sup>a</sup>		Remarks
			Clockwise		
1.70	-2.2	0	98		
	-1.1		96		
	0		90		
	1.2		100		
	2.4		114		
	4.5		123		
	6.6		131		
	8.9		97		
	11.1		0		Stopped rolling; aero lockup
	↓				
17.9	0		Small oscillation angle		
1.70	-2.3	45	102		
	-1.3		81		
	-.1		83		
	1.3		105		
	2.2		104		
	4.3		128		
	↓				
	10.8		207		Roll rate increasing with $\alpha$ ; $\alpha > 11^\circ$ ; rpm > 500
2.16	-1.2	0	93		
	0		97		
	1.1		109		
	2.2		122		
	3.3		136		
	5.5		154		
	7.6		164		Steady rolling
	↓				
	16.7		138		
	18.9		0		Stopped rolling; aero lockup
↓					
24.8	0				

<sup>a</sup>When viewed from the rear.

TABLE III.- Continued

M	$\alpha$ , deg	$\phi_C$ , deg	Tail-fin roll rate, rpm <sup>a</sup>		Remarks			
			Clockwise					
2.16	-1.3	45	82		Steady rolling			
	0		84					
	1.0		95					
	2.1		95					
	3.3		104					
	5.4		150					
	7.6		207					
	↓							
	12.0		151					
	14.3		0					
	↓							
	24.5		0					
2.36	-1.3	0	109		Stopped rolling; aero lockup			
	-.1		121					
	.8		103					
	2.0		95					
	3.1		147					
	5.2		123					
	7.3		110					
	9.6		0					
	↓							
	24.4		0					
	2.36		-1.0	45		88		Stopped rolling; aero lockup
			.4			71		
1.3		105						
2.3		93						
3.4		108						
5.6		168						
7.8		178						
10.0		156						
12.2		0						
↓								
24.2		0						

<sup>a</sup>When viewed from the rear.

TABLE III.- Concluded

M	$\alpha$ , deg	$\phi_C$ , deg	Tail-fin roll rate, rpm <sup>a</sup>		Remarks
				Clockwise	
2.86	-2.7	0		51	
	-1.5		67		
	-.4		87		
	.7		104		
	2.1		80		
	3.8		99		
	5.9		123	Steady rolling	
	↓				
	14.7		133		
	17.0		0	Stopped rolling; aero lockup	
	↓				
22.6	0				
2.86	-2.6	45		84	Low roll rates
	-1.5		58		
	-.5		65		
	.6		71		
	1.7		73		
	3.8		105	Steady rolling	
	↓				
	10.3		42		
	12.5		0	Stopped rolling; aero lockup	
	↓				
22.5	0				

<sup>a</sup>When viewed from the rear.

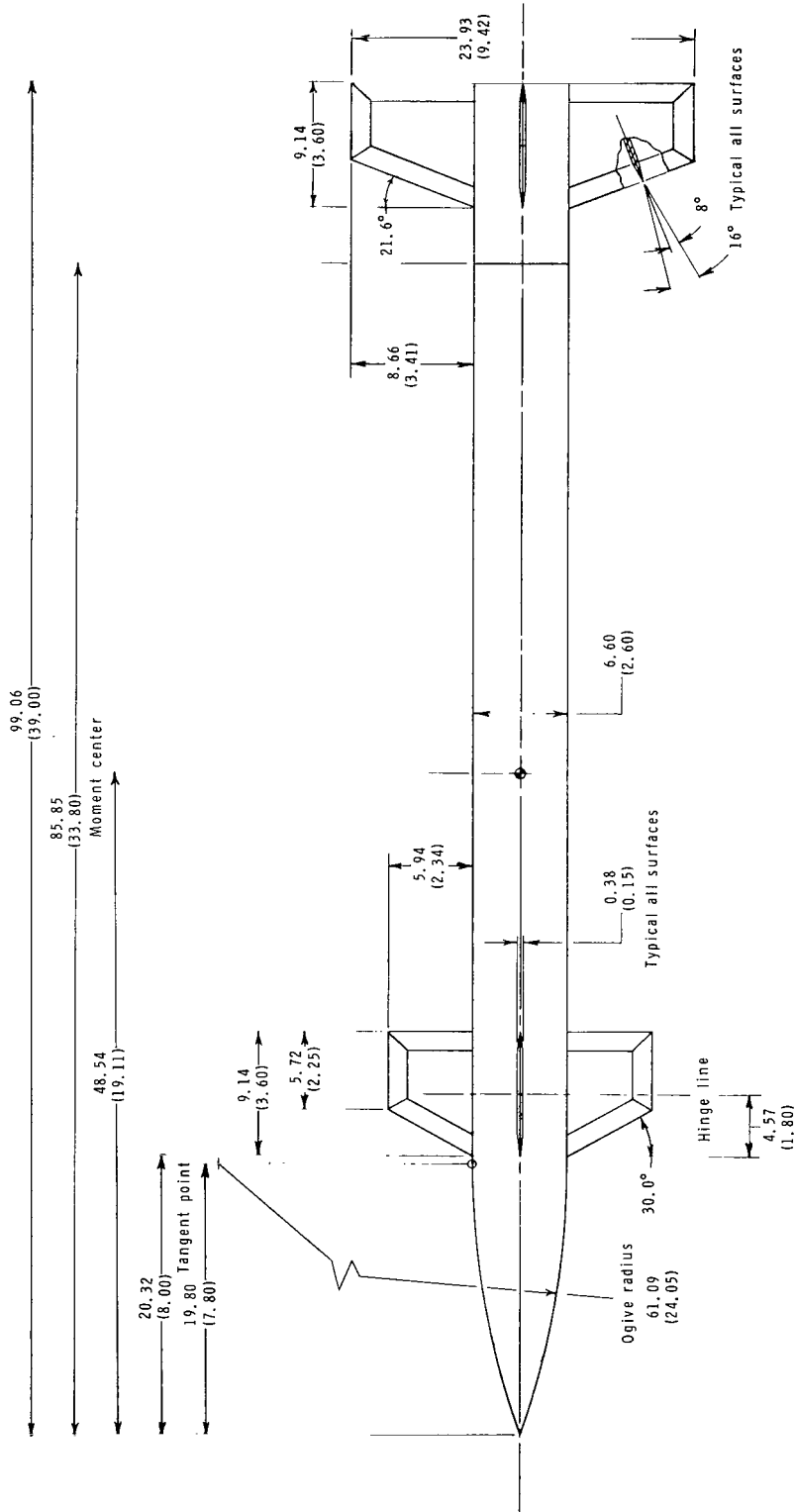
TABLE IV.- SUMMARY OF TEST DATA FROM FREE-ROLLING TAIL CONFIGURATION

WITH VERTICAL CANARDS DEFLECTED 5° FOR POSITIVE YAW CONTROL

M	$\alpha$ , deg	$\phi_C$ , deg	Tail-fin roll rate, rpm <sup>a</sup>		Remarks
			Clockwise	Counterclockwise	
1.70	-2.2	0	360		Roll direction changed Roll rate increasing with $\alpha$ Excessive roll rate
	-1.1		134		
	0			80	
	1.0			314	
	2.1			463	
2.16	-1.3	0	152		Low roll rate  Excessive roll rate
	0			53	
	1.1			240	
	2.2			430	
	3.3			517	
2.36	-1.3	0	191		Very low roll rate both directions Roll rate increasing with $\alpha$  Excessive roll rate
	-.2			36	
	.9			187	
	2.0			360	
	3.0			500	
2.86	6.7		590		
	-2.7	0	351		Roll direction changed Roll rate increasing with $\alpha$  Stopped rolling; "stable" aero lockup
	-1.5		177		
	-.5		55		
	.6			84	
	1.7			206	
	3.9			439	
	5.8			527	
	8.3			507	
	10.3			354	
	12.5			94	
14.1			0		
↓					
22.7		0			

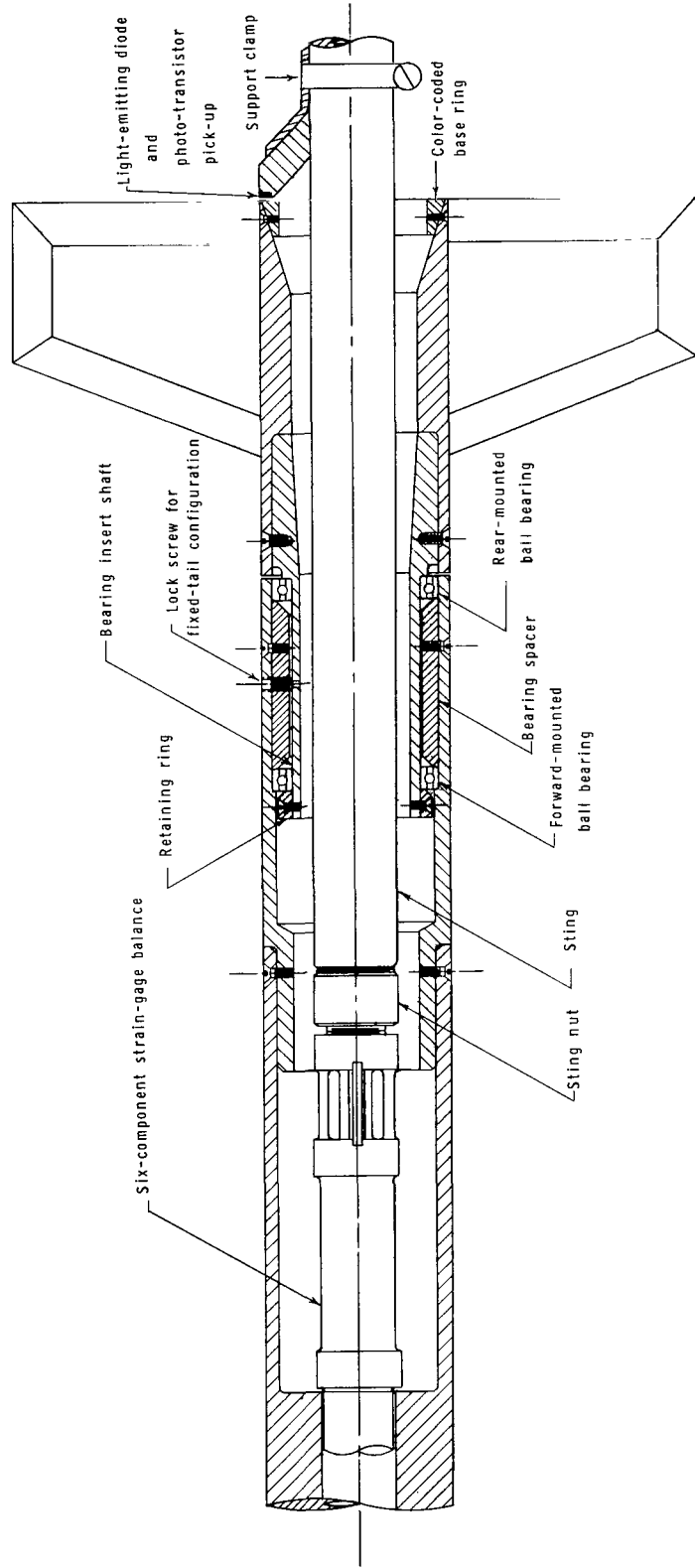
<sup>a</sup>When viewed from the rear.





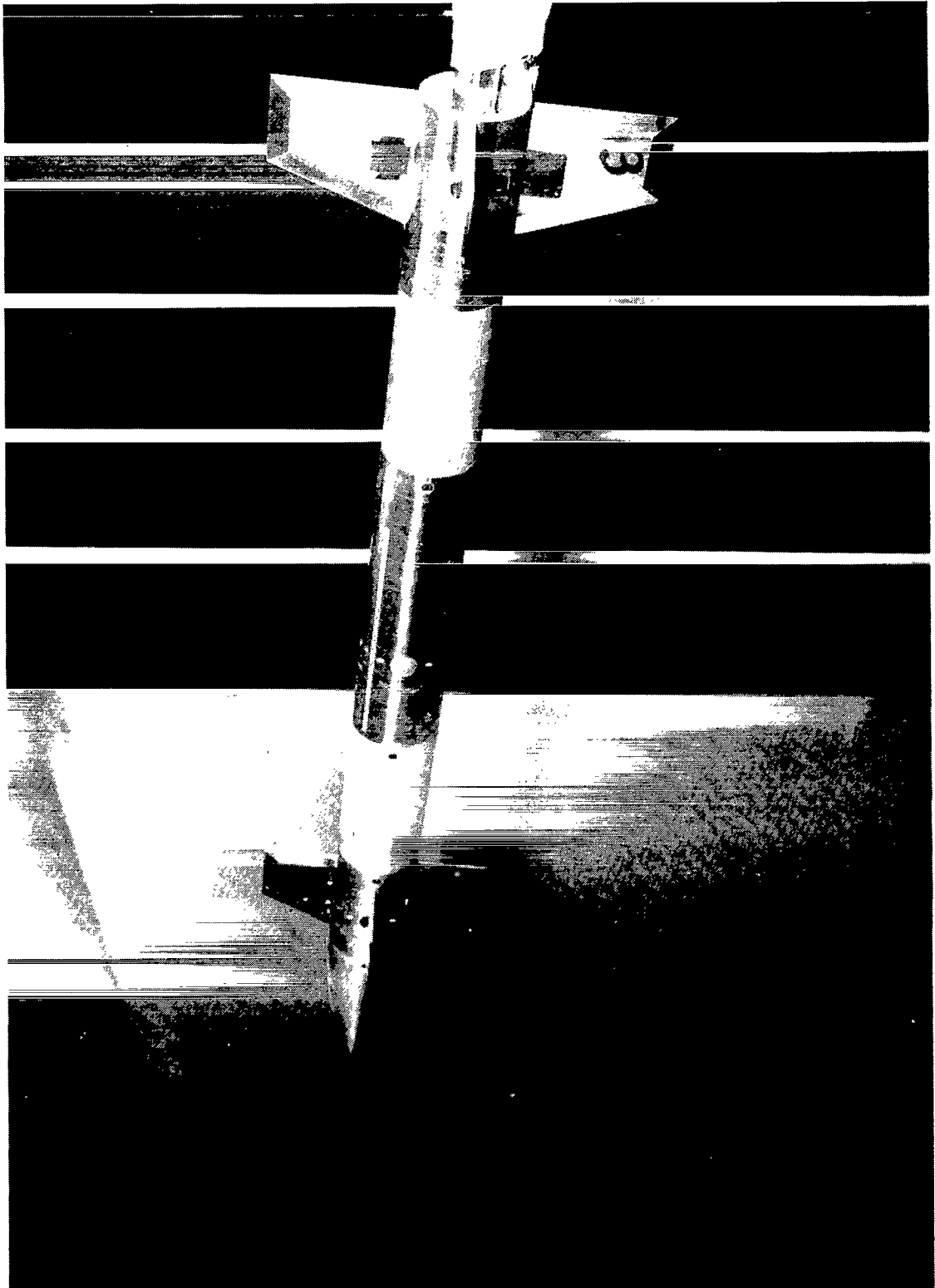
(a) Complete model.

Figure 1.- Model details. All dimensions are in centimeters (inches) unless otherwise indicated.



(b) Ball-bearing spindle assembly and sting support.

Figure 1.- Concluded.



L-76-3409

Figure 2.- Model.

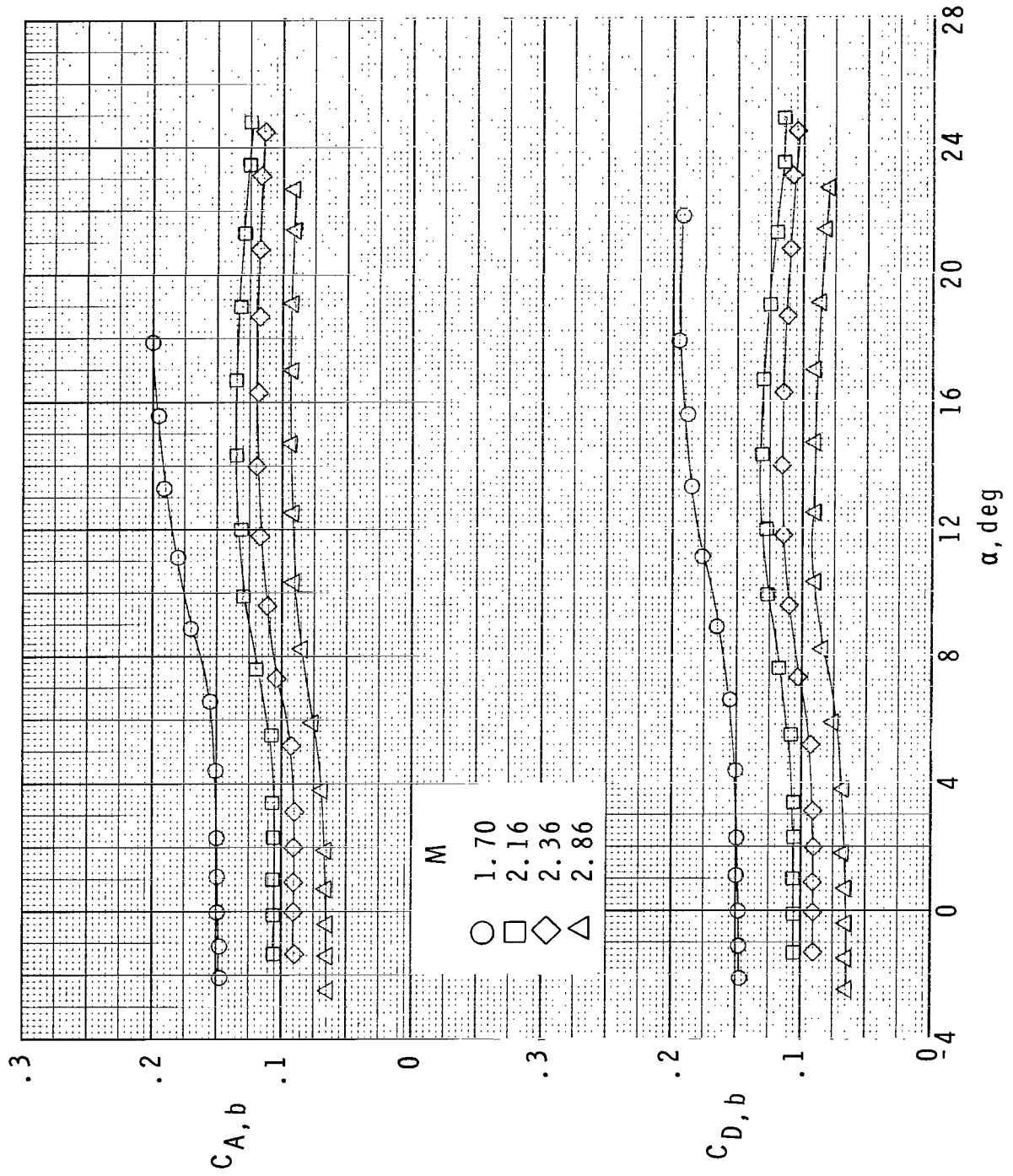
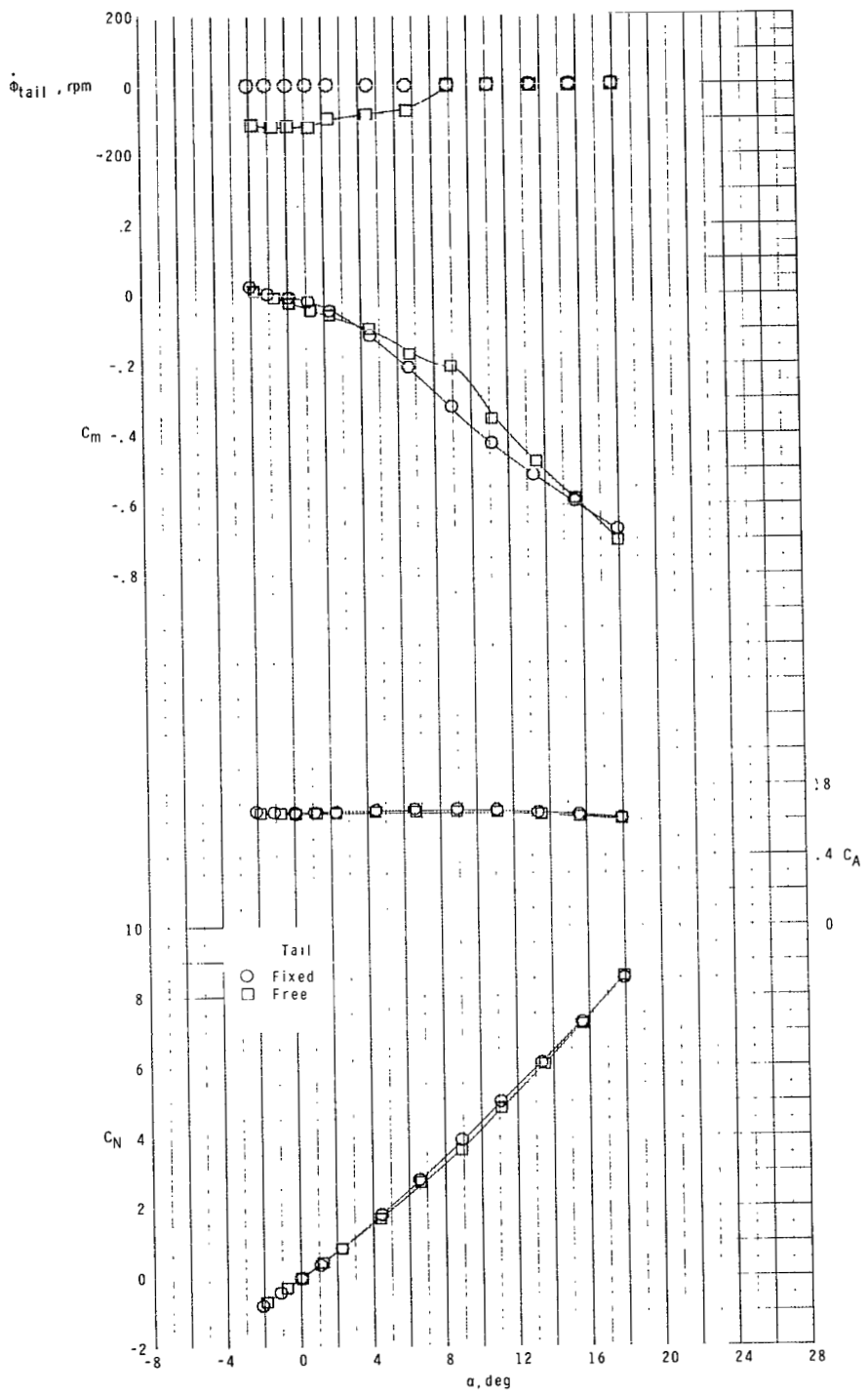
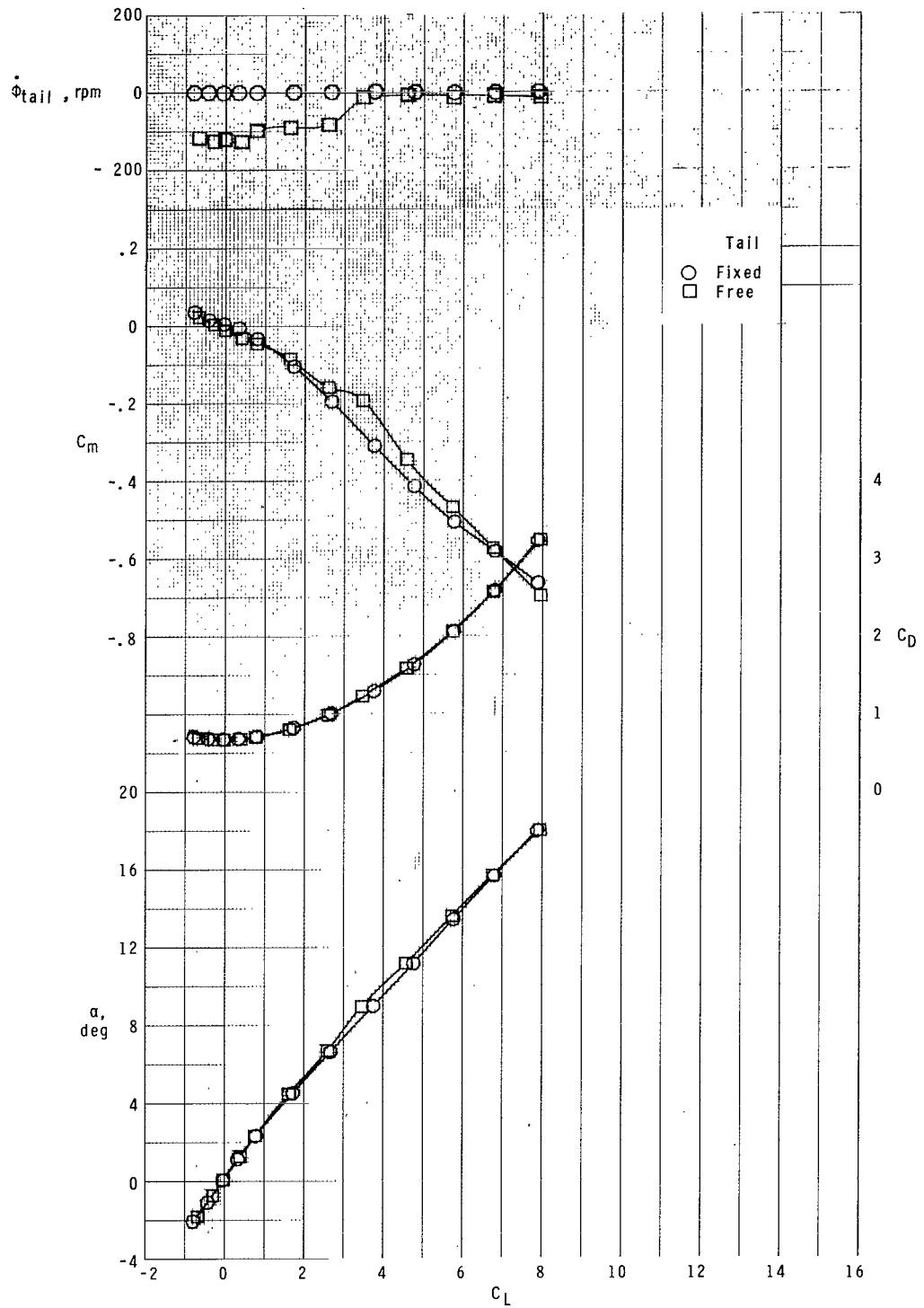


Figure 3.- Typical variation of measured  $C_{A,b}$  and  $C_{D,b}$  with angle of attack.



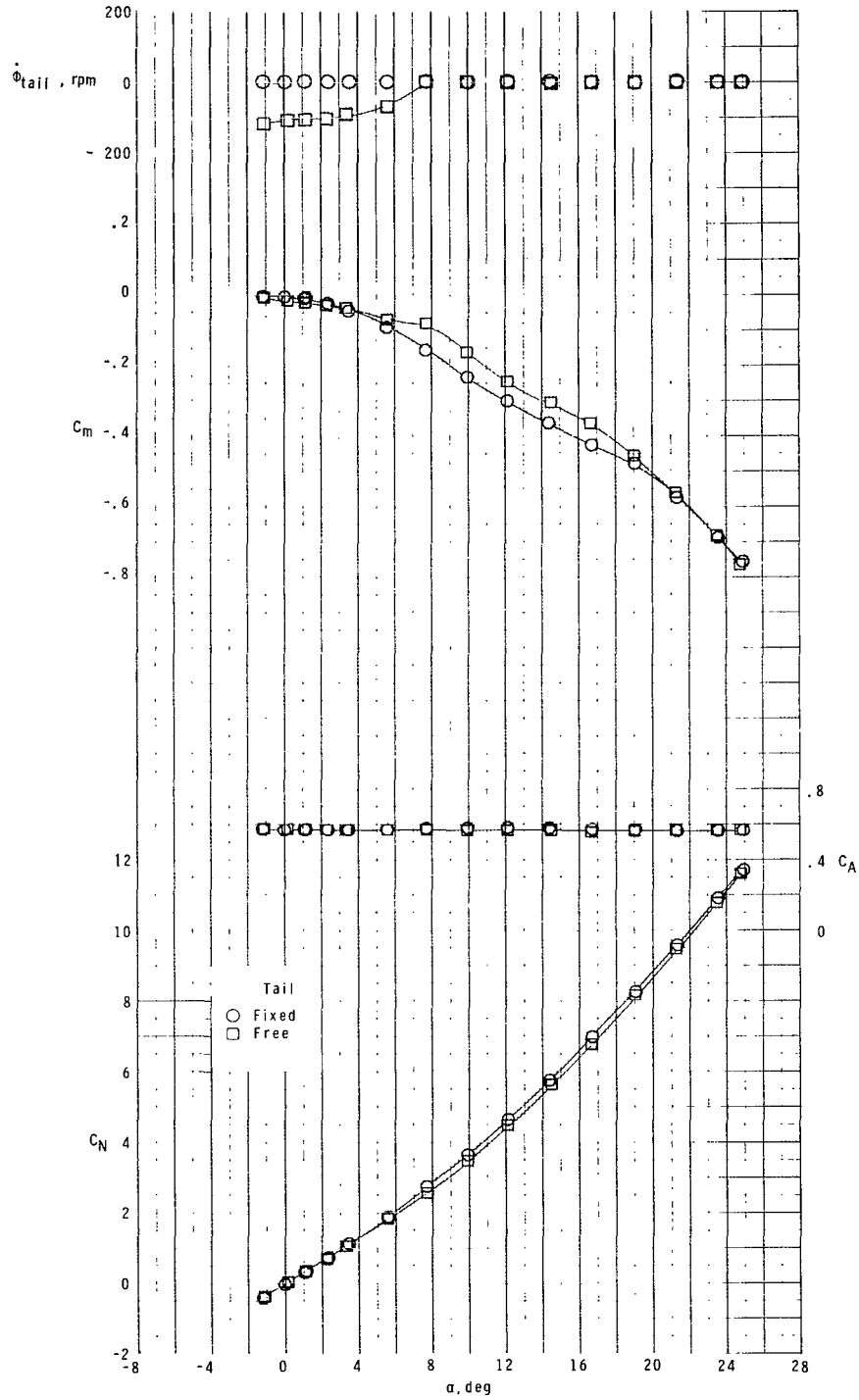
(a)  $M = 1.70$ .

Figure 4.- Effect of free-rolling tail on longitudinal aerodynamic characteristics of model with zero control deflection at  $\phi_C = 0^\circ$ .



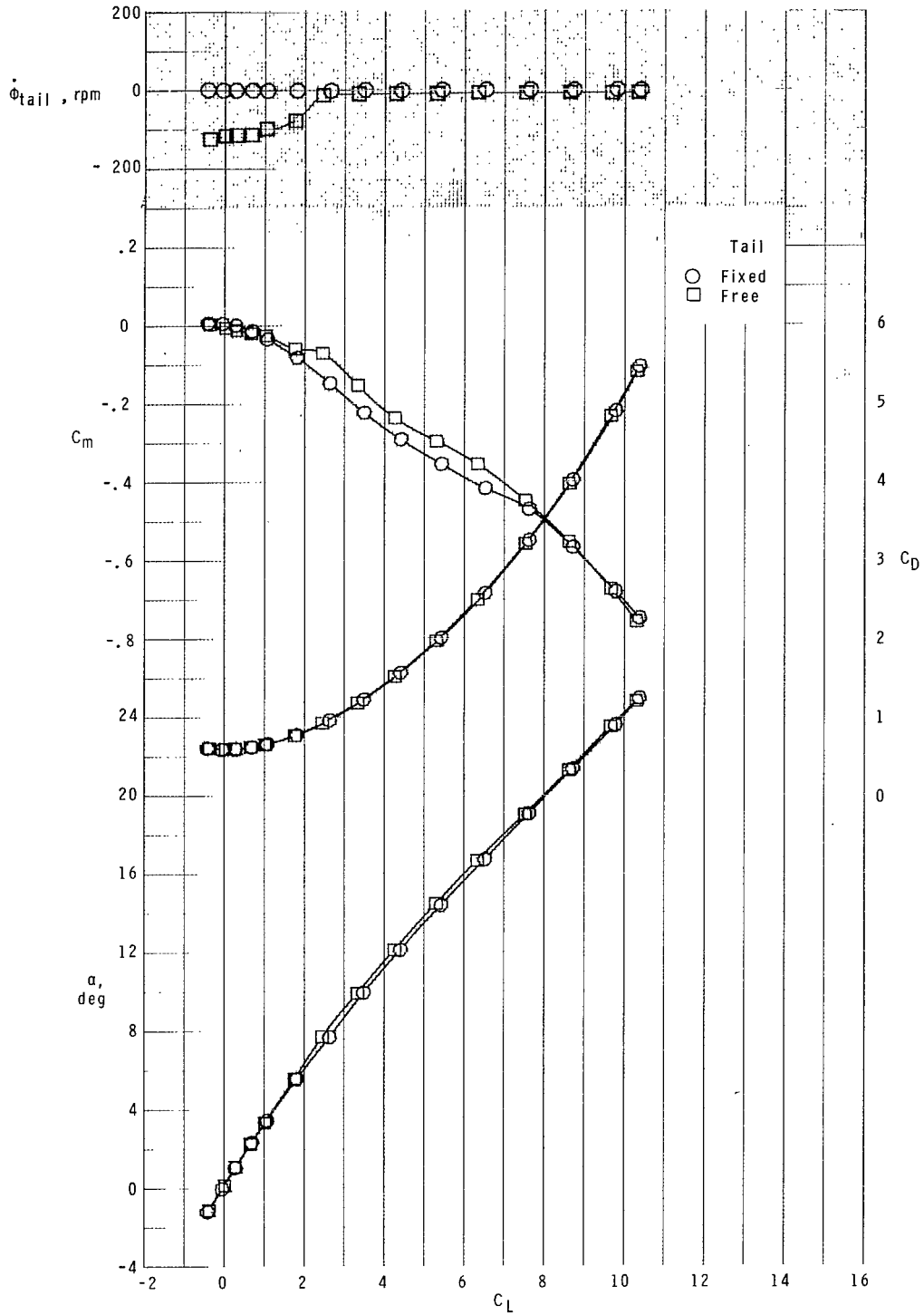
(a) Concluded.

Figure 4.- Continued.



(b)  $M = 2.16$ .

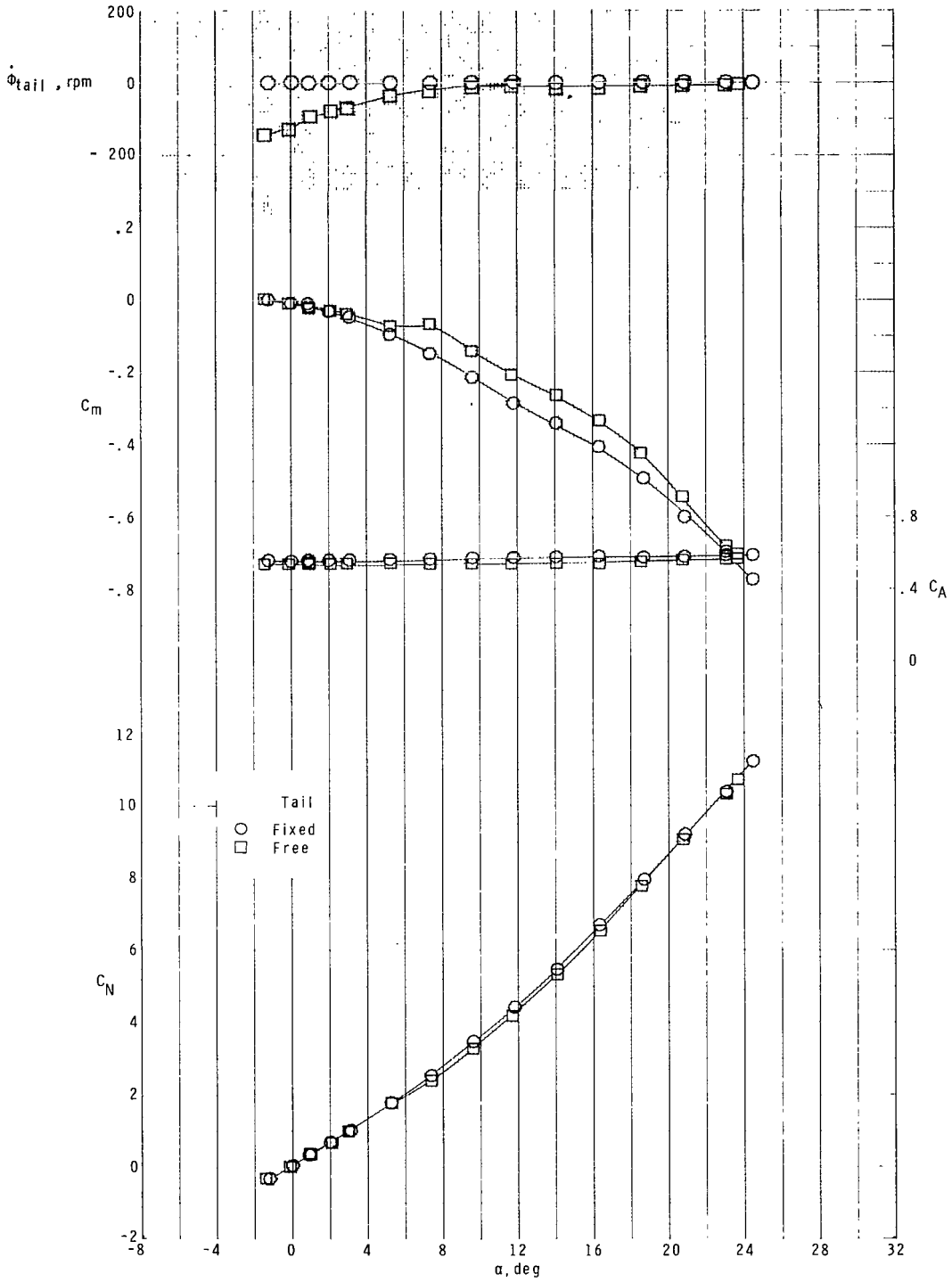
Figure 4.- Continued.



(b) Concluded.

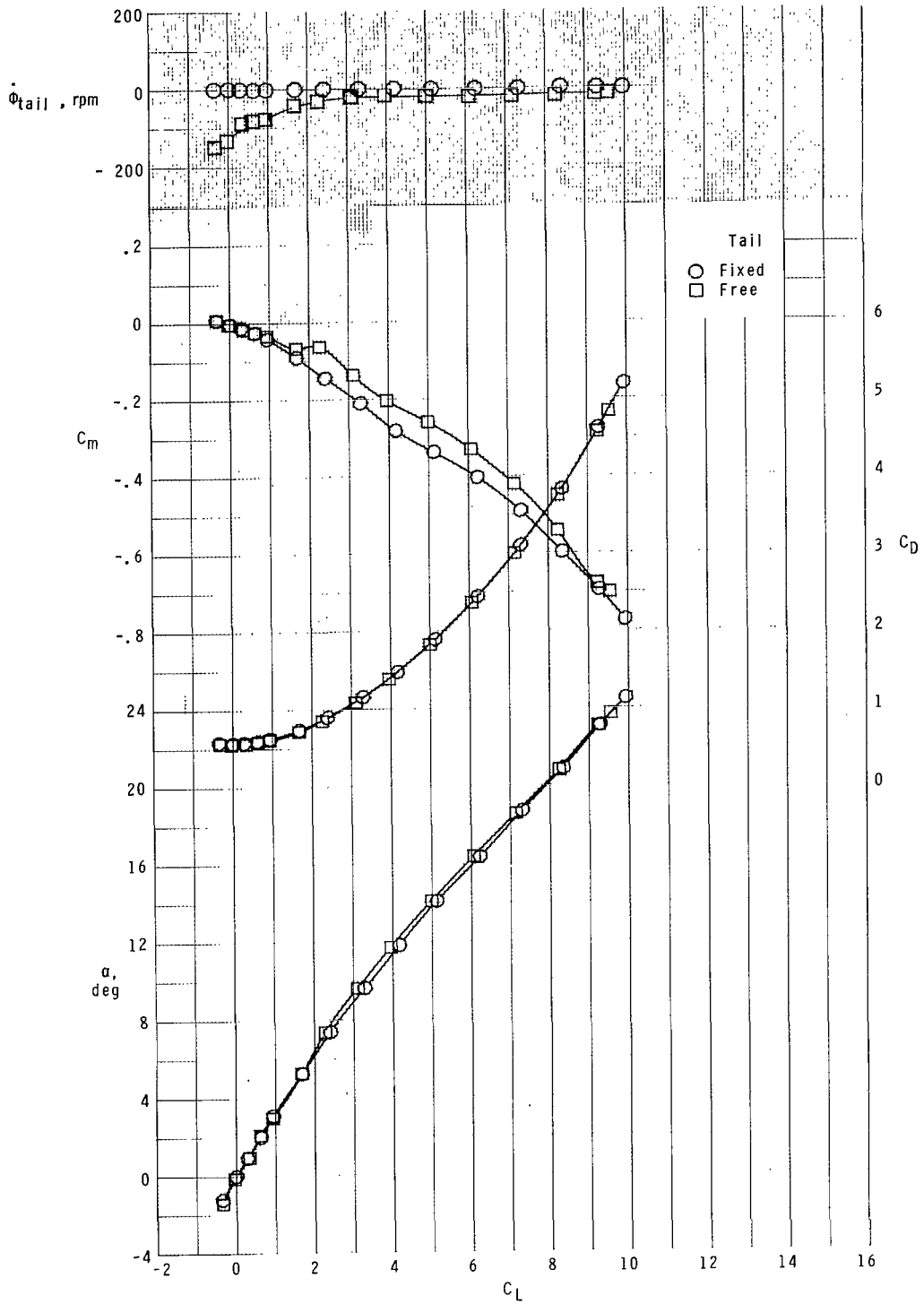
Figure 4.- Continued.





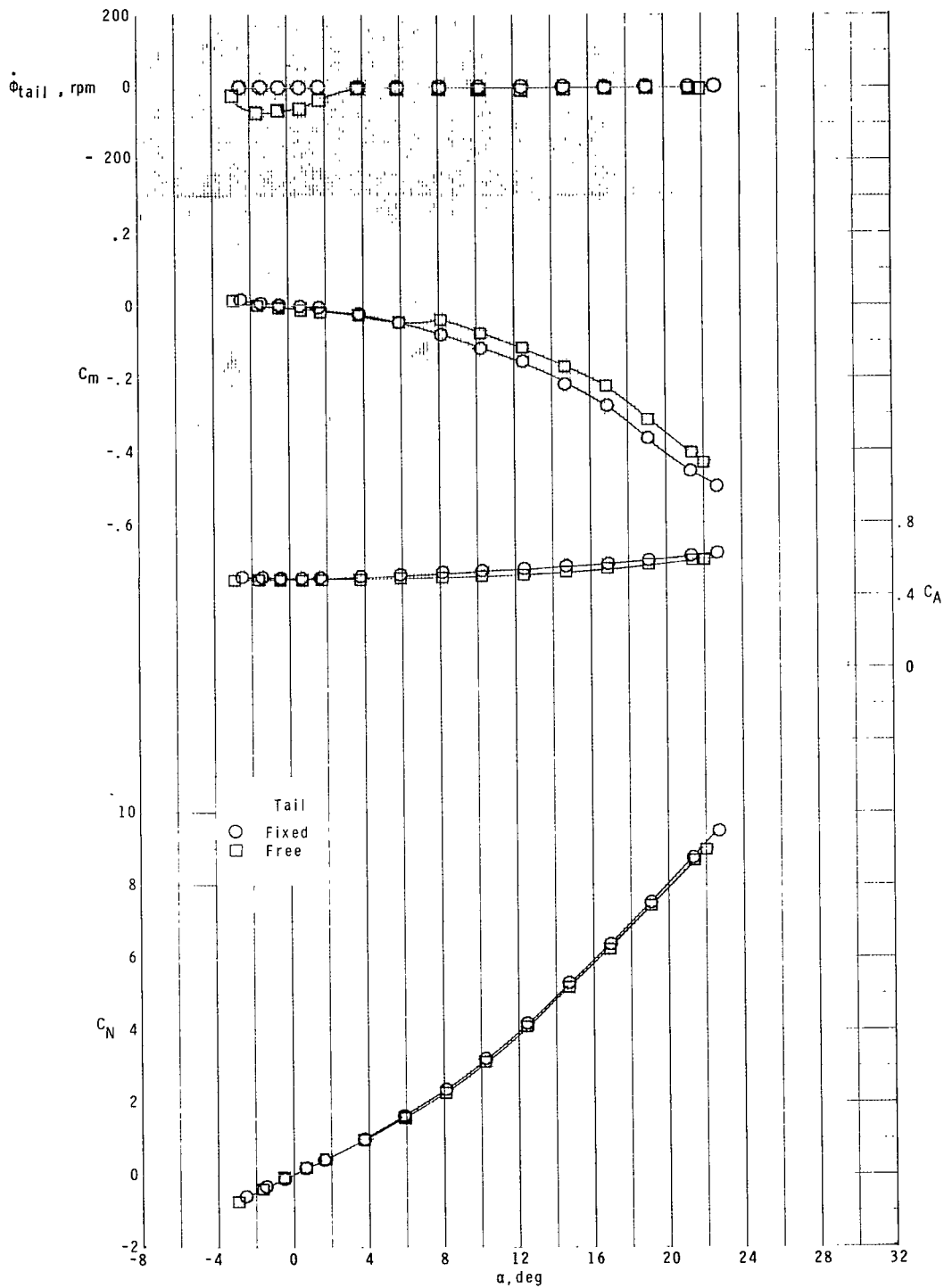
(c)  $M = 2.36$ .

Figure 4.- Continued.



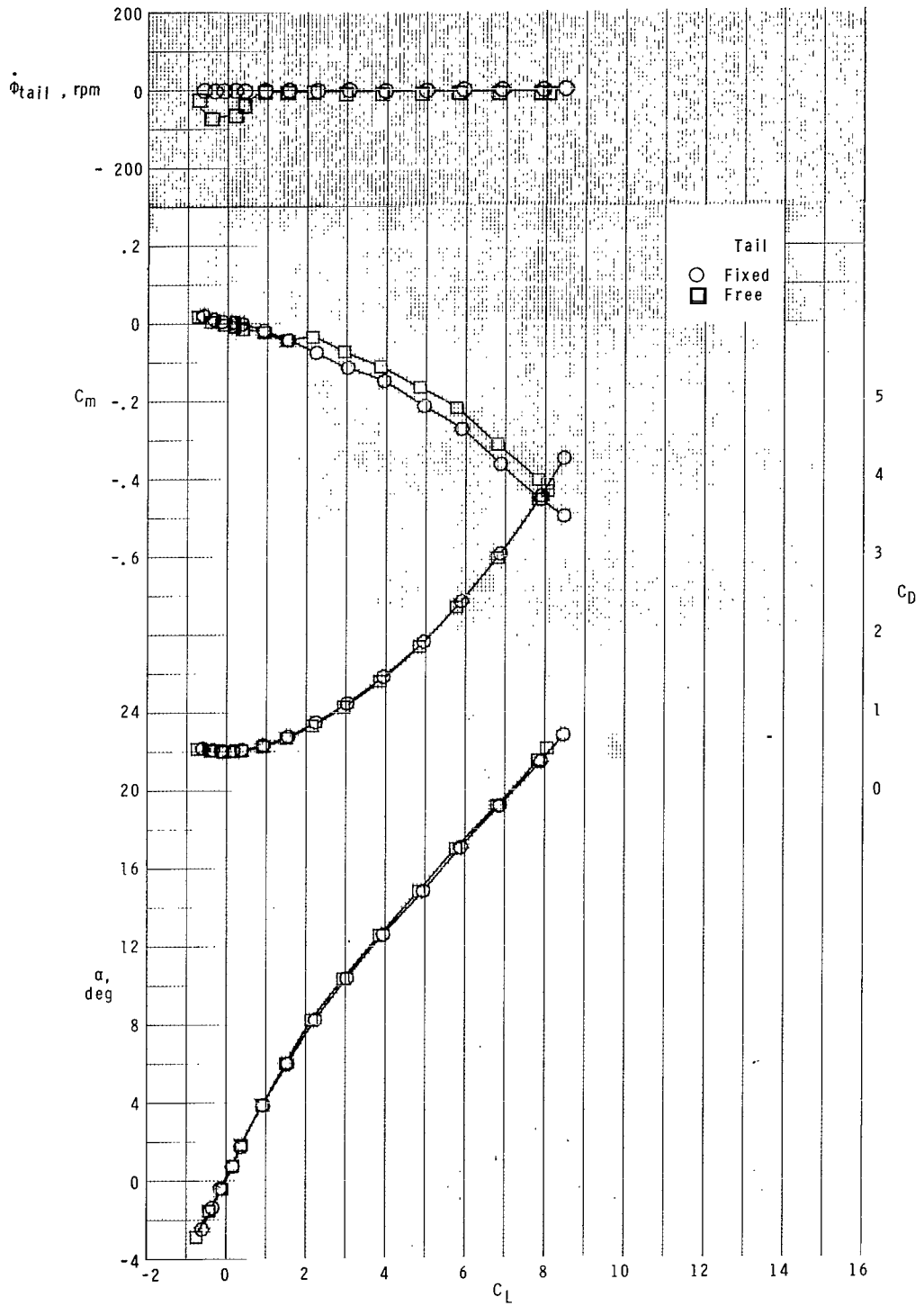
(c) Concluded.

Figure 4.- Continued.



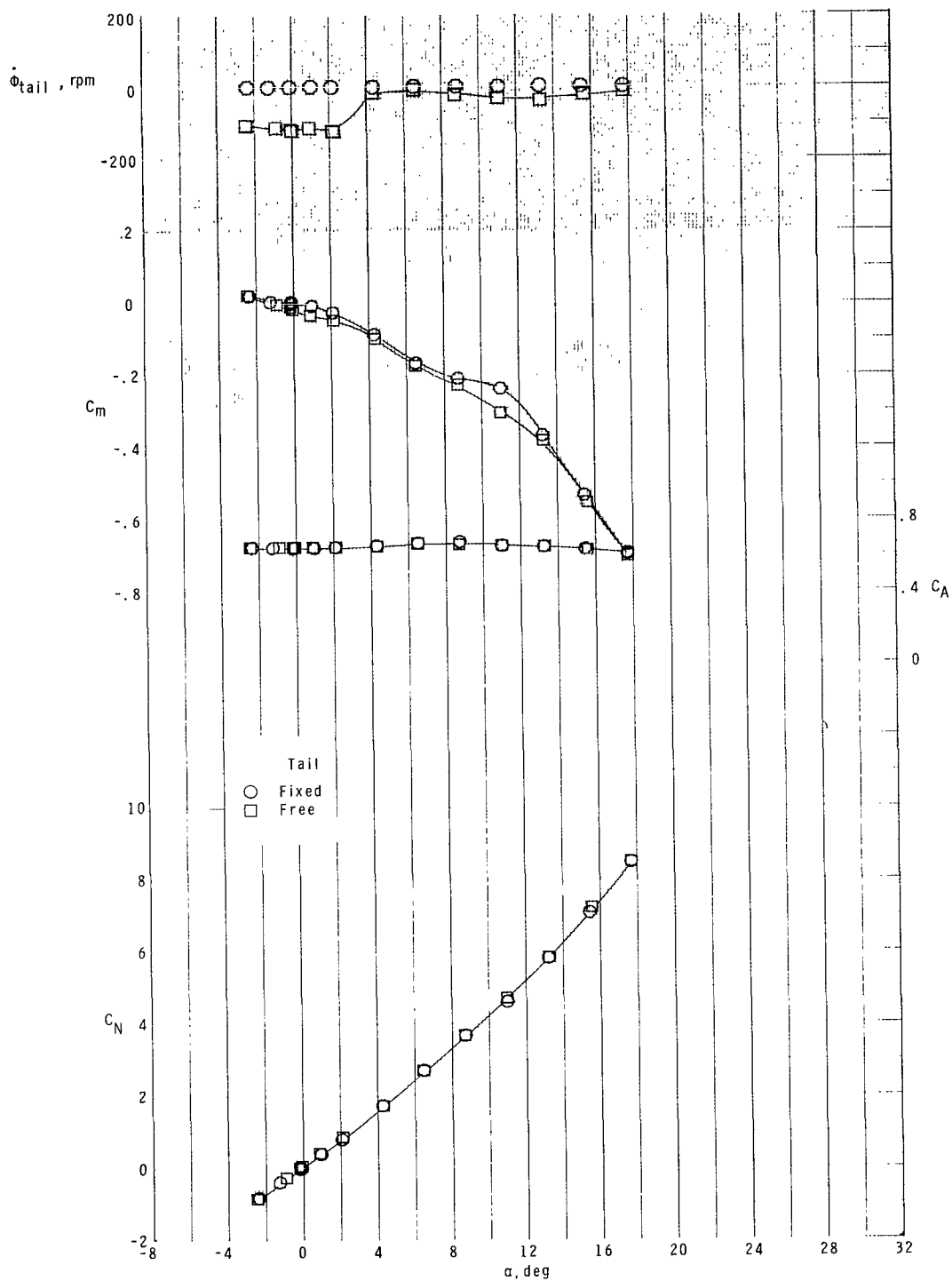
(d)  $M = 2.86$ .

Figure 4.- Continued.



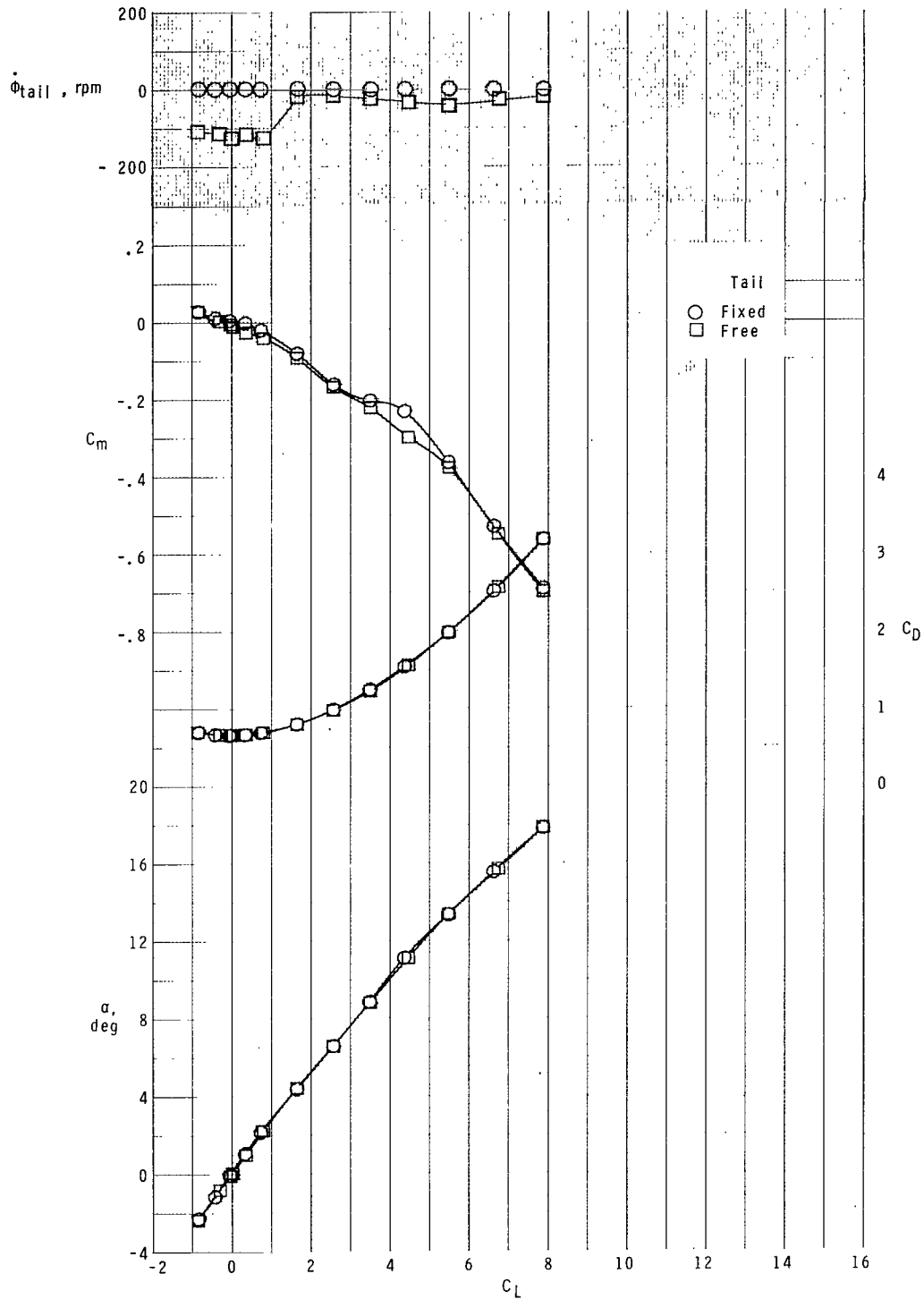
(d) Concluded.

Figure 4.- Concluded.



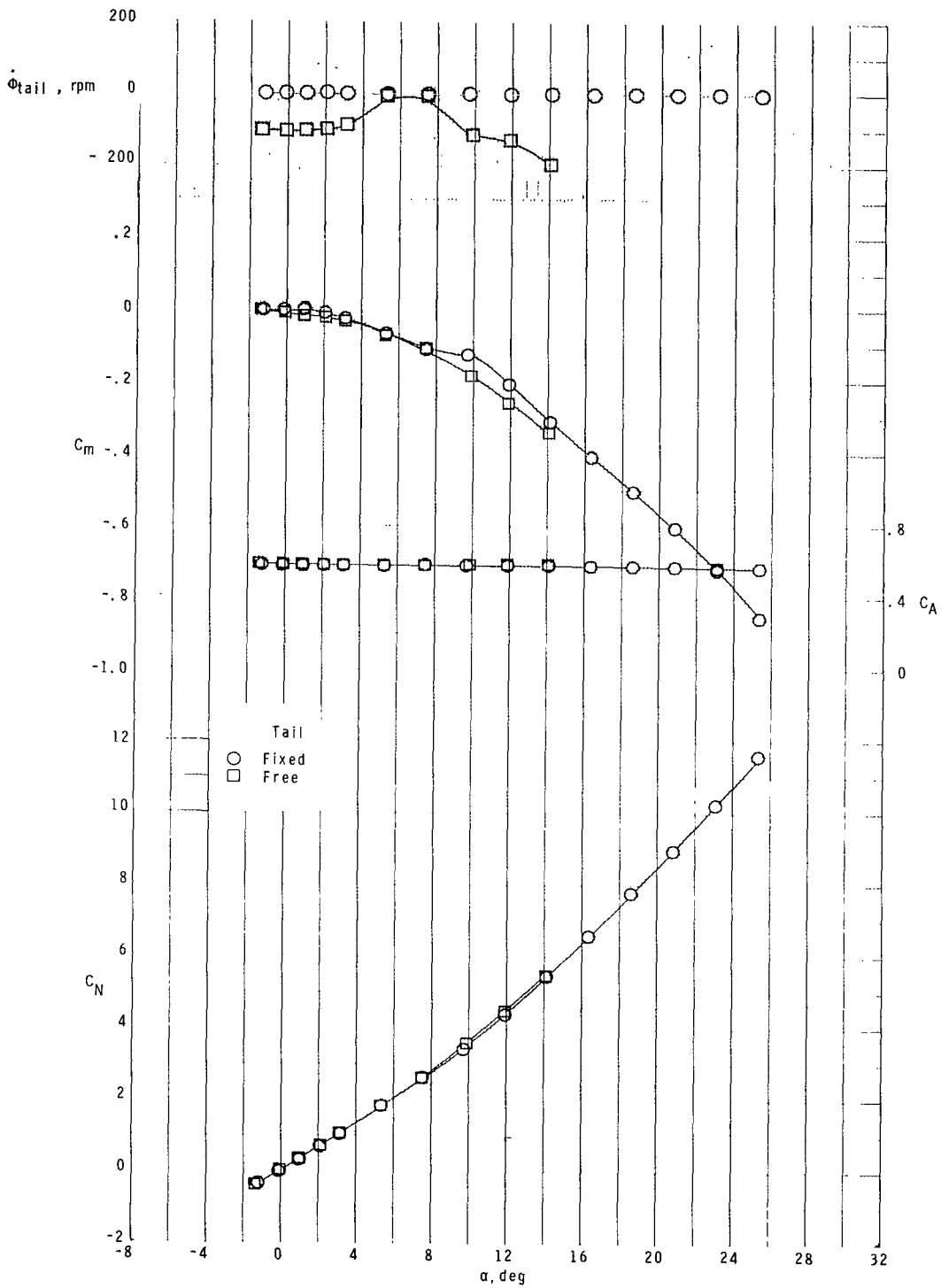
(a)  $M = 1.70$ .

Figure 5.- Effect of free-rolling tail on longitudinal aerodynamic characteristics of model with zero control deflection at  $\phi_C = 45^\circ$ .



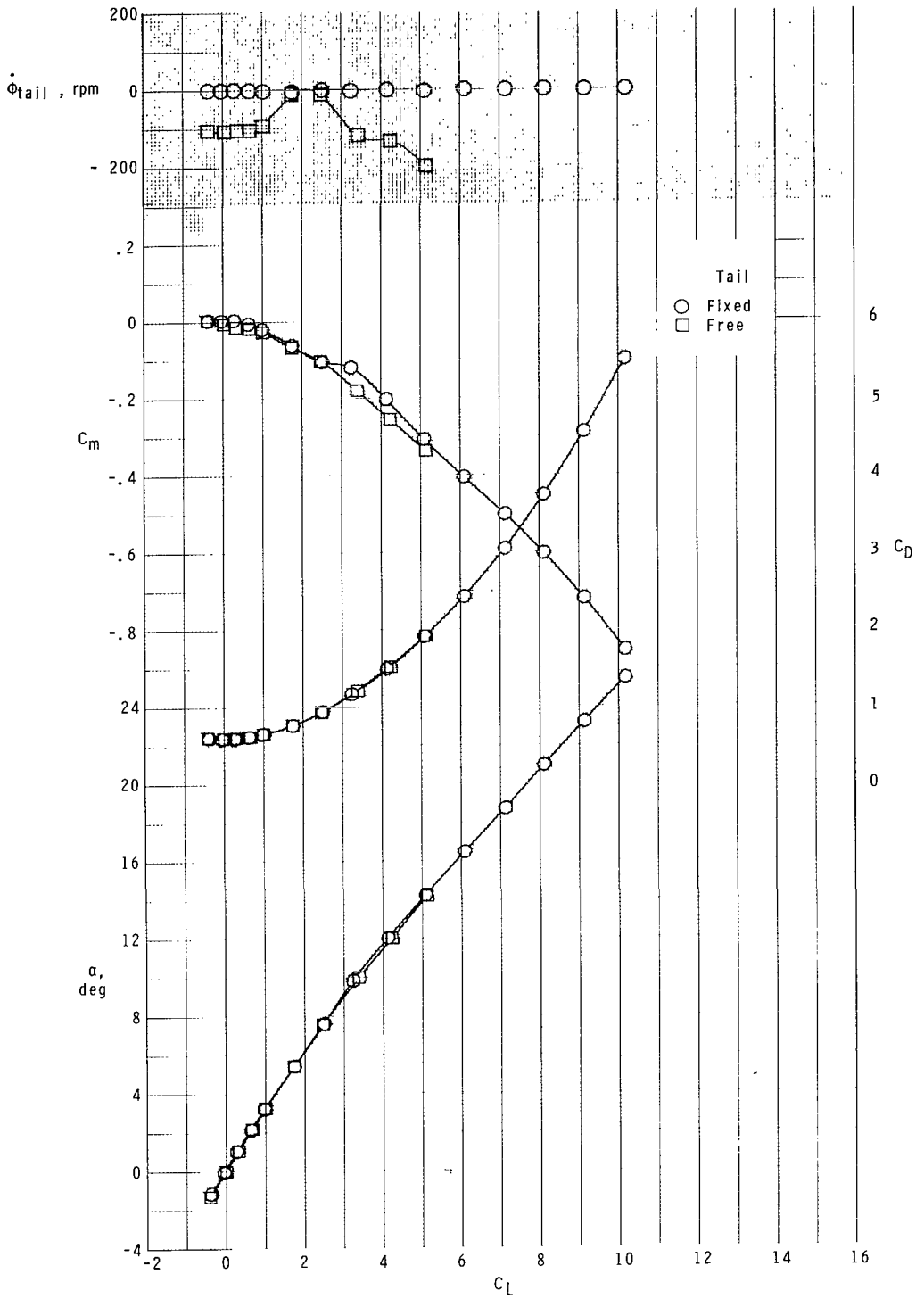
(a) Concluded.

Figure 5.- Continued.



(b)  $M = 2.16$ .

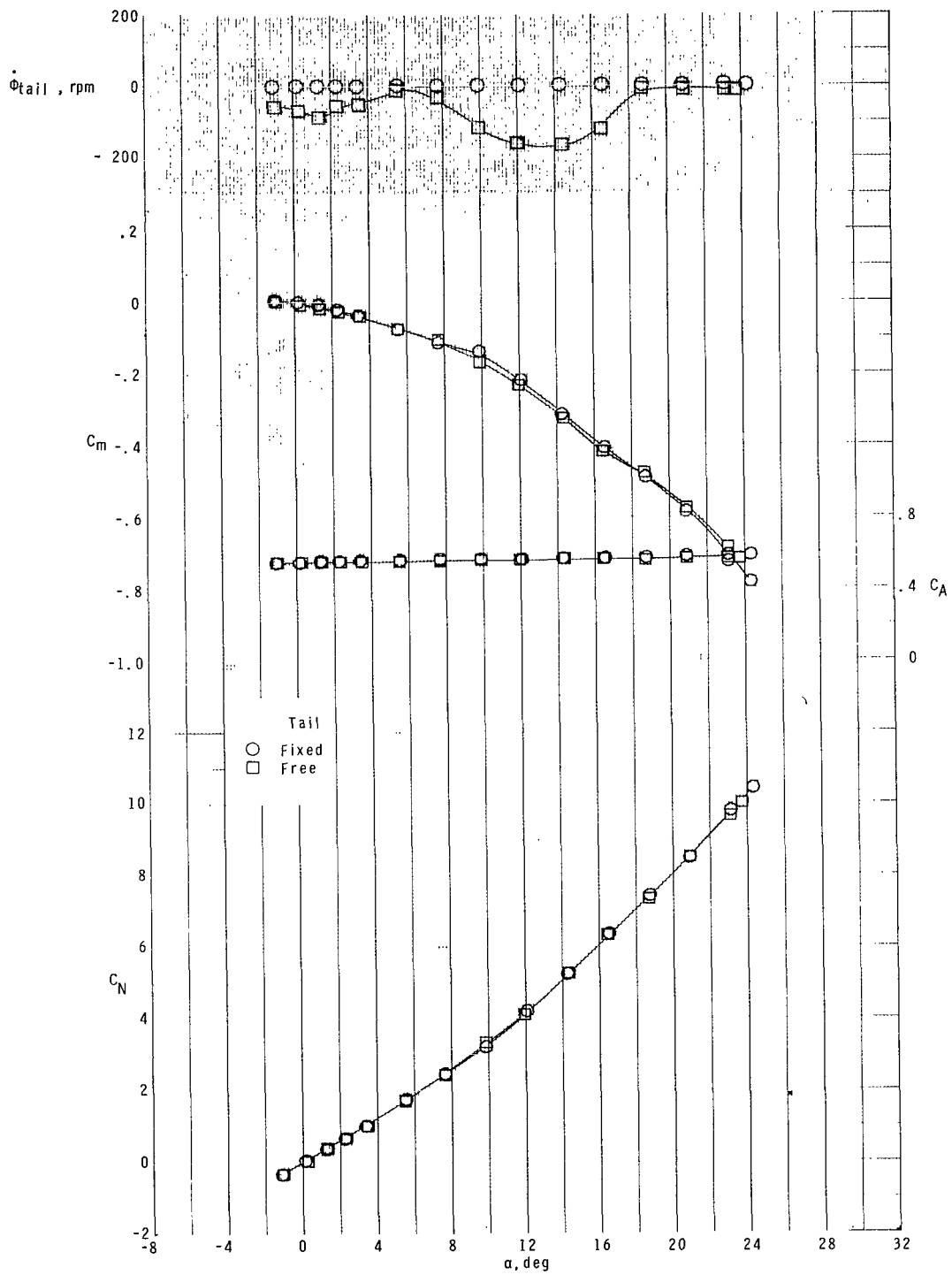
Figure 5.- Continued.



(b) Concluded.

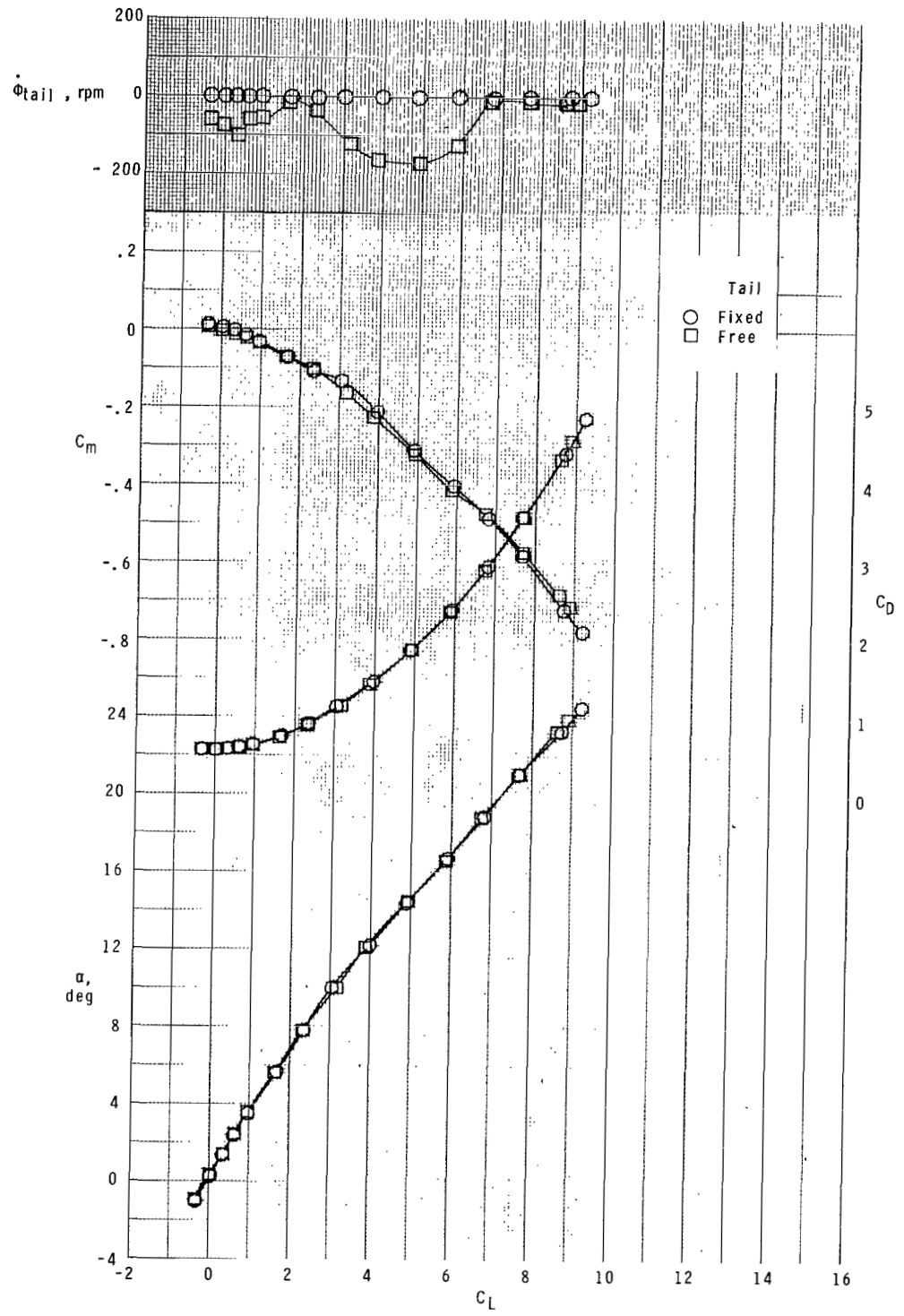
Figure 5.- Continued.





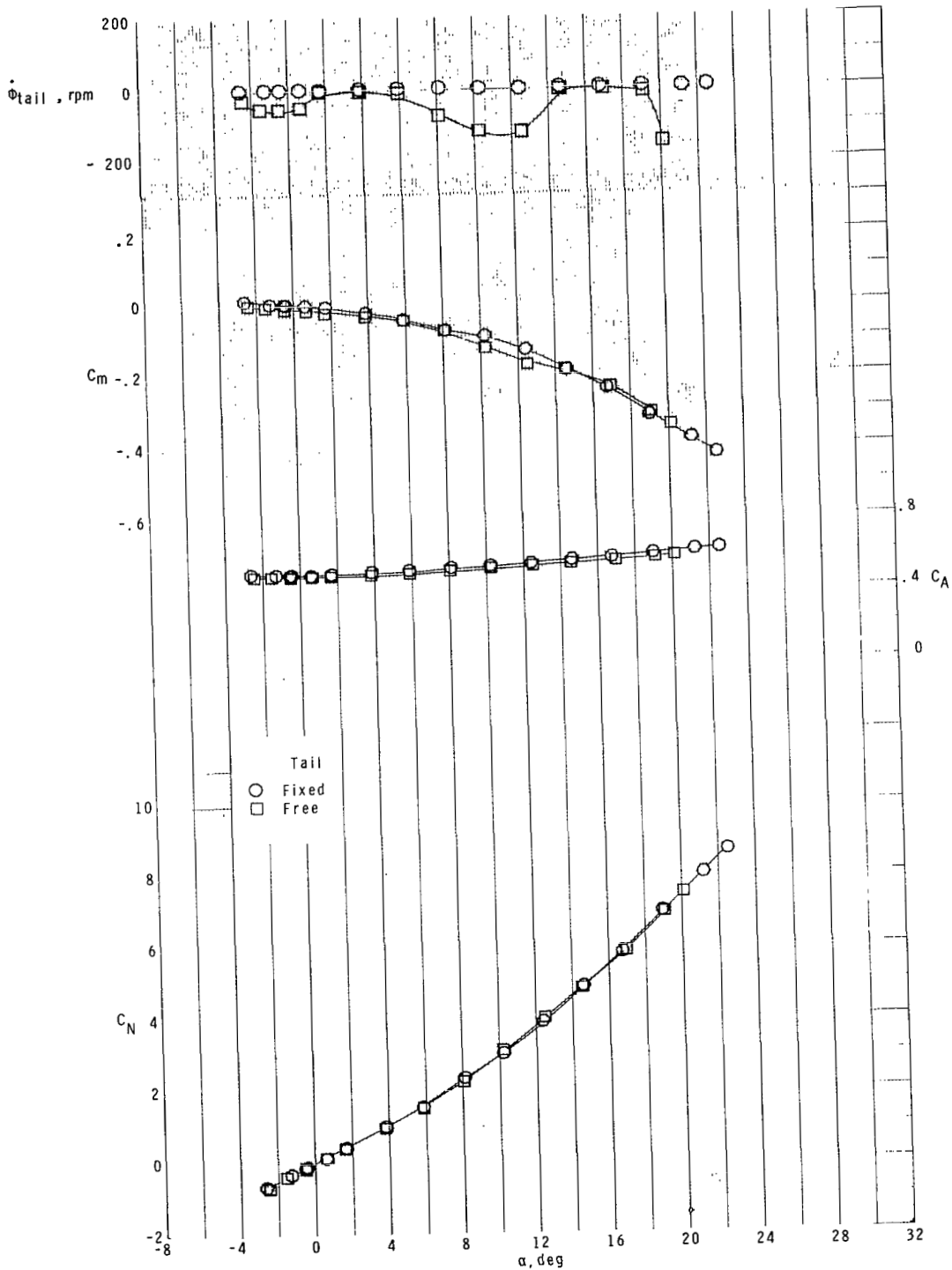
(c)  $M = 2.36$ .

Figure 5.- Continued.



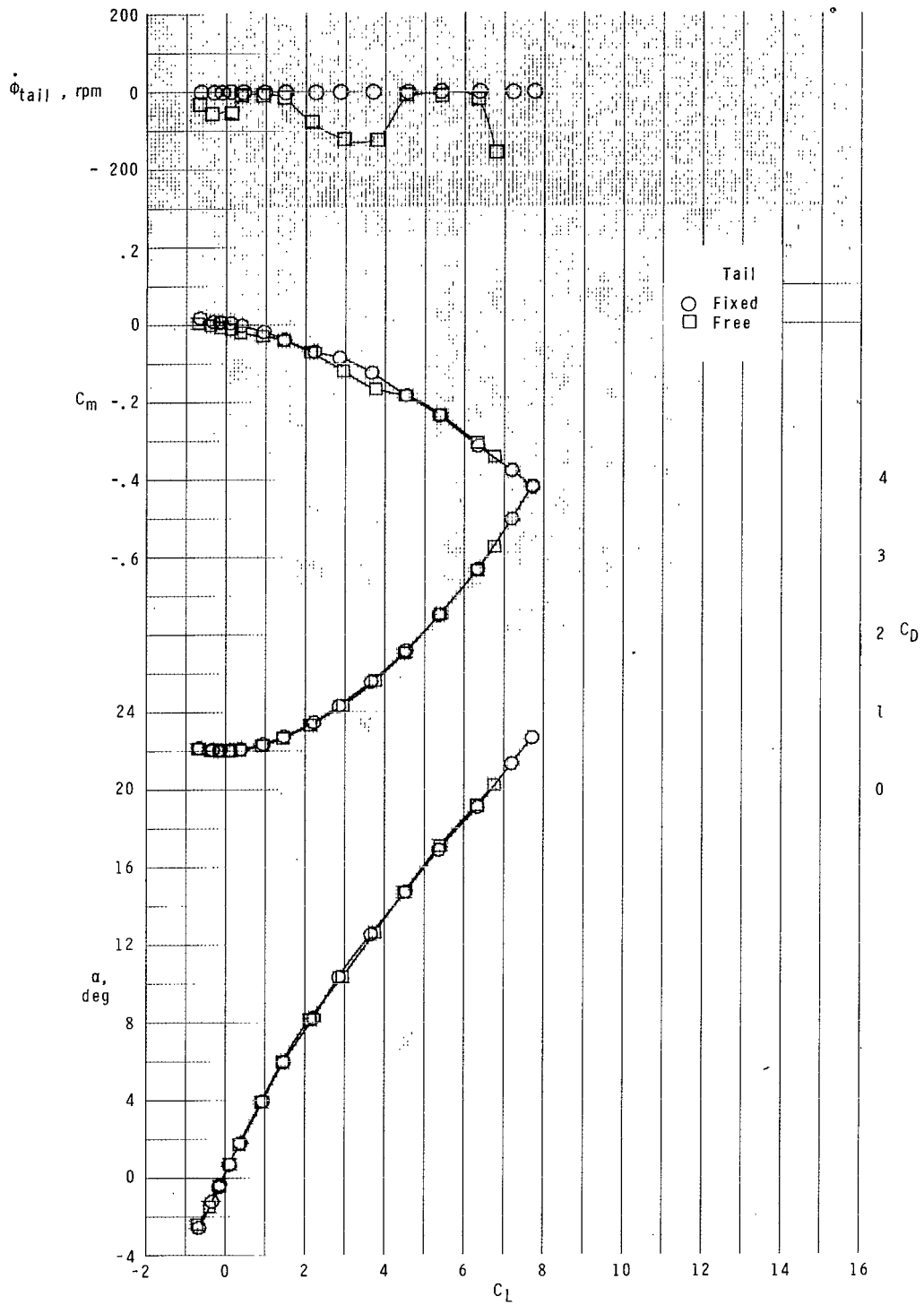
(c) Concluded.

Figure 5.- Continued.



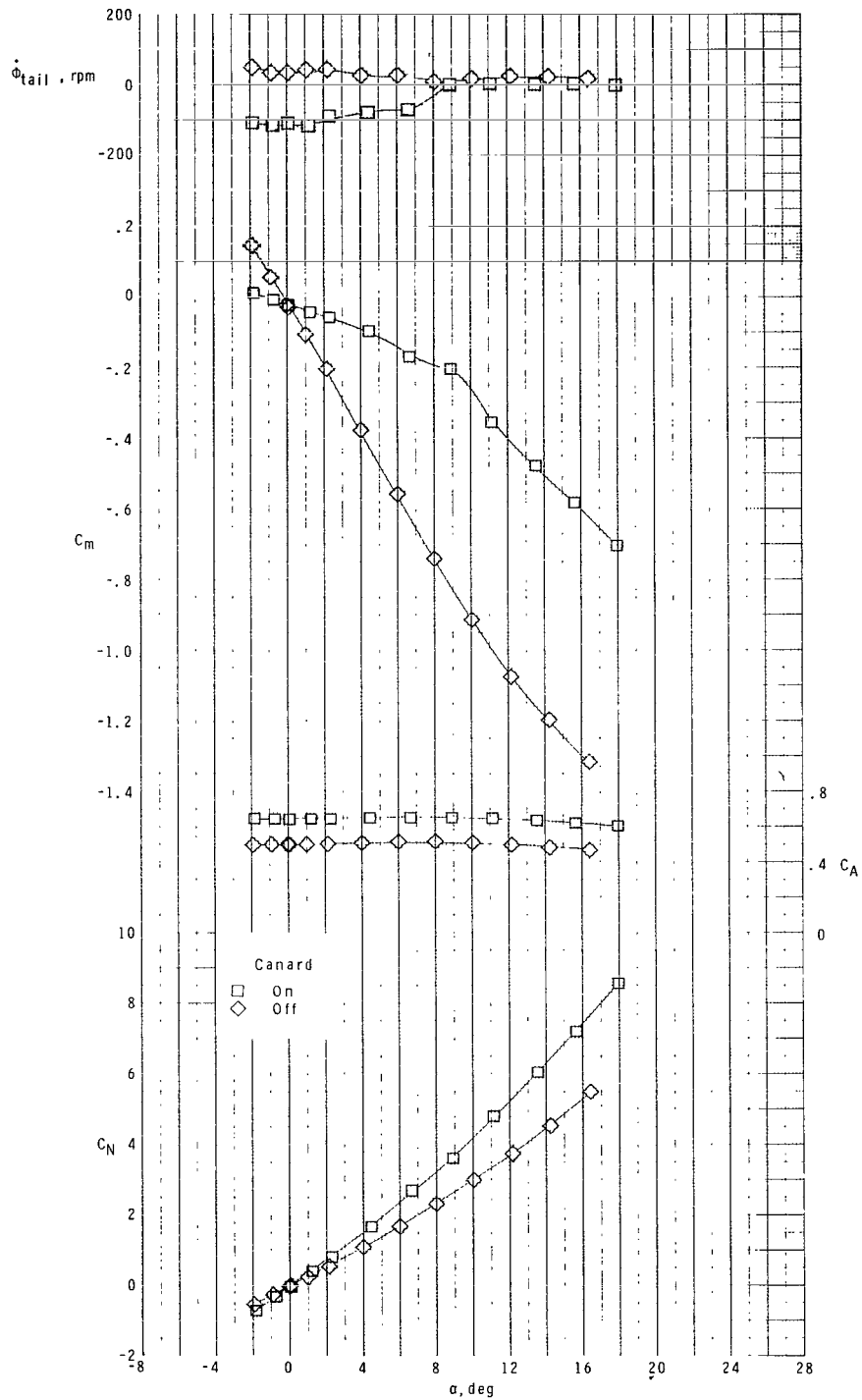
(d)  $M = 2.86$

Figure 5.- Continued.



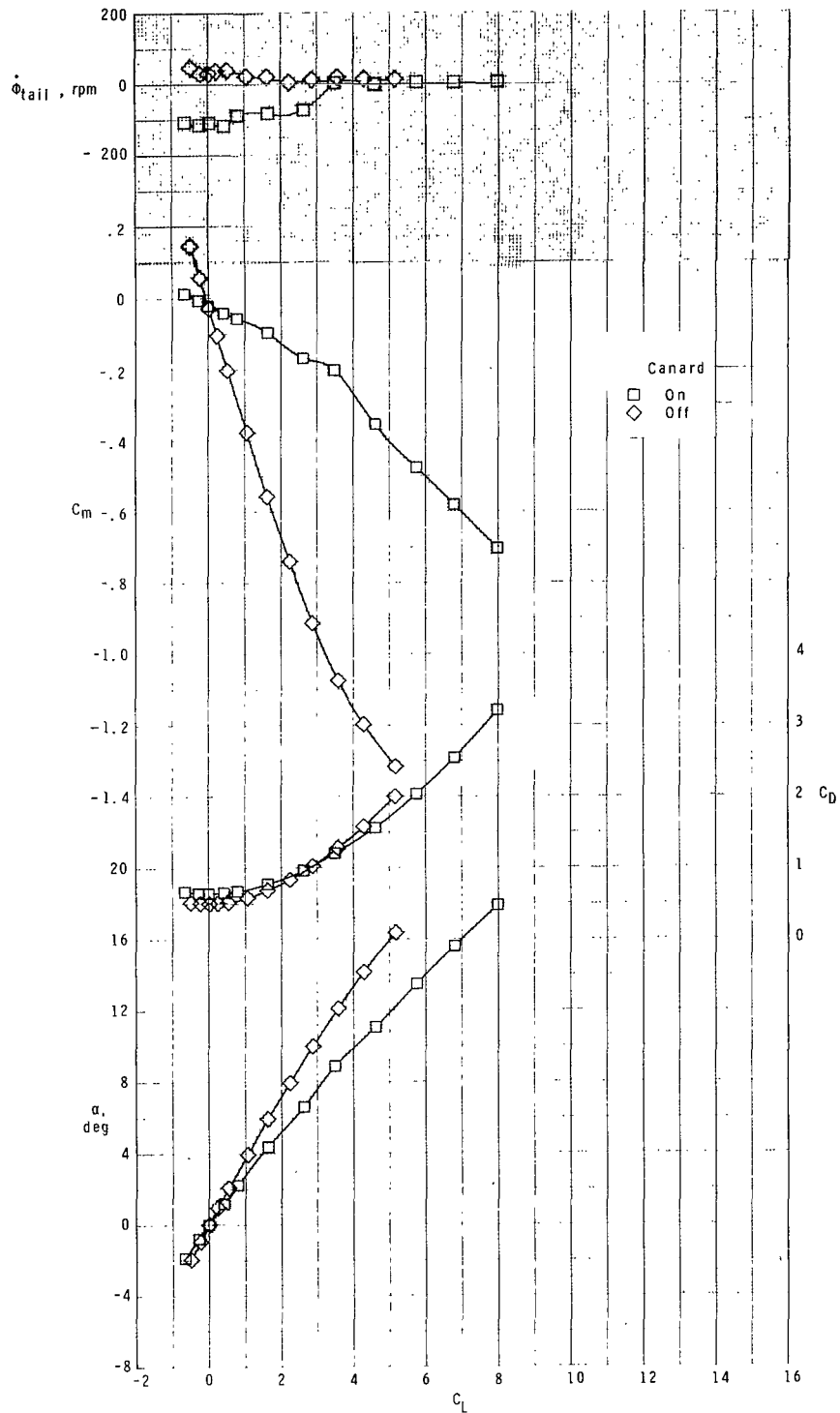
(d) Concluded.

Figure 5.- Concluded.



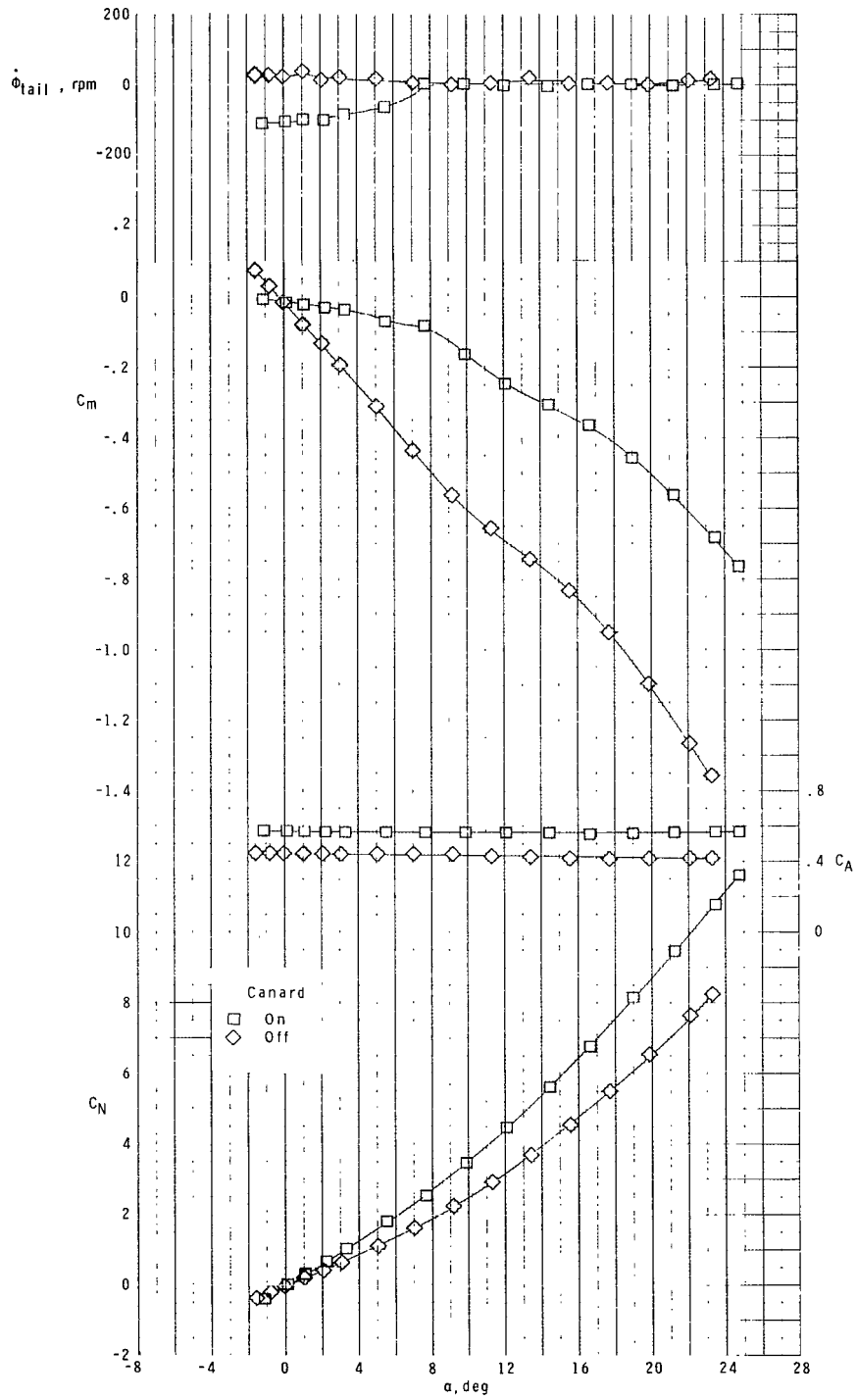
(a)  $M = 1.70$ .

Figure 6.- Effect of canards on longitudinal aerodynamic characteristics of model with free-rolling tail at  $\phi_C = 0^\circ$ .



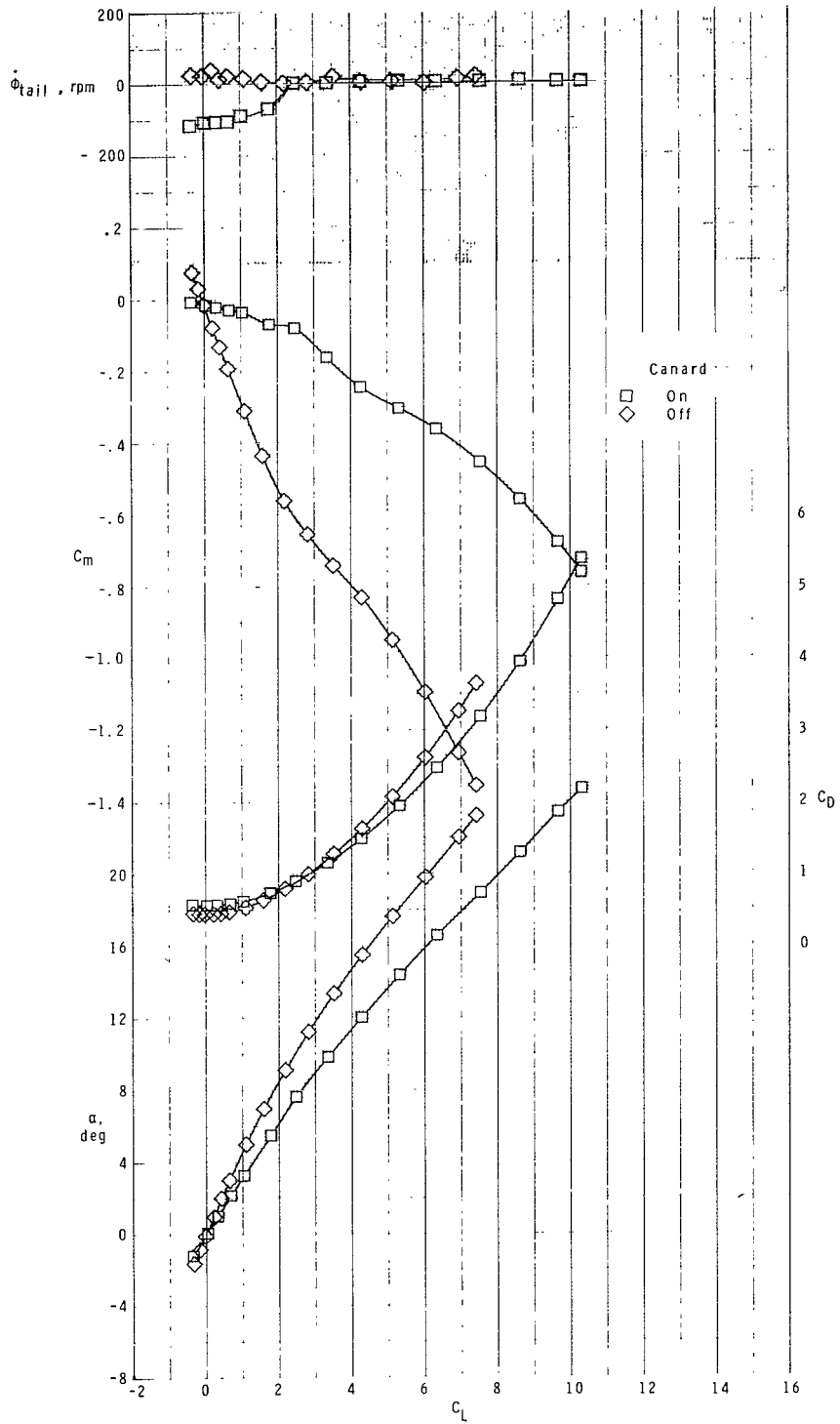
(a) Concluded.

Figure 6.- Continued.



(b)  $M = 2.16$ .

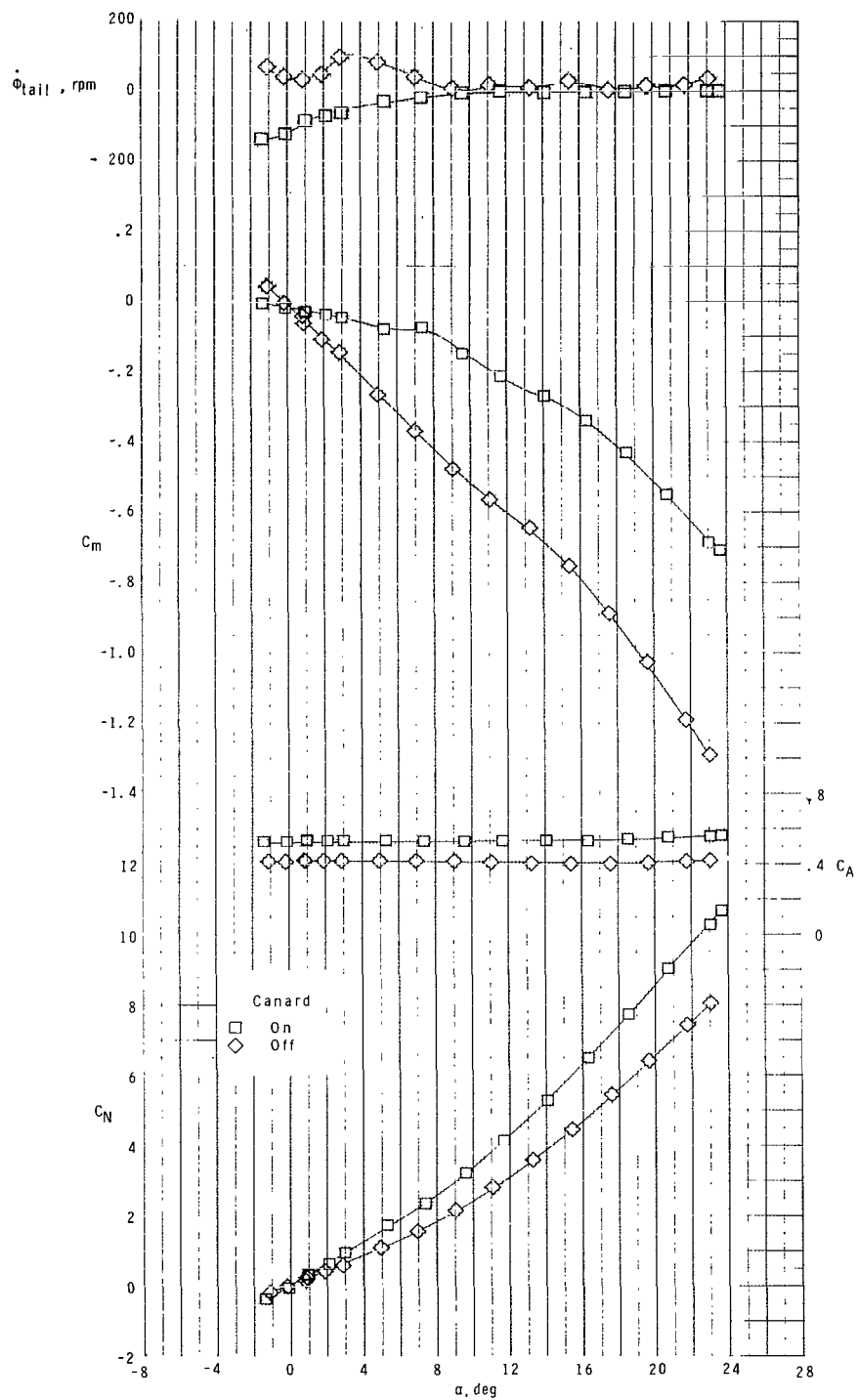
Figure 6.- Continued.



(b) Concluded.

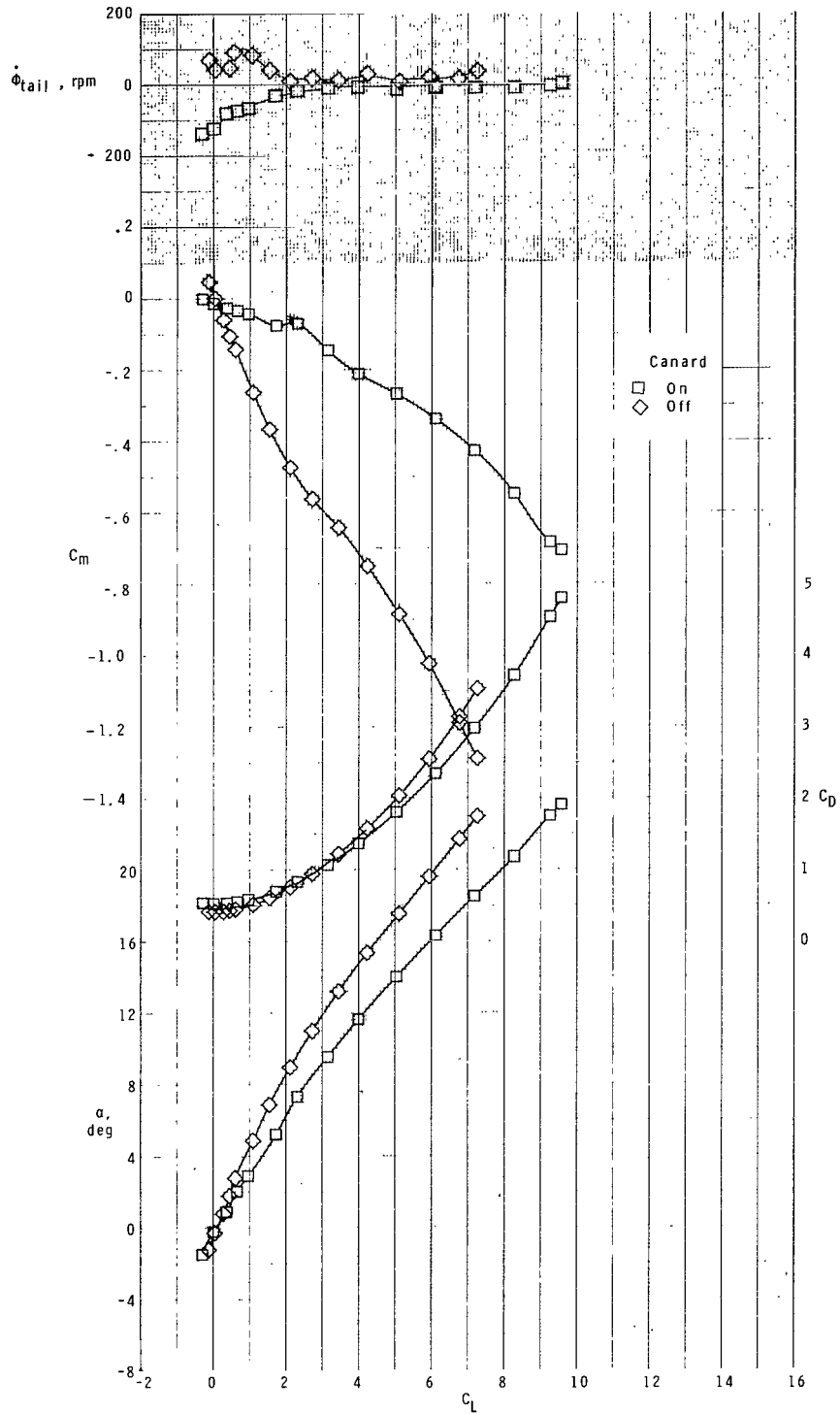
Figure 6.- Continued.





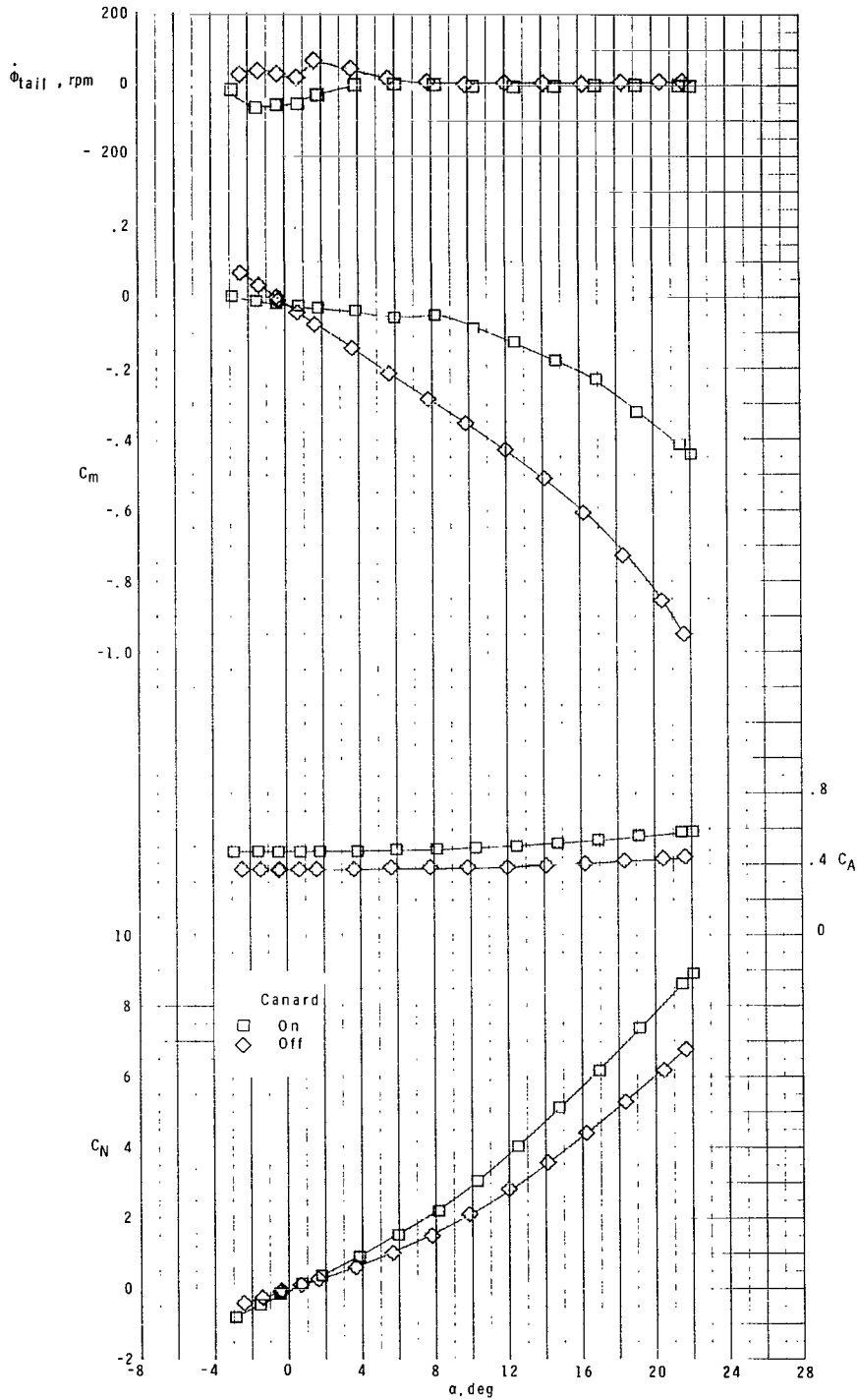
(c)  $M = 2.36$ .

Figure 6.- Continued.



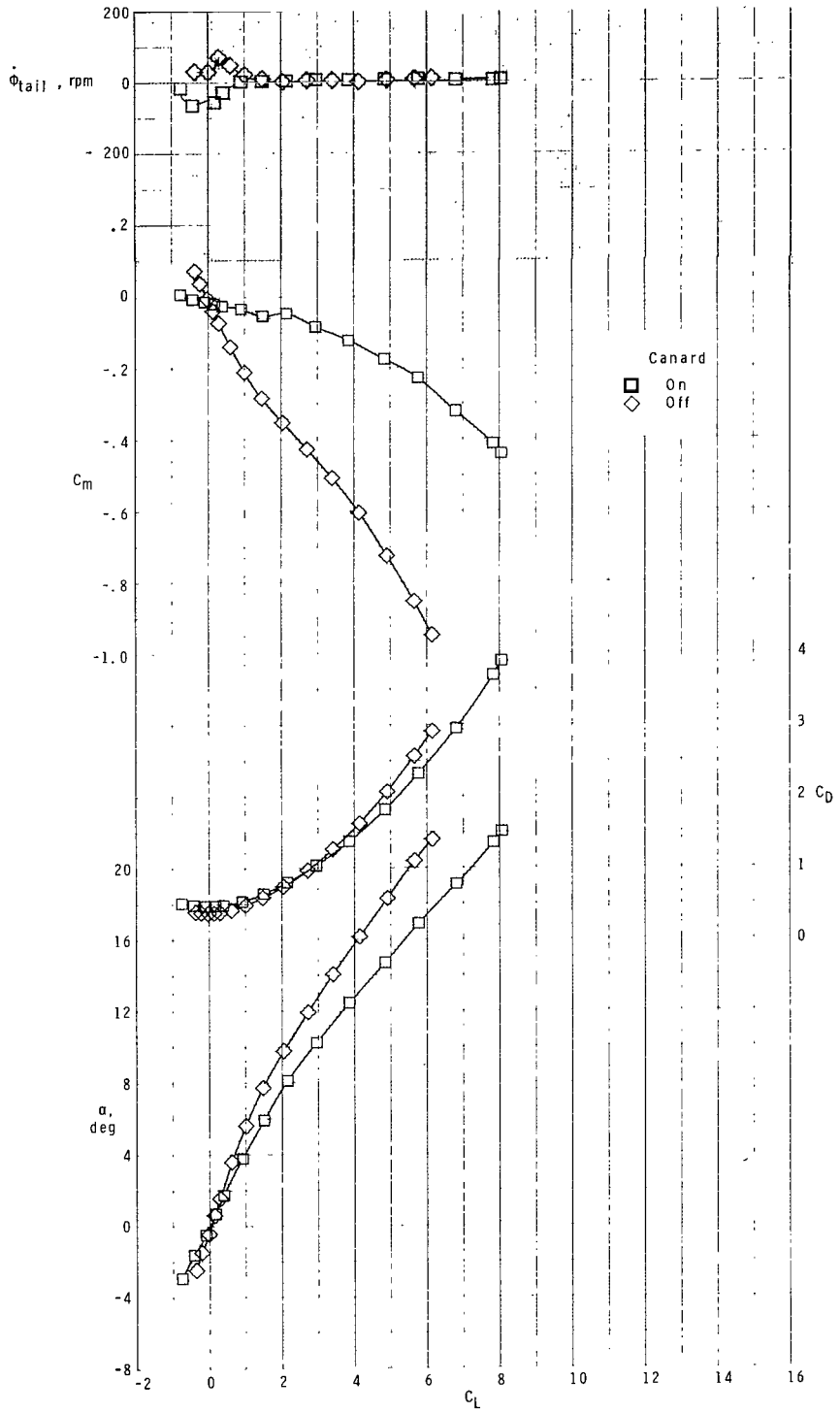
(c) Concluded.

Figure 6.- Continued.



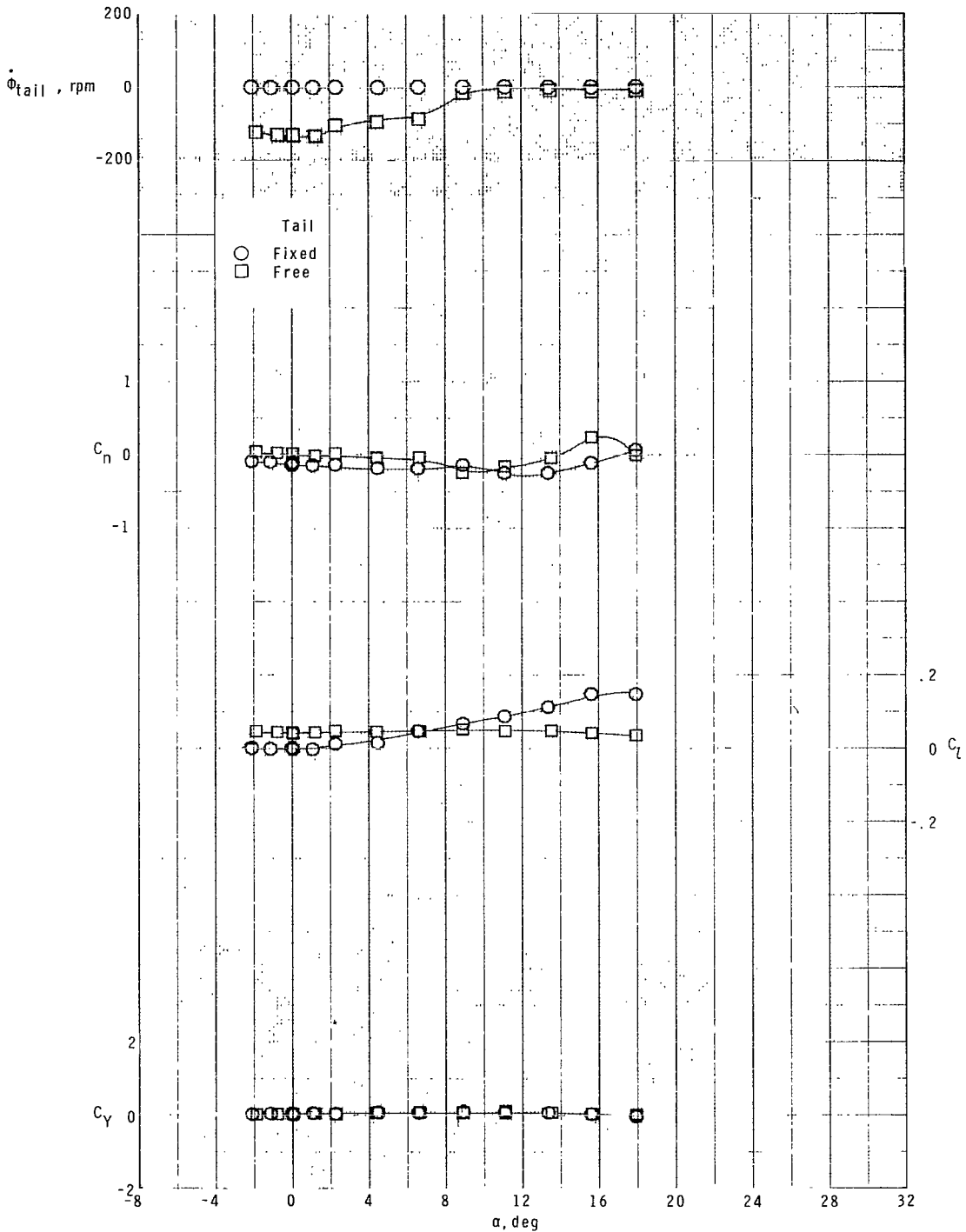
(d)  $M = 2.86$ .

Figure 6.- Continued.



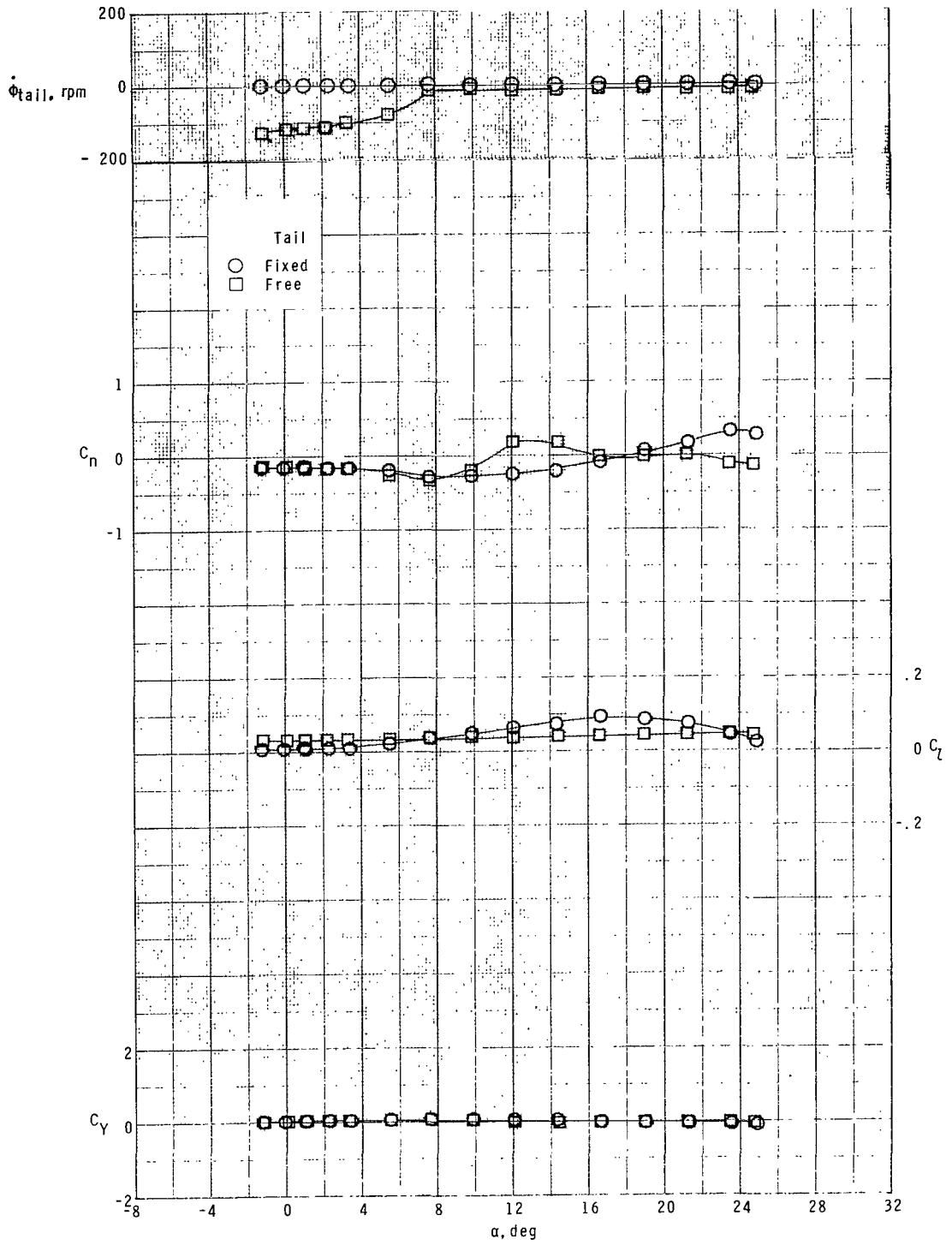
(d) Concluded.

Figure 6.- Concluded.



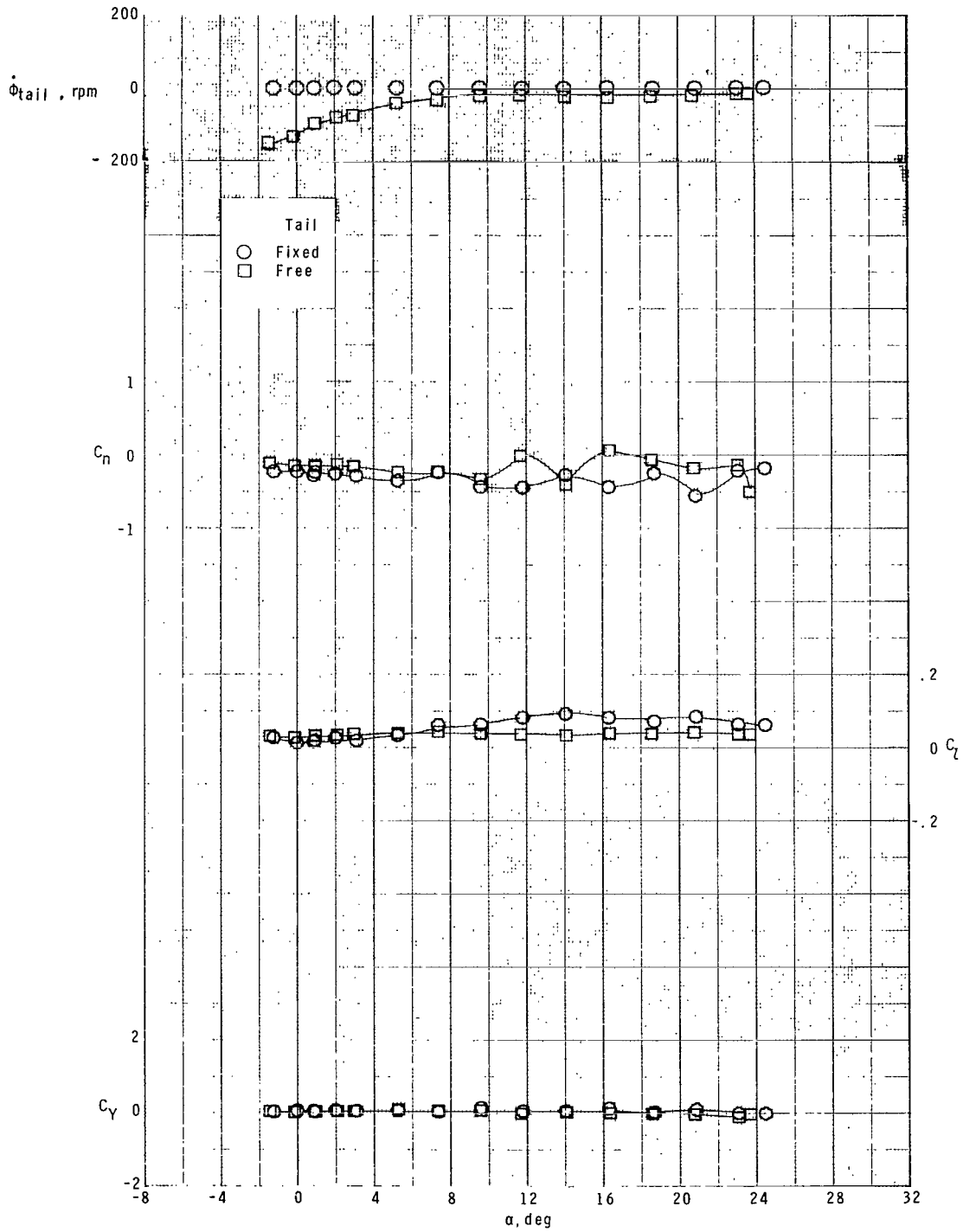
(a)  $M = 1.70$ .

Figure 7.- Effect of free-rolling tail on lateral aerodynamic characteristics of model with zero control deflection at  $\phi_C = 0^\circ$ .



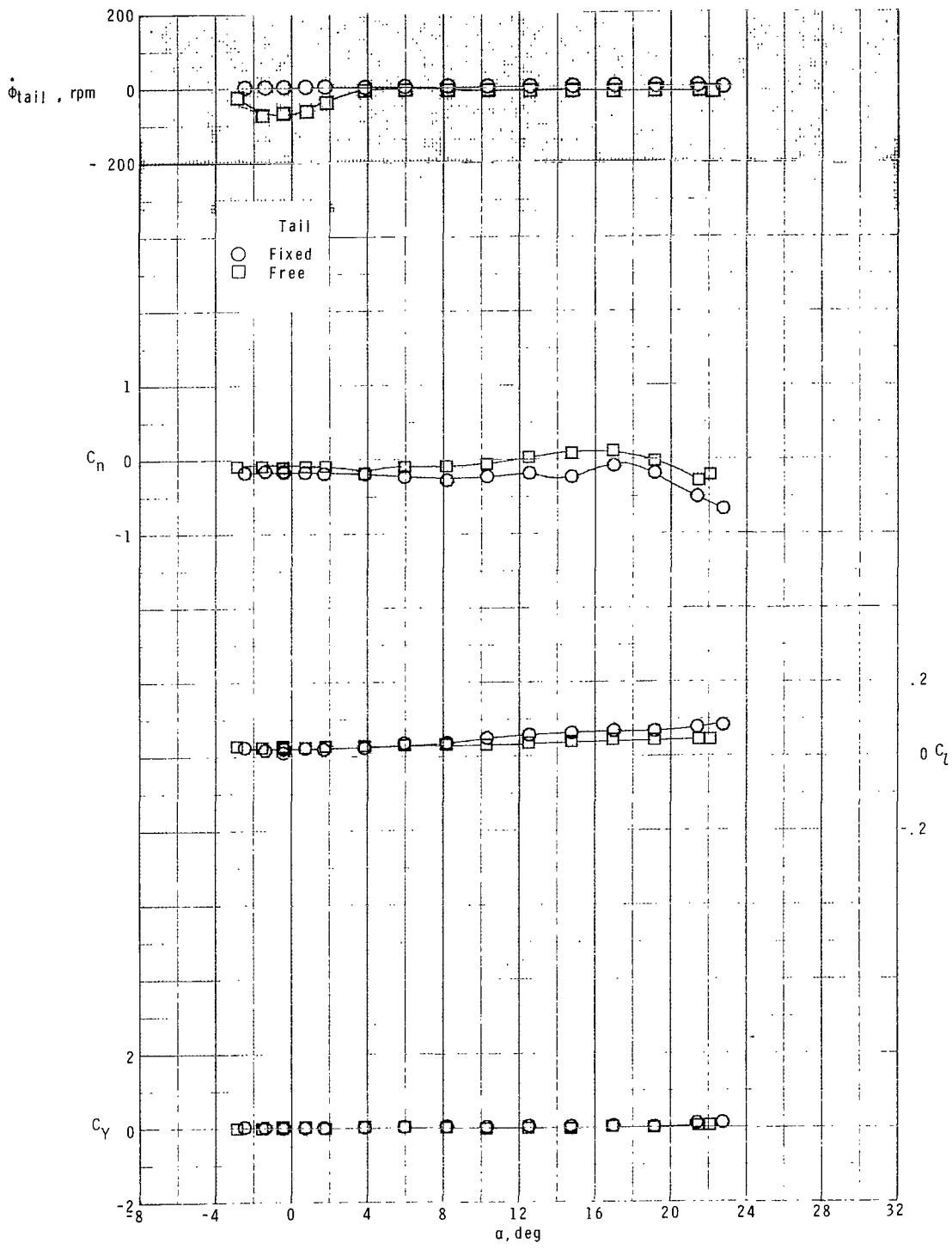
(b)  $M = 2.16$ .

Figure 7.- Continued.



(c)  $M = 2.36$ .

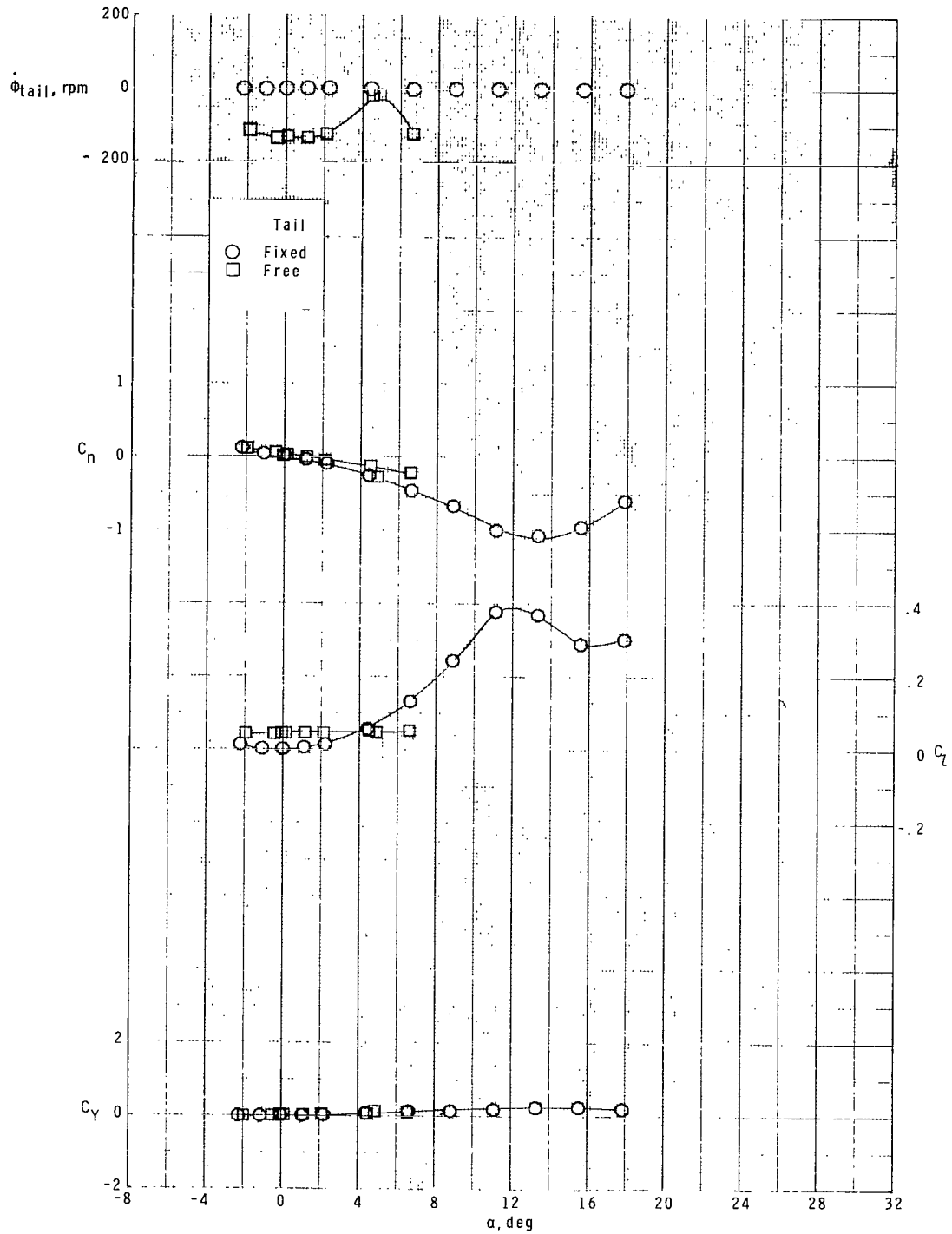
Figure 7.- Continued.



(d) M = 2.86.

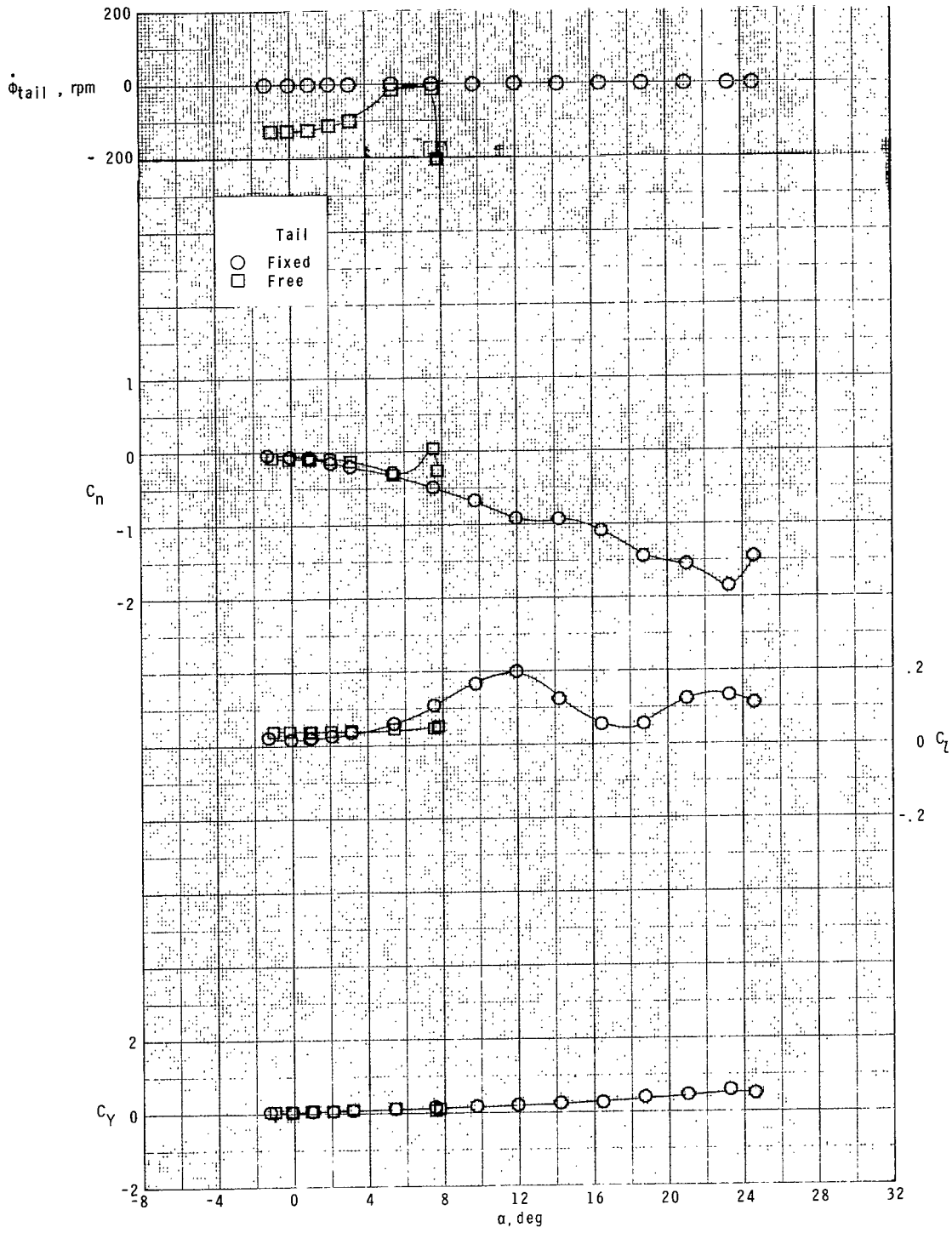
Figure 7.- Concluded.





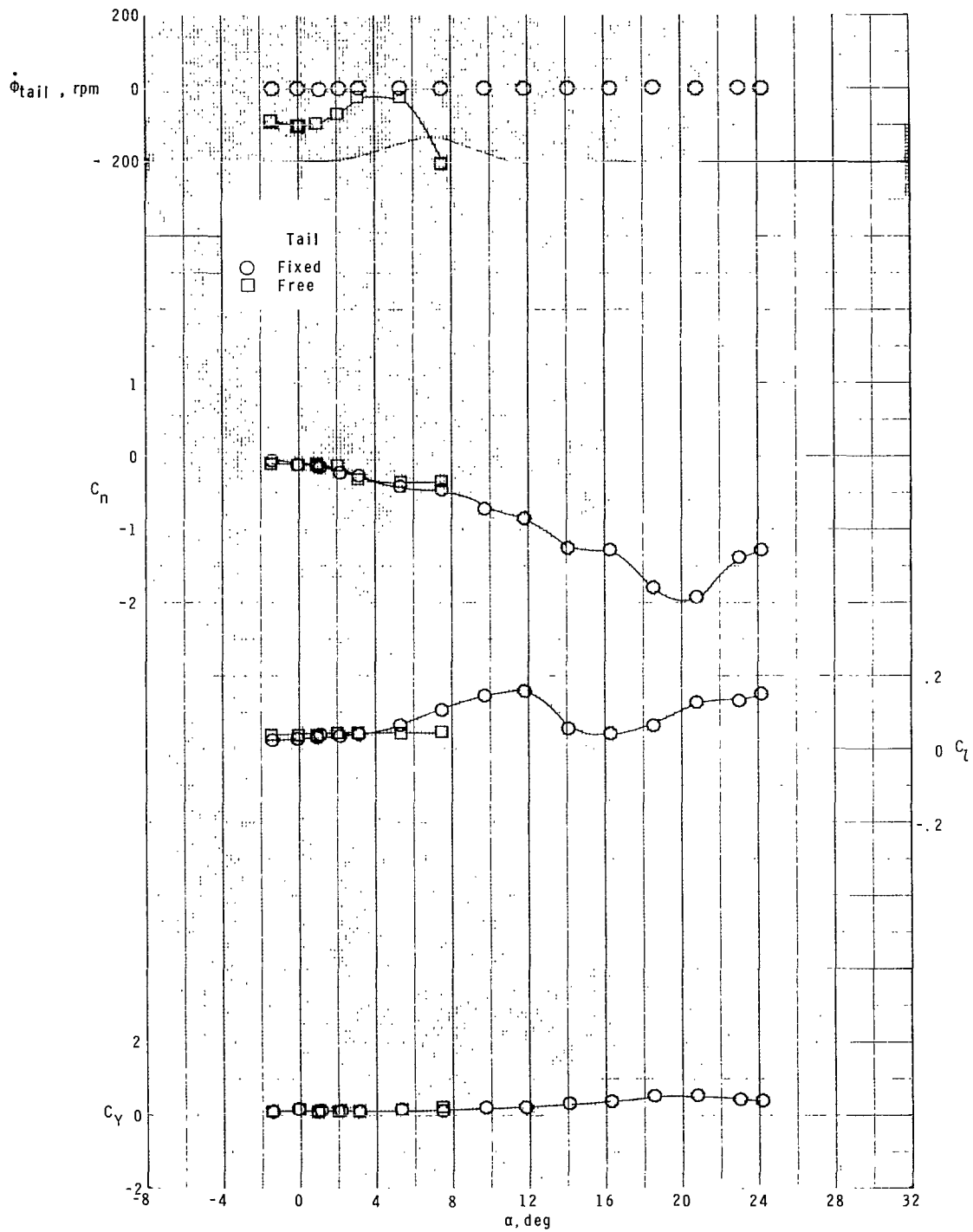
(a)  $M = 1.70$ .

Figure 8.- Effect of free-rolling tail on lateral aerodynamic characteristics of model with zero control deflection at  $\phi_c = 26.6^\circ$ .



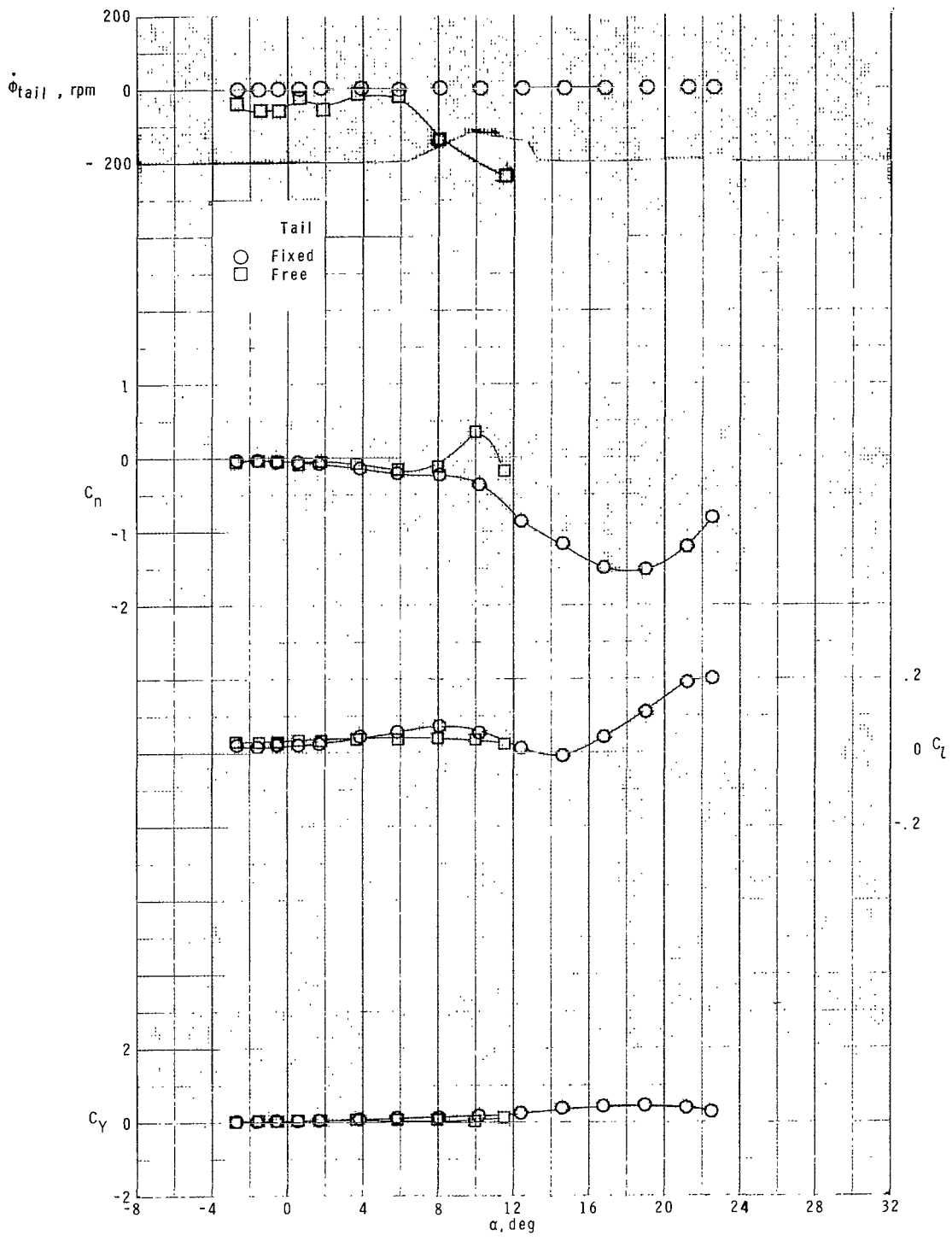
(b)  $M = 2.16$ .

Figure 8.- Continued.



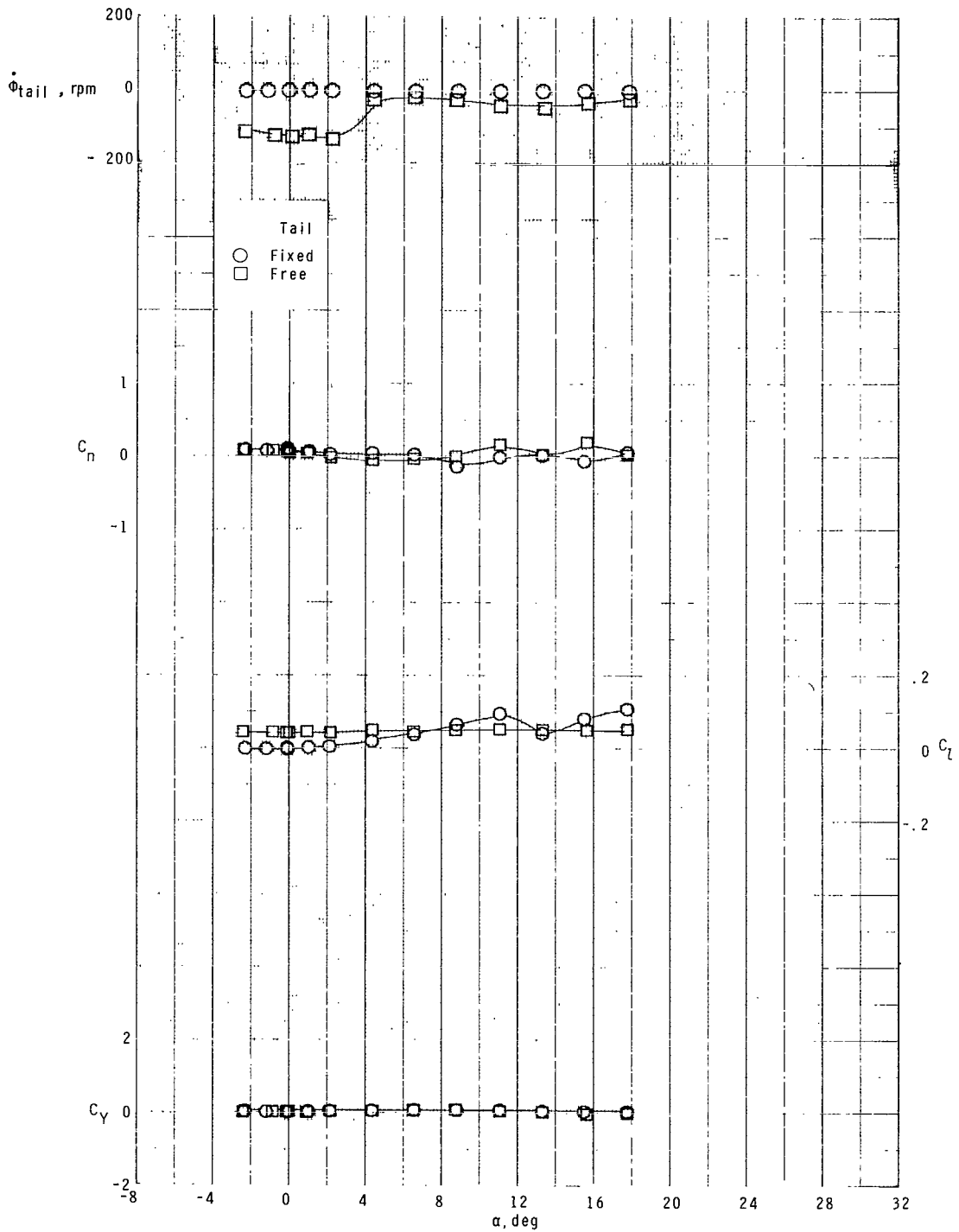
(c)  $M = 2.36$ .

Figure 8.- Continued.



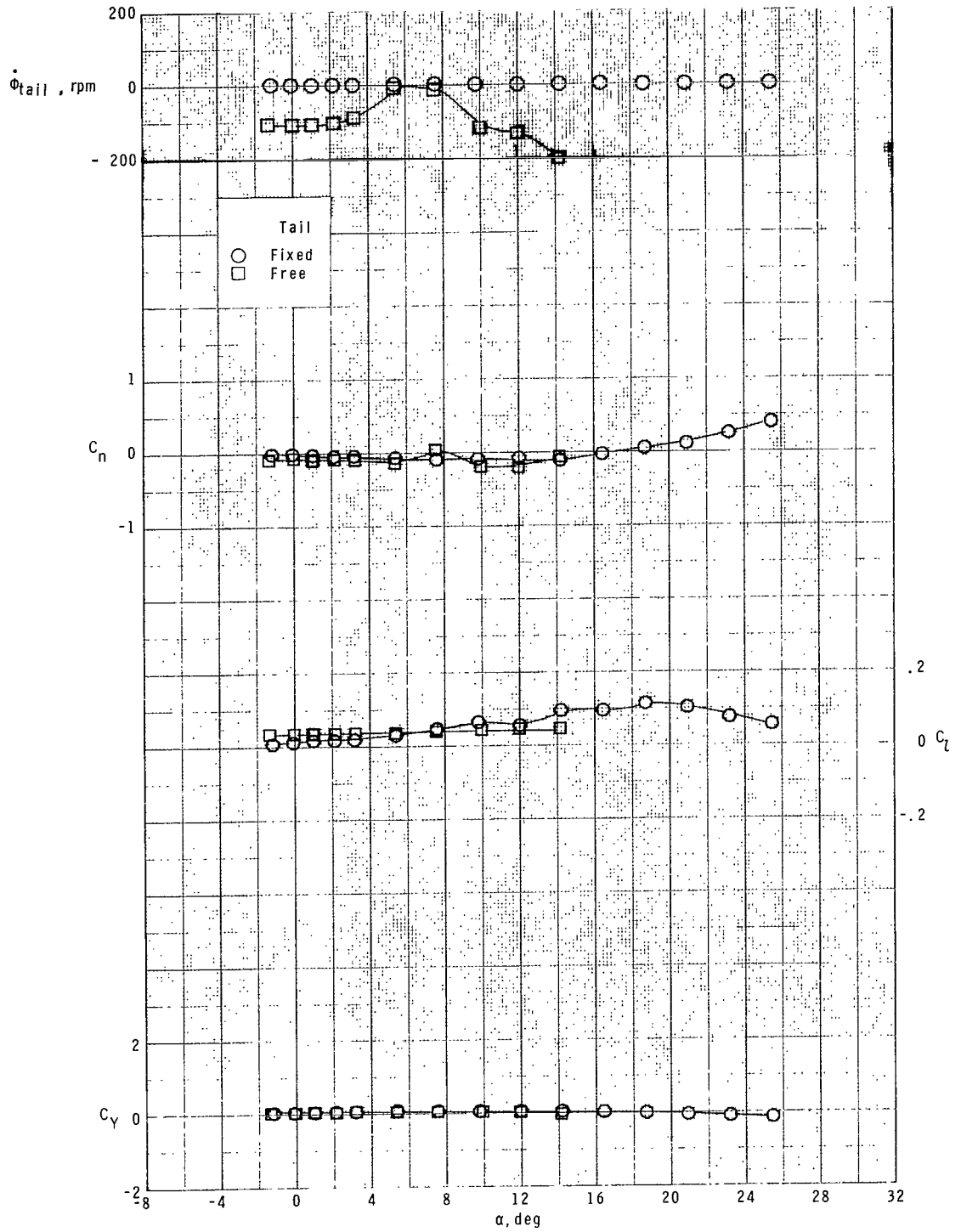
(d)  $M = 2.86$ .

Figure 8.- Concluded.



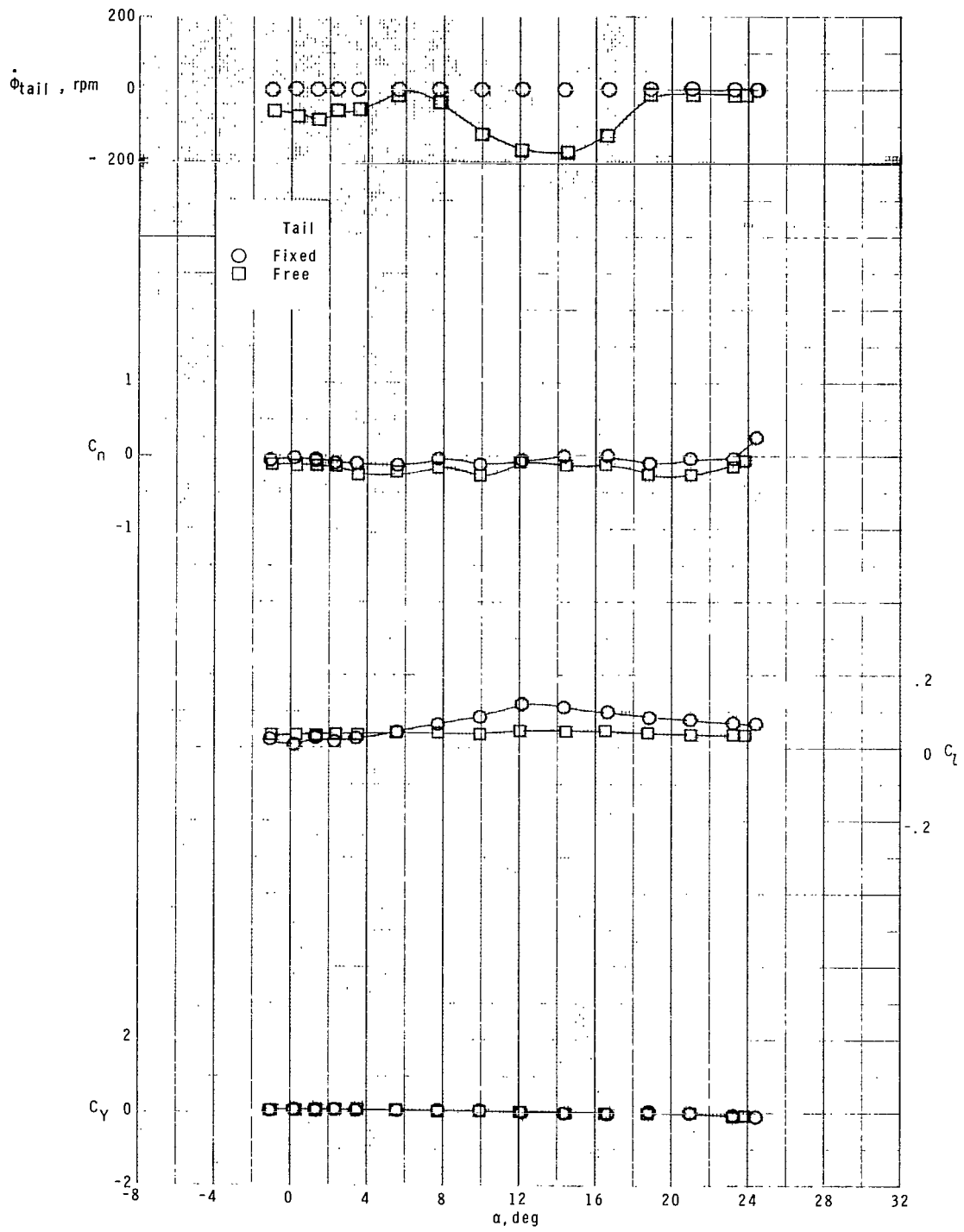
(a)  $M = 1.70$ .

Figure 9.- Effect of free-rolling tail on lateral aerodynamic characteristics of model with zero control deflection at  $\phi_C = 45^\circ$ .



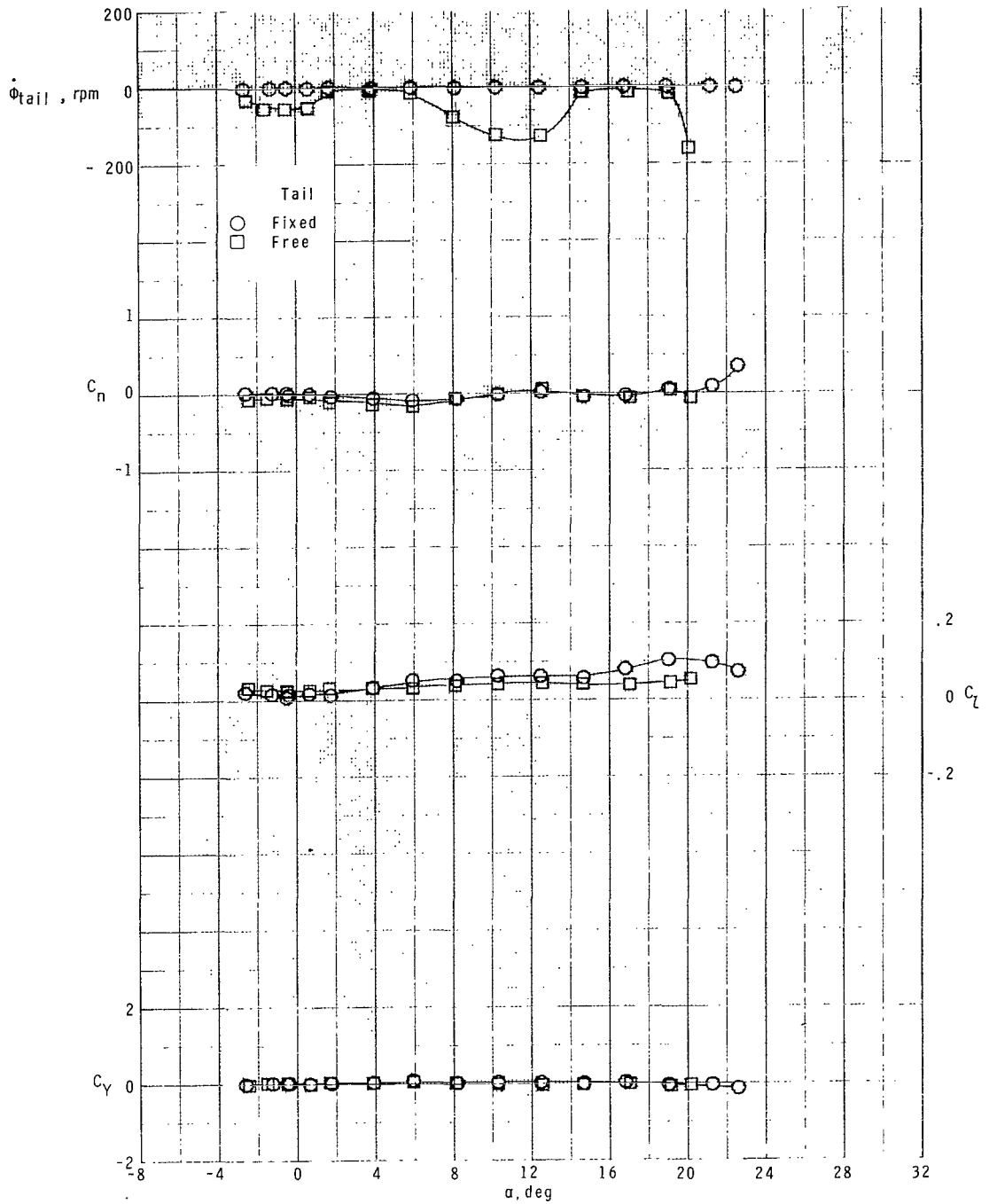
(b)  $M = 2.16$ .

Figure 9.- Continued.



(c)  $M = 2.36.$

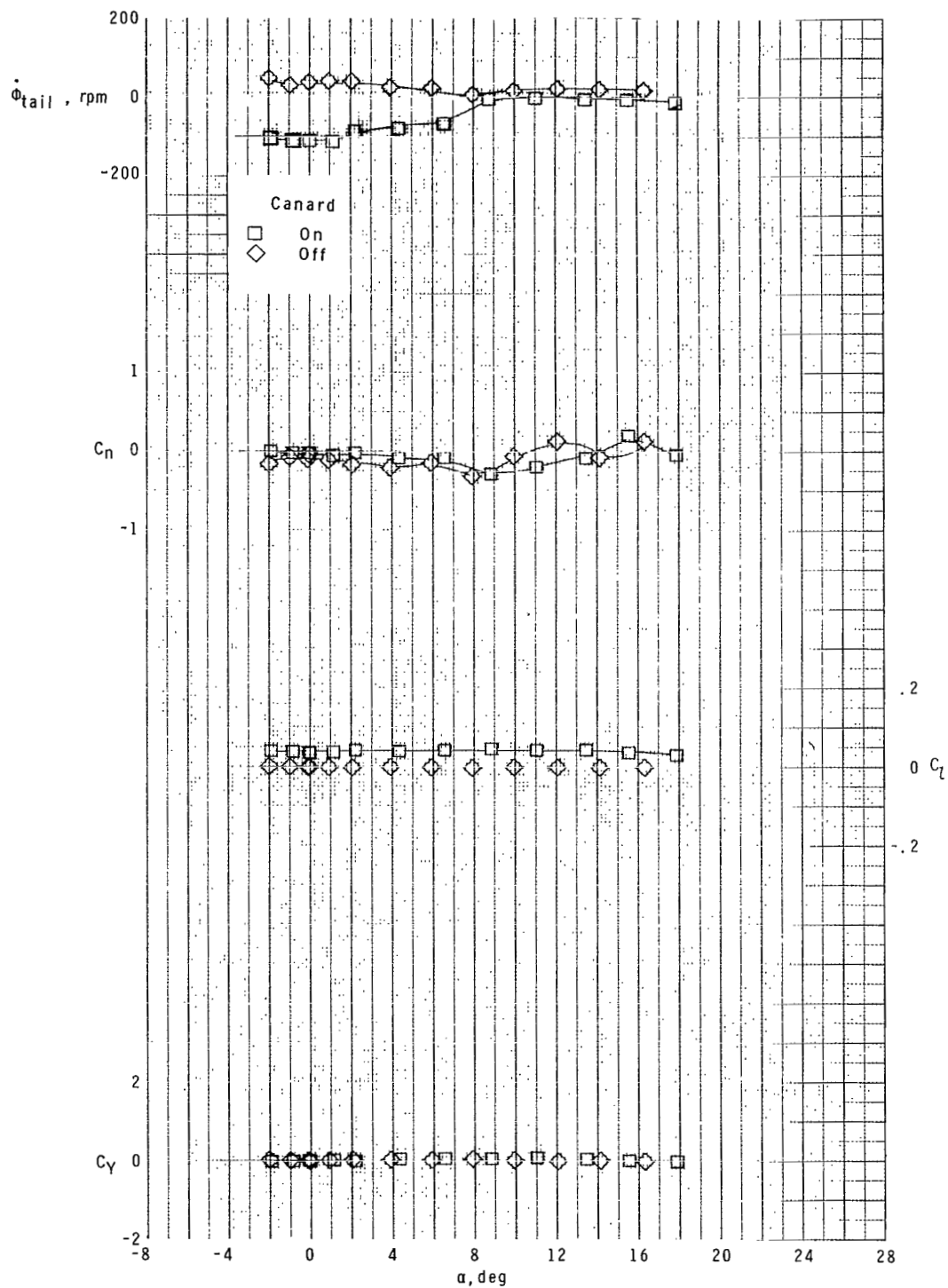
Figure 9.- Continued.



(d)  $M = 2.86$ .

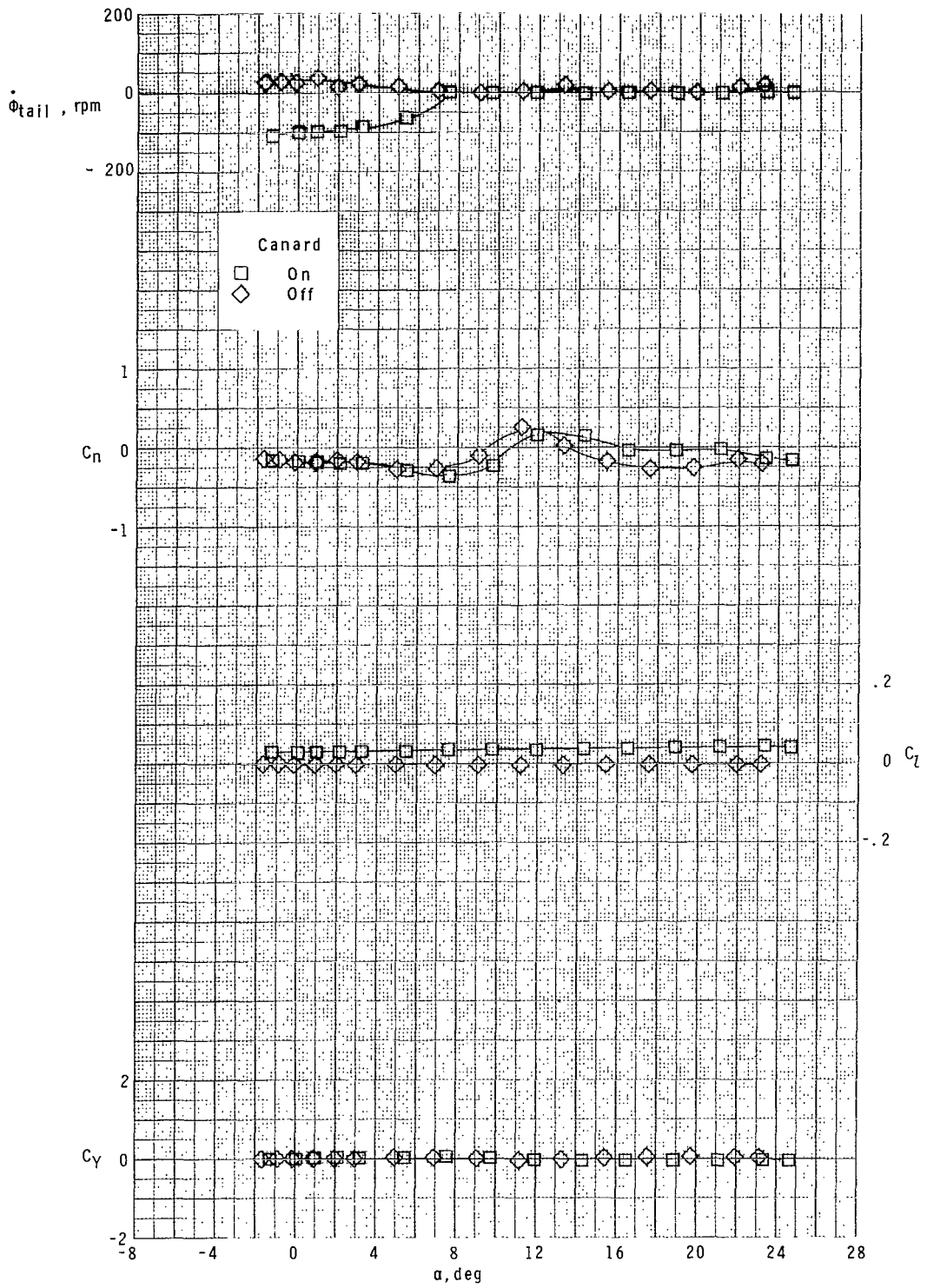
Figure 9.- Concluded.





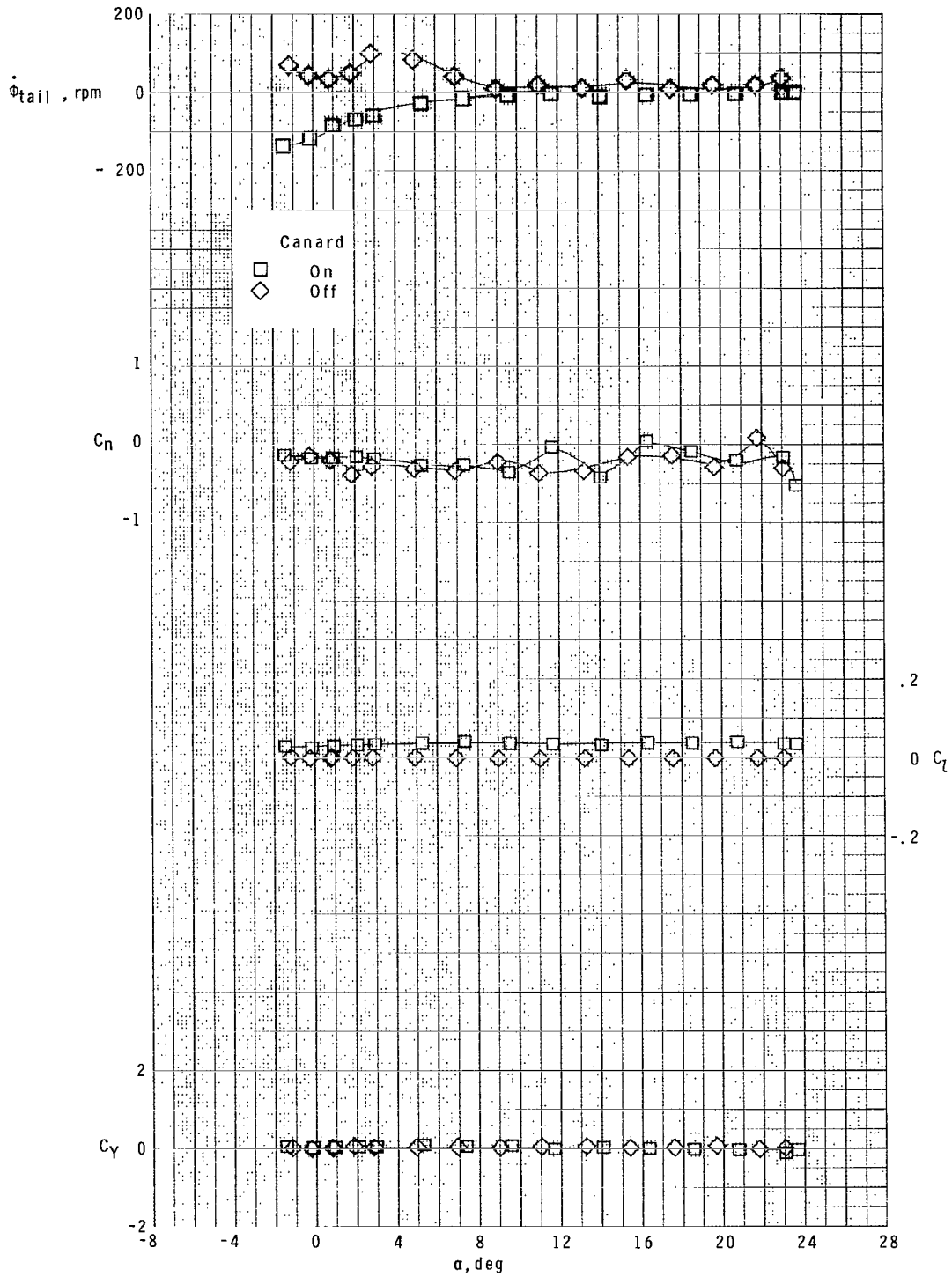
(a)  $M = 1.70$ .

Figure 10.- Effect of canards on lateral aerodynamic characteristics of model with a free-rolling tail at  $\phi_C = 0^\circ$ .



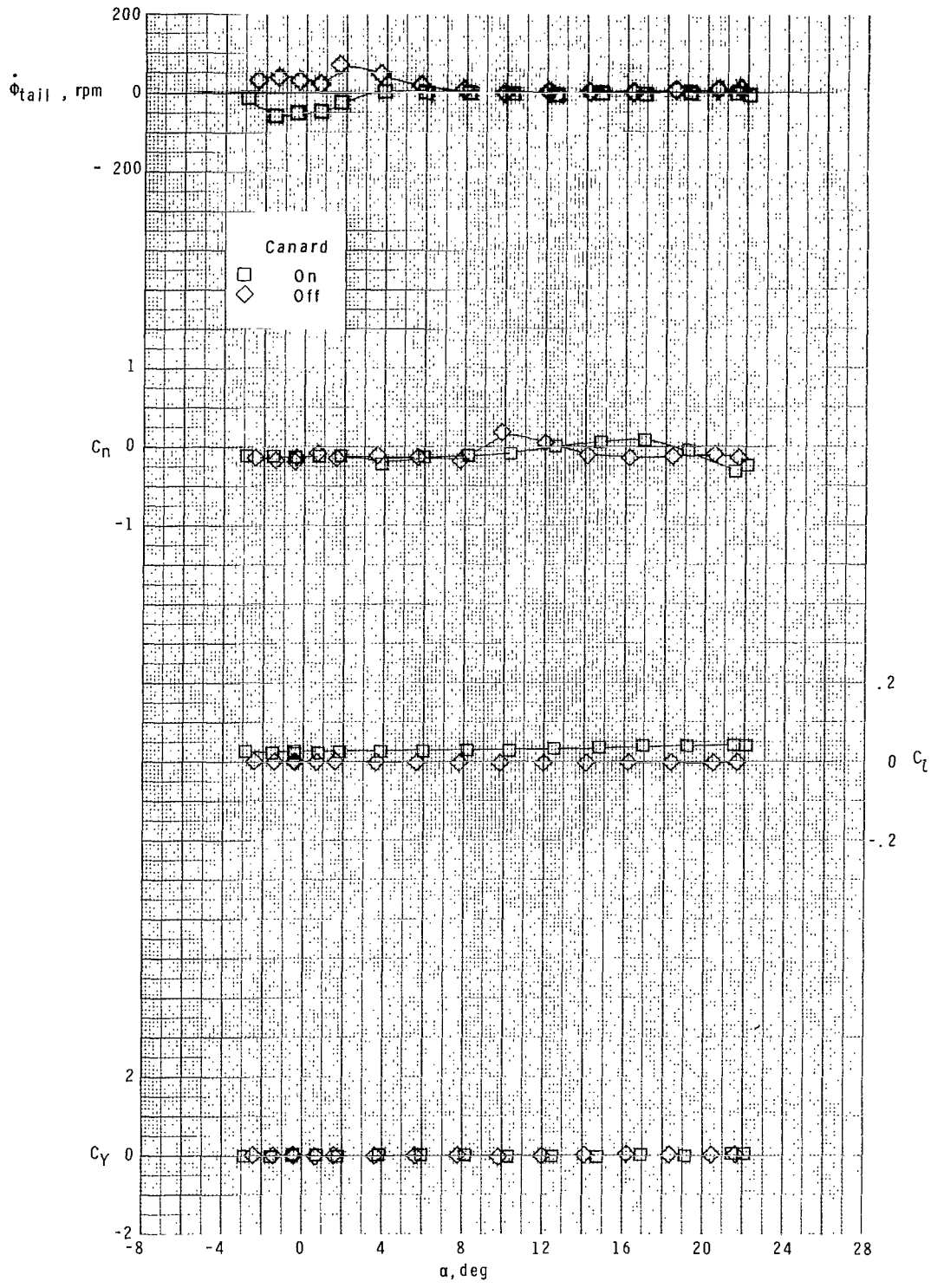
(b)  $M = 2.16$ .

Figure 10.- Continued.



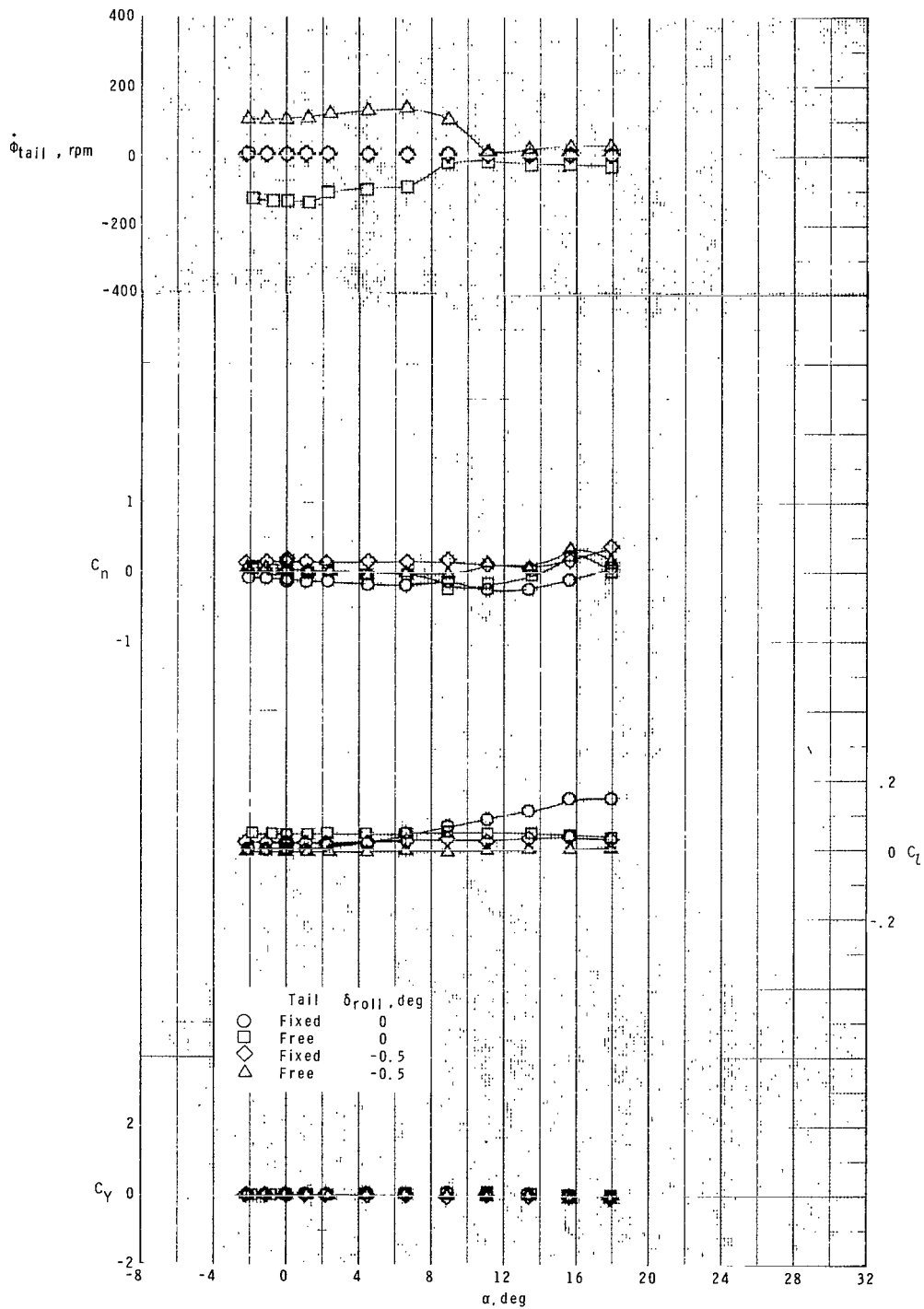
(c)  $M = 2.36$ .

Figure 10.- Continued.



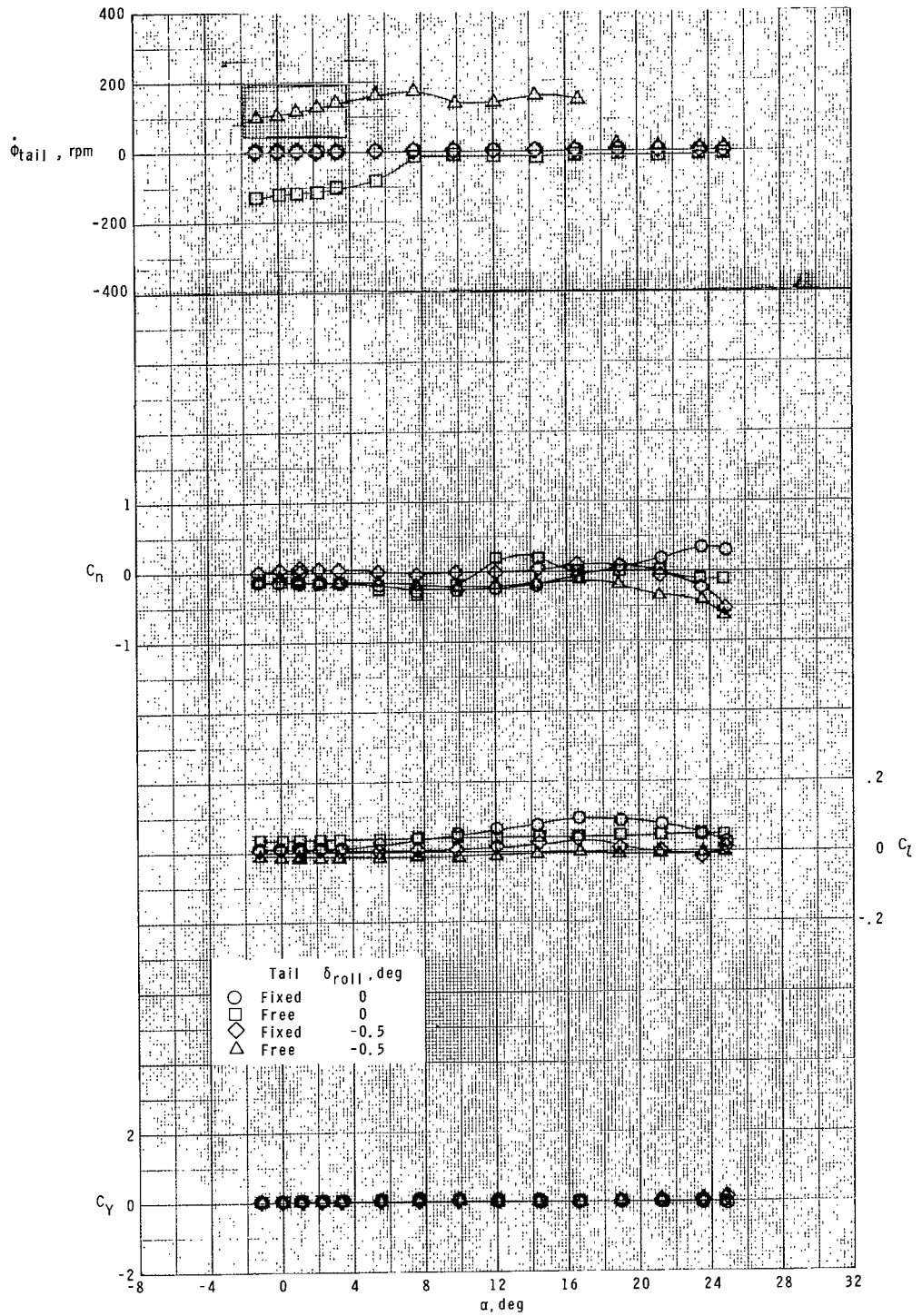
(d)  $M = 2.86$ .

Figure 10.- Concluded.



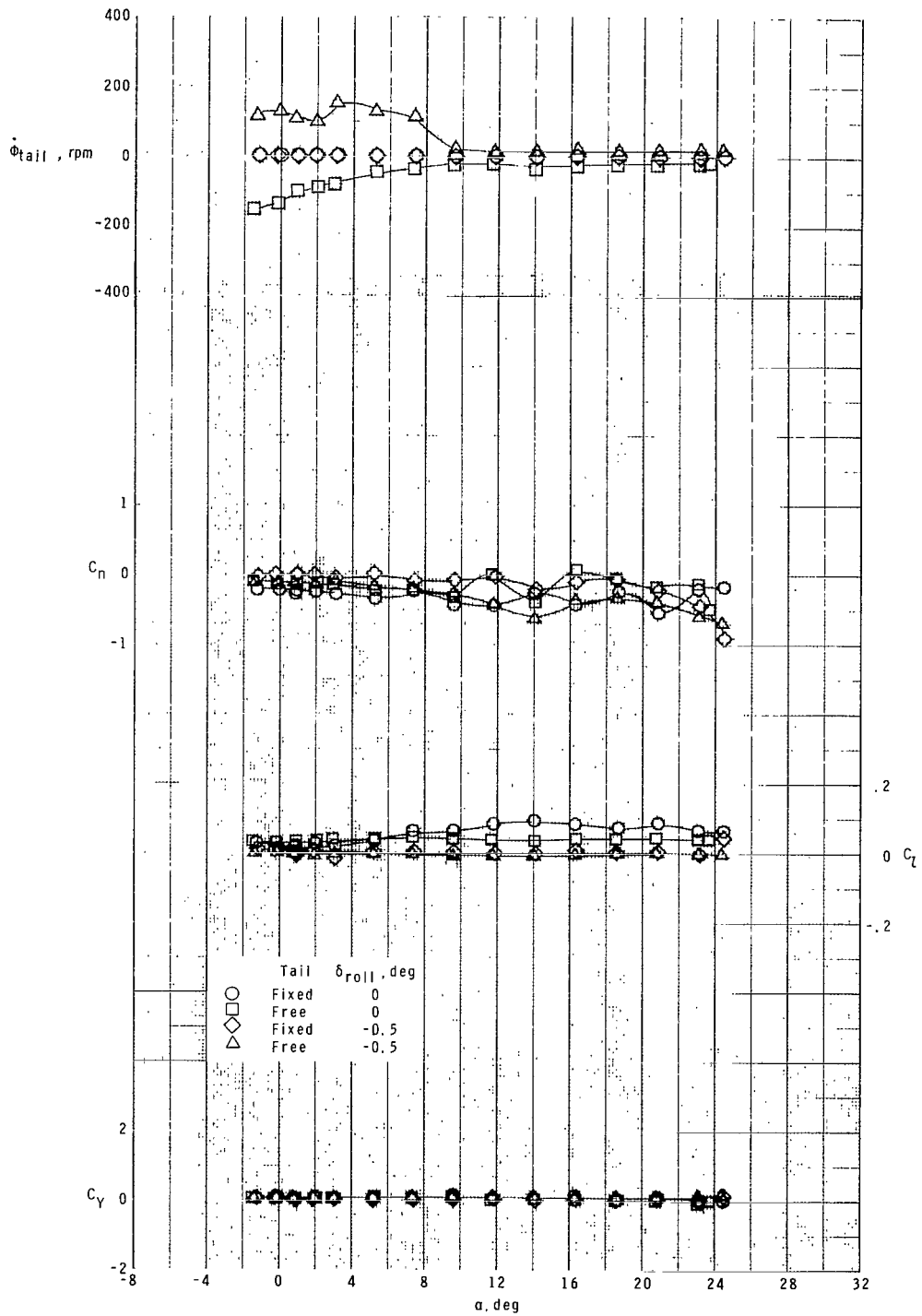
(a)  $M = 1.70$ .

Figure 11.- Roll-control characteristics of model with fixed and free-rolling tail at  $\phi_C = 0^\circ$ . Two canards deflected.



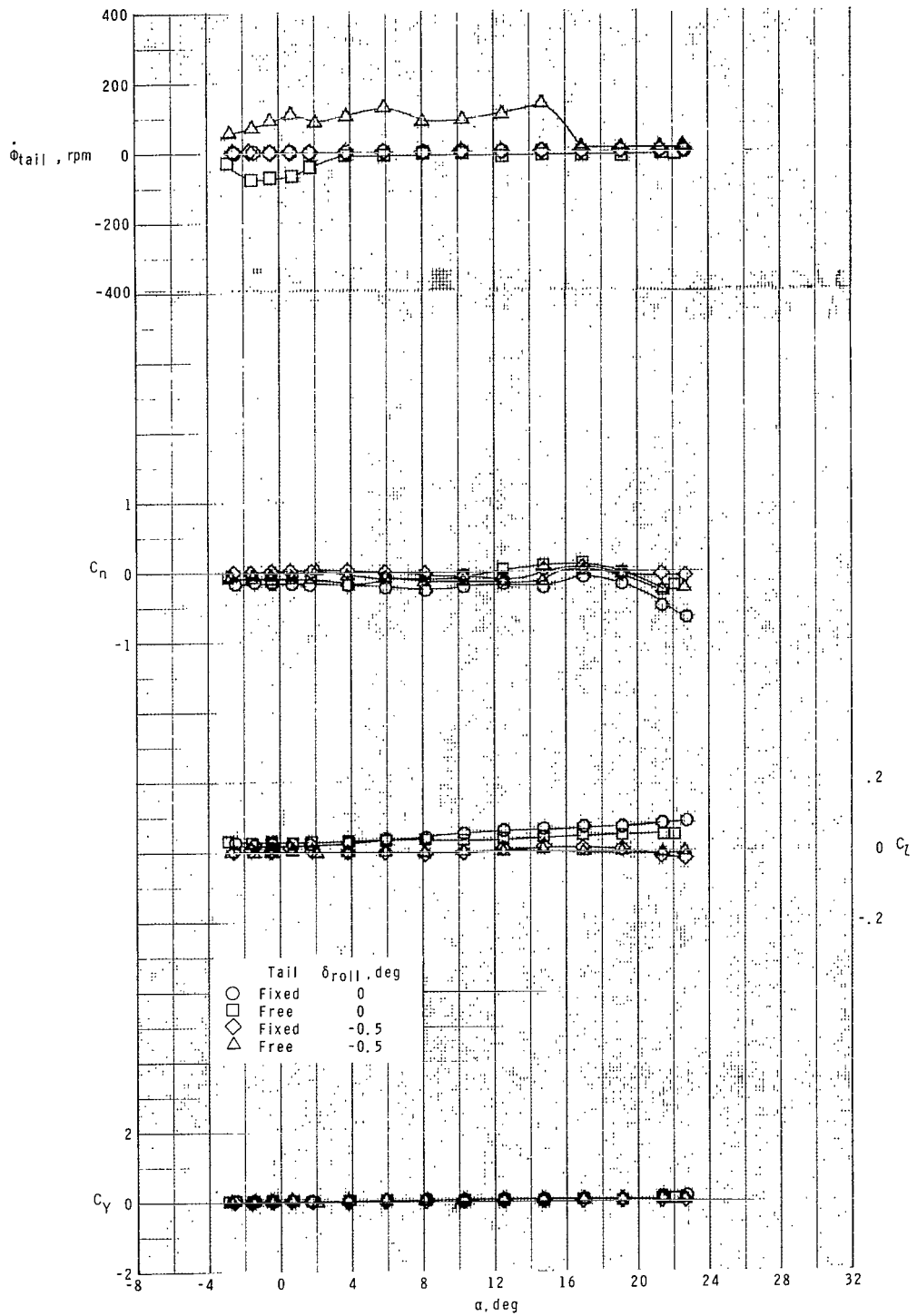
(b)  $M = 2.16$ .

Figure 11.- Continued.



(c)  $M = 2.36$ .

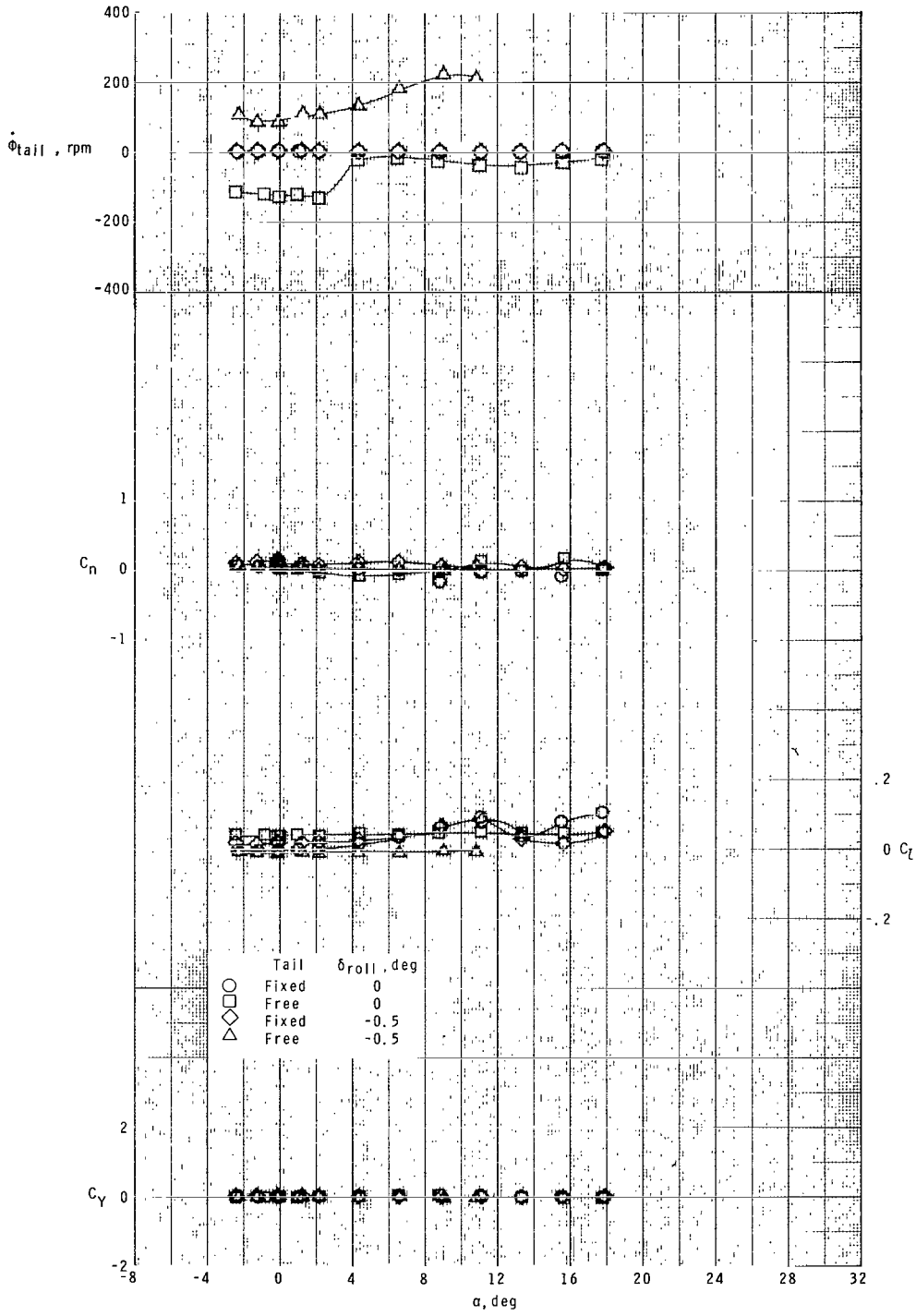
Figure 11.- Continued.



(d)  $M = 2.86$ .

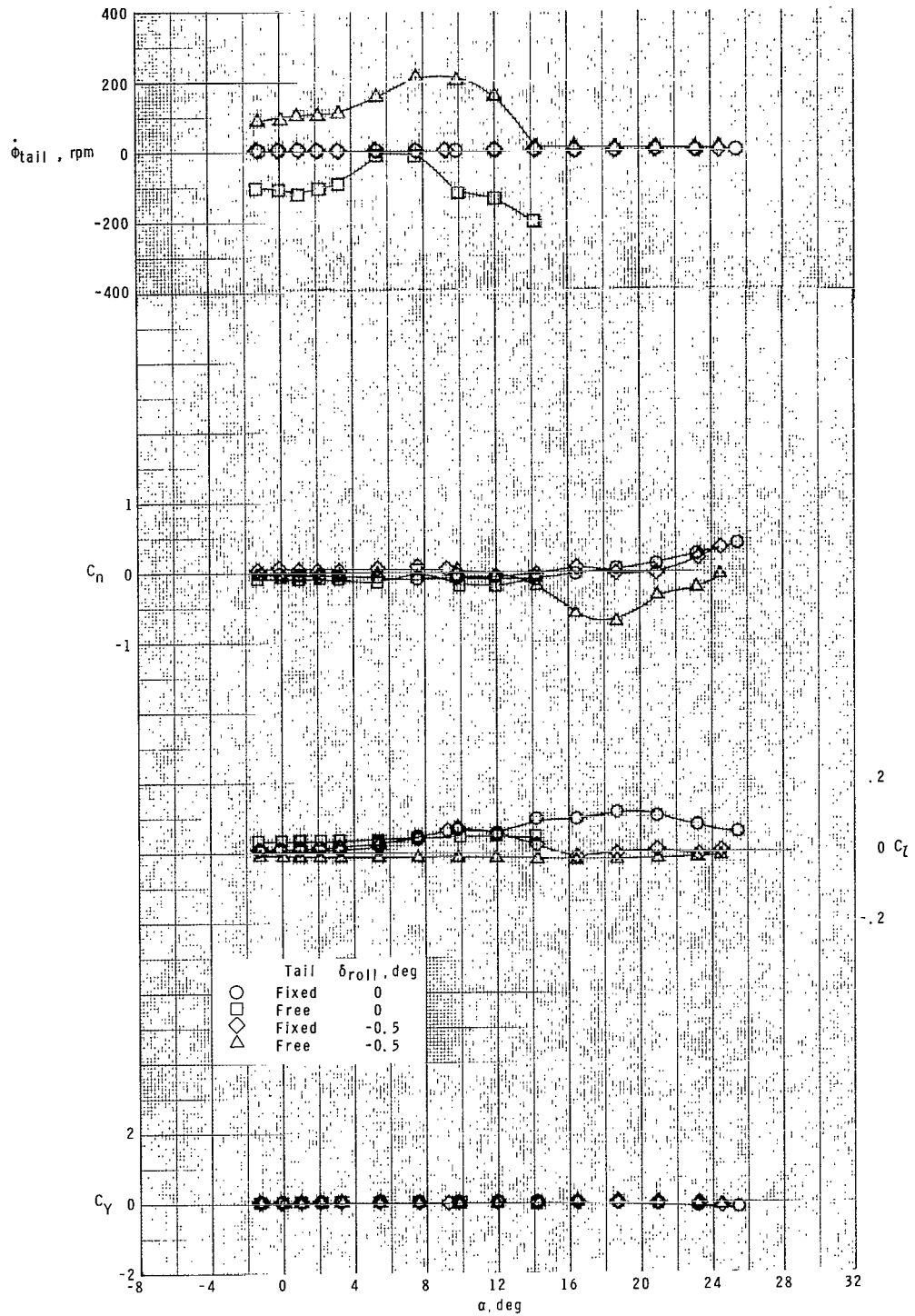
Figure 11.- Concluded.





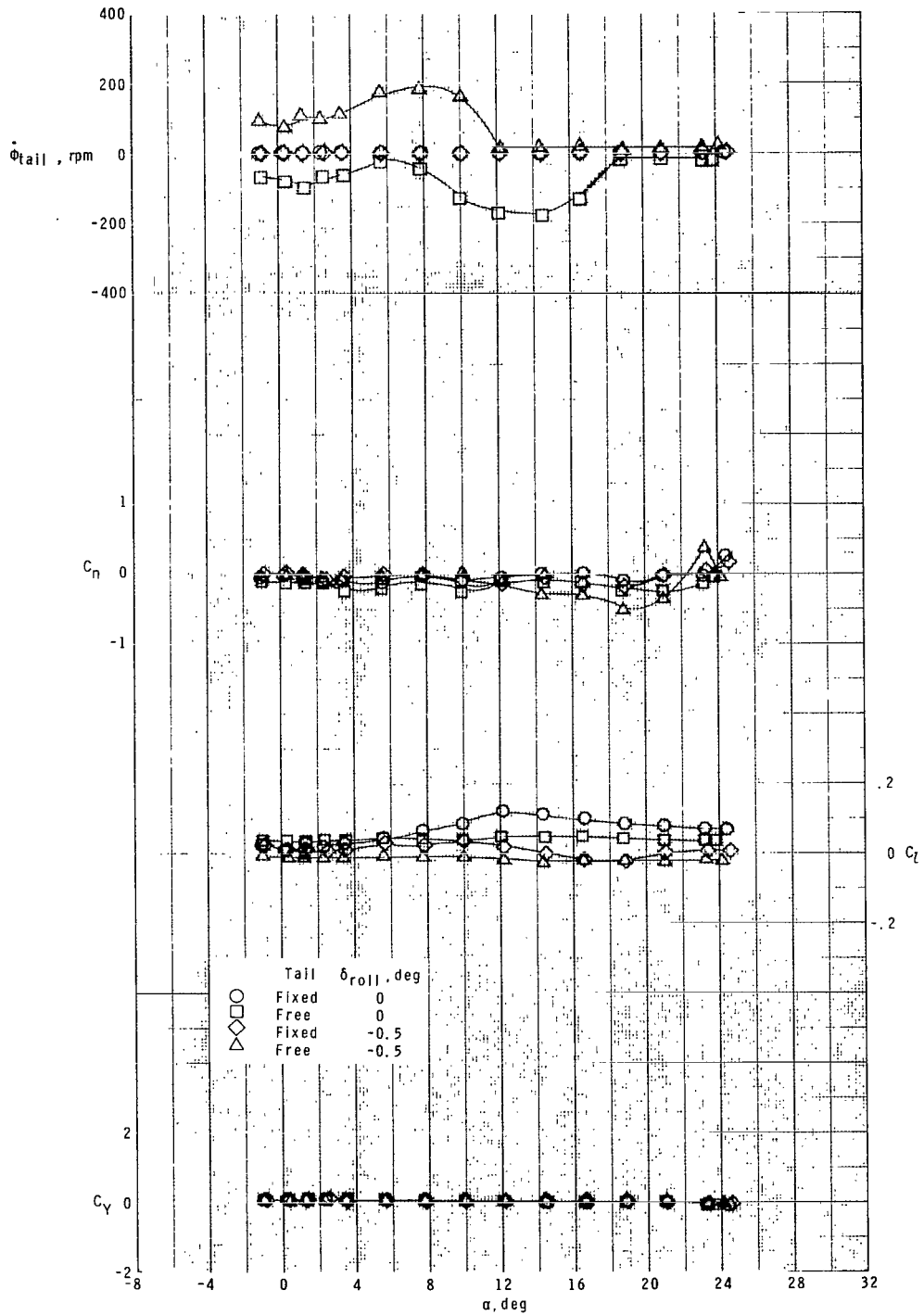
(a)  $M = 1.70$ .

Figure 12.- Roll-control characteristics of model with fixed and free-rolling tail at  $\phi_c = 45^\circ$ . Two canards deflected.



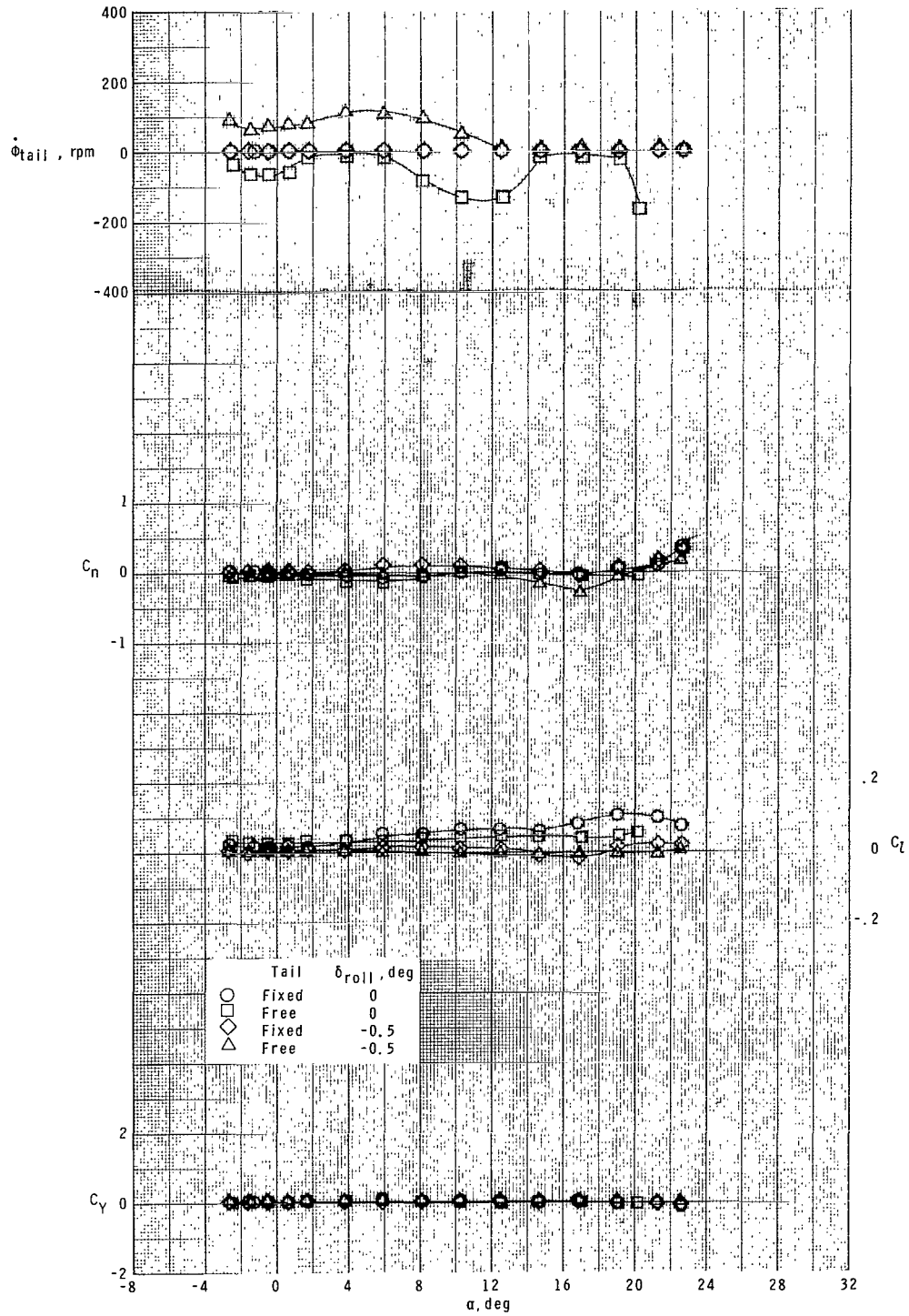
(b)  $M = 2.16$ .

Figure 12.- Continued.



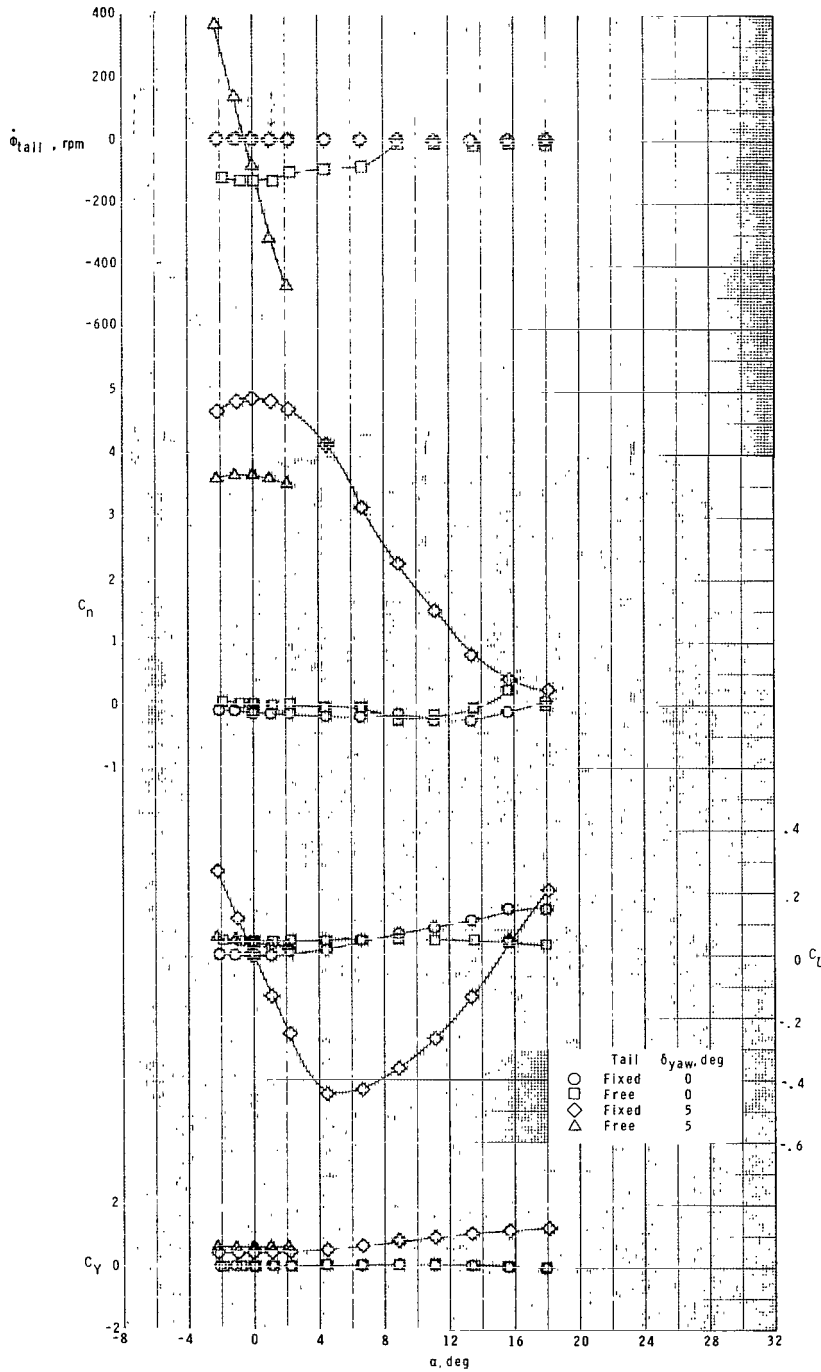
(c)  $M = 2.36.$

Figure 12.- Continued.



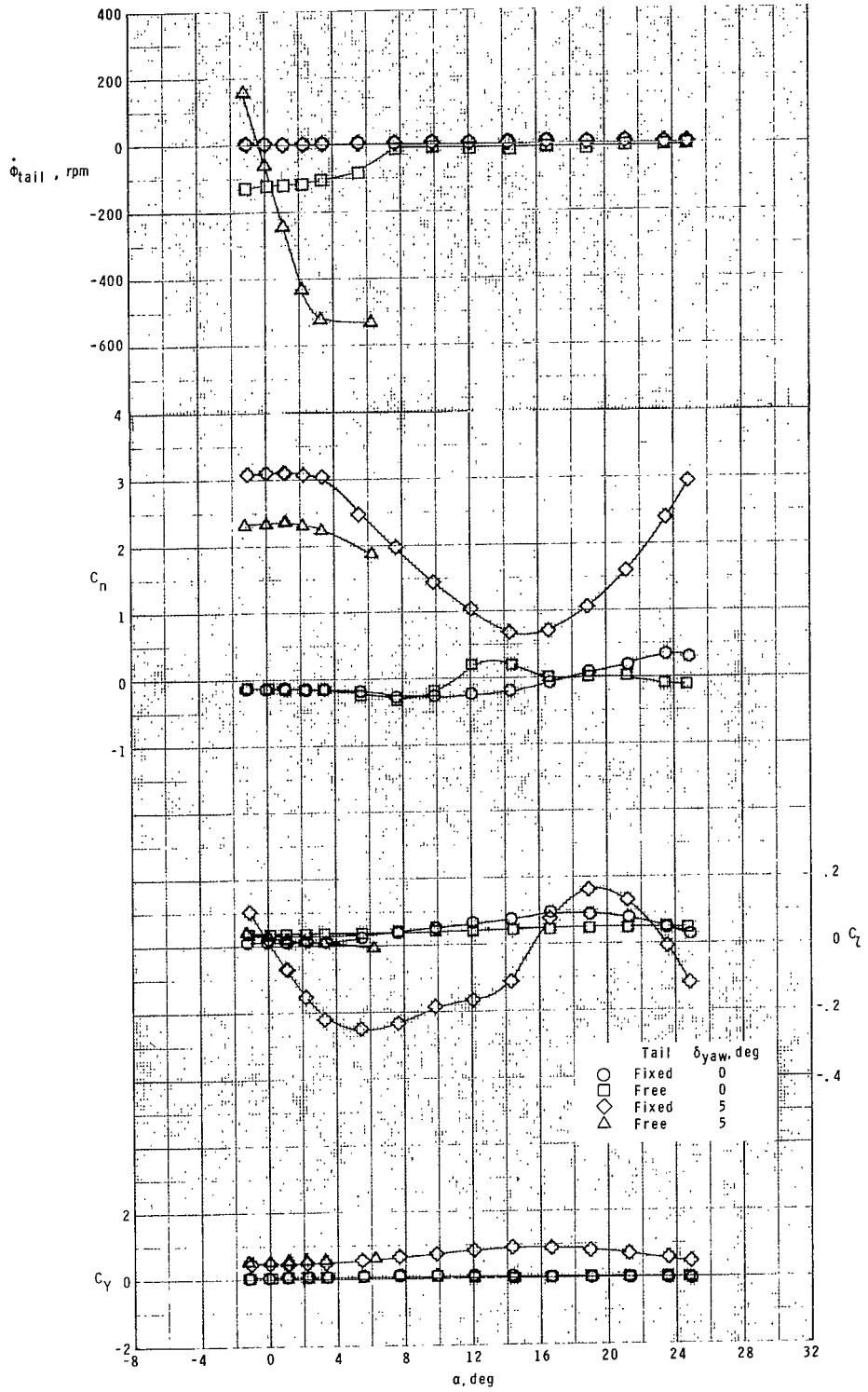
(d)  $M = 2.86$ .

Figure 12.- Concluded.



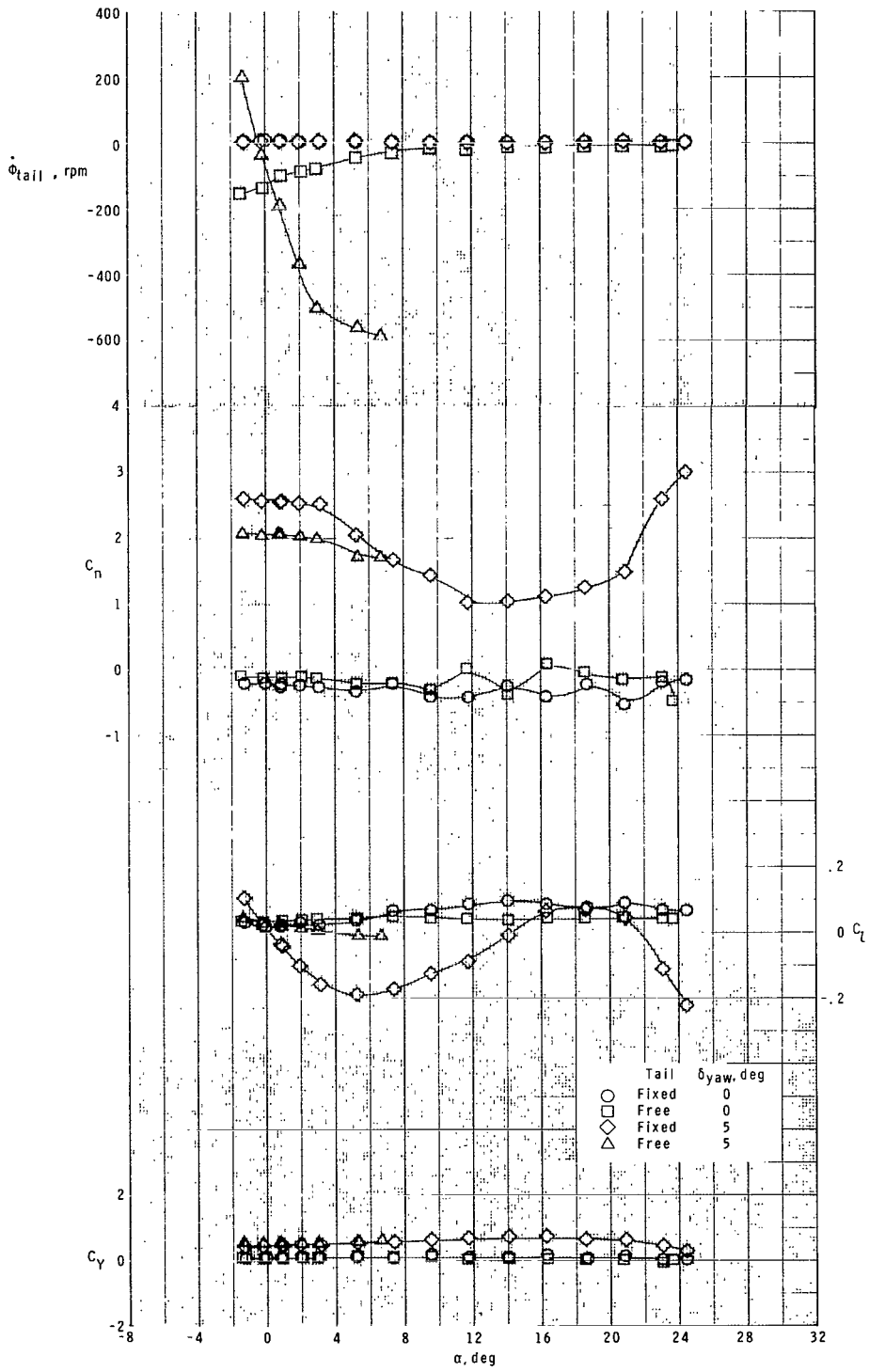
(a)  $M = 1.70$ .

Figure 13.- Yaw-control characteristics of model with fixed and free-rolling tail at  $\phi_C = 0^\circ$ . Vertical canards deflected.



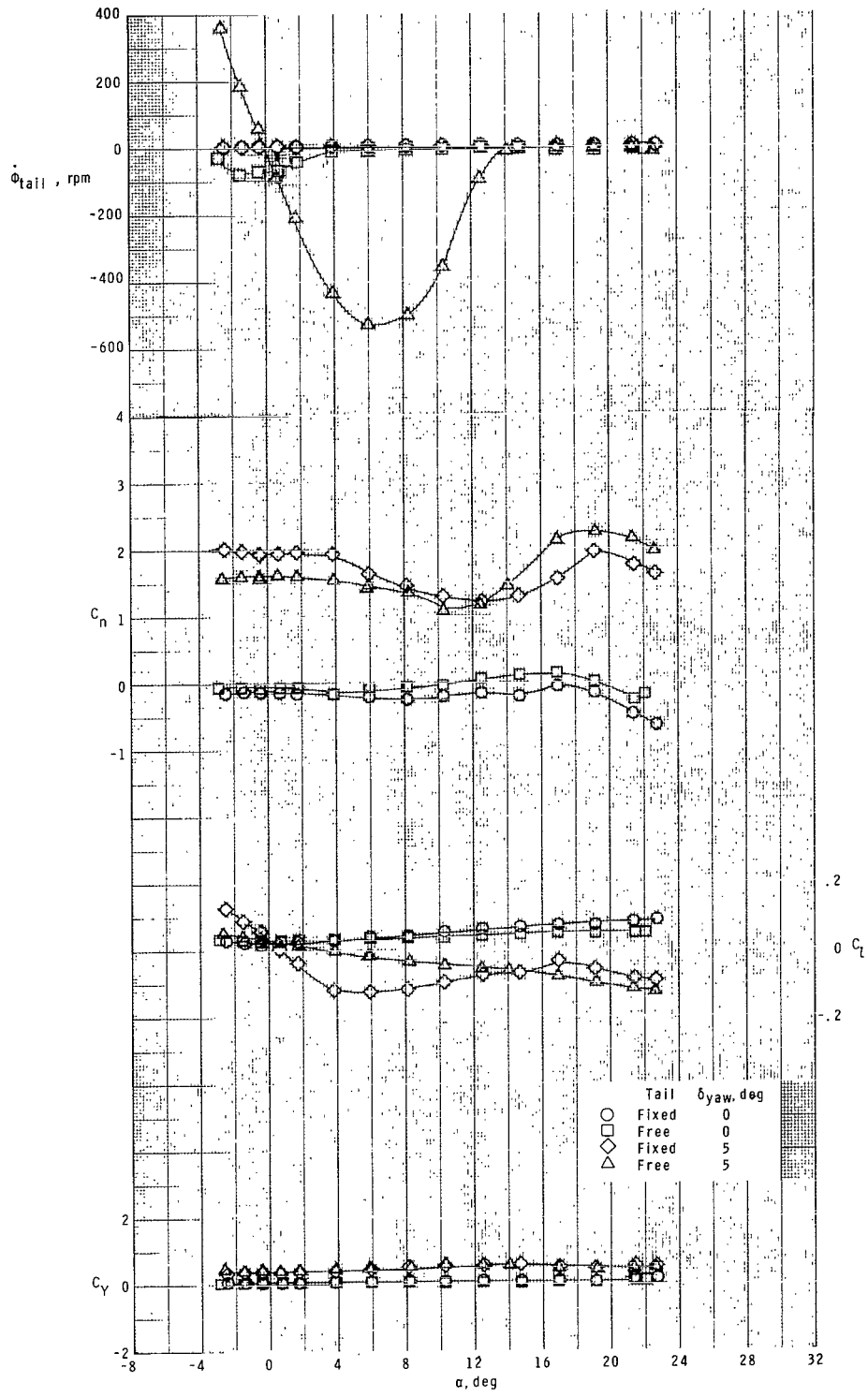
(b)  $M = 2.16$ .

Figure 13.- Continued.



(c)  $M = 2.36$ .

Figure 13.- Continued.



(d)  $M = 2.86$ .

Figure 13.- Concluded.





1. Report No. NASA TP-1316		2. Government Accession No.		3. Recipient's Catalog No.	
4. Title and Subtitle WIND-TUNNEL INVESTIGATION AT SUPERSONIC SPEEDS OF A CANARD-CONTROLLED MISSILE WITH FIXED AND FREE-ROLLING TAIL FINS				5. Report Date September 1978	
7. Author(s) A. B. Blair, Jr.				6. Performing Organization Code	
9. Performing Organization Name and Address NASA Langley Research Center Hampton, VA 23665				8. Performing Organization Report No. L-12297	
12. Sponsoring Agency Name and Address National Aeronautics and Space Administration Washington, DC 20546				10. Work Unit No. 505-11-23-03	
15. Supplementary Notes				11. Contract or Grant No.	
16. Abstract <p>A wind-tunnel investigation was made at free-stream Mach numbers from 1.70 to 2.86 to determine the effects of fixed and free-rolling tail-fin afterbodies on the static longitudinal and lateral aerodynamic characteristics of a cruciform canard-controlled missile model. The effect of small canard roll- and yaw-control deflections was also investigated. The results indicate that the fixed and free-rolling tail configurations have about the same lift-curve slope and longitudinal stability level at low angles of attack. For the free-rolling tail configuration, the canards provide conventional roll control with no roll-control reversal at low angles of attack. The free-rolling tail configuration reduced induced roll due to model roll angle and canard yaw control.</p>				13. Type of Report and Period Covered Technical Paper	
17. Key Words (Suggested by Author(s)) Cruciform missile Canard control Free-rolling tail				14. Sponsoring Agency Code	
18. Distribution Statement Unclassified - Unlimited				Subject Category 02	
19. Security Classif. (of this report) Unclassified		20. Security Classif. (of this page) Unclassified		21. No. of Pages 76	
				22. Price* \$6.00	

\* For sale by the National Technical Information Service, Springfield, Virginia 22161

NASA-Langley, 1978



National Aeronautics and  
Space Administration

THIRD-CLASS BULK RATE

Postage and Fees Paid  
National Aeronautics and  
Space Administration  
NASA-451



Washington, D.C.  
20546

Official Business

Penalty for Private Use, \$300

8 1 1U,A, 090878 S00903DS  
DEPT OF THE AIR FORCE  
AF WEAPONS LABORATORY  
ATTN: TECHNICAL LIBRARY (SUL)  
KIRTLAND AFB NM 87117

**NASA**

POSTMASTER:

If Undeliverable (Section 158  
Postal Manual) Do Not Return

---

**S**